DEEP LEARNING FOR ISLANDING DETECTION OF GRID-CONNECTED PHOTOVOLTAIC SYSTEMS

by

Omar Allan

A thesis submitted to the
School of Graduate and Postdoctoral Studies in partial
fulfillment of the requirements for the degree of

Master of Applied Science

in

The Electrical and Computer Engineering

Faculty of Engineering and Applied Science

University of Ontario Institute of Technology (Ontario Tech University)

Oshawa, ON Canada

January 2021

THESIS EXAMINATION INFORMATION

Submitted by: **Omar Allan**

Master of Applied Science (MASC) in **Electrical and Computer Engineering**

Thesis title: DEEP LEARNING FOR ISLANDING DETECTION OF GRID-CONNECTED PHOTOVOLTAIC SYSTEMS

An oral defense of this thesis took place on January 18, 2021 in front of the following examining committee:

Examining Committee:

Chair of Examining Committee	Dr. Ying Wang
Research Supervisor	Dr. Walid Morsi Ibrahim
Examining Committee Member	Dr. Mohamed Youssef
Thesis Examiner	Dr. Marc Rosen

The above committee determined that the thesis is acceptable in form and content and that a satisfactory knowledge of the field covered by the thesis was demonstrated by the candidate during an oral examination. A signed copy of the Certificate of Approval is available from the School of Graduate and Postdoctoral Studies.

ABSTRACT

Over the past decade, the integration of renewable-based distribution energy resources within the smart distribution system has been steadily growing. Despite the numerous advantages of integrating these renewable energy resources in reducing the greenhouse gas emissions and releasing the transmission line capacity, there are many operational challenges involving the protection when considering the unintentional islanding of these resources. Typically, when faults occur, an island or multiple islands may be formed throughout the electrical power distribution system. When the island includes one or more distributed energy resource, there is usually a serious potential hazard for the working personnel and hence the IEEE Standard 1547 recommends the distributed generation to cease to supply within 2 seconds of the formation of the island. Thus, there is a need for detecting the island and disconnecting the distributed generation within two seconds to fully comply with the IEEE Standard. In the literature, several methods for islanding detection have been proposed, which can be classified as communication-based, active or passive methods. The communication-based methods are expensive to implement while the active methods typically inject harmonic distortion into the distribution system to detect the island, which will lead to power quality degradation. On the other hand, the passive methods are preferred over other detection methods because they are inexpensive to implement and they do not affect the system power quality. The passive methods rely on identifying the islanding features in the local measurement of the voltage and current signals, which needs to be fed to the machine learning algorithms that have been proposed in the literature. However, identifying such features a priori is a very complex task in particular when considering inverter-based renewable energy resources. The work in this thesis uses deep learning to discover the features of the islanding as part of the classification process rather than identifying the features a priori as in the previous work and hence enhancing the capability of the passive methods. The results of testing the proposed passive islanding approach show an outstanding performance of the proposed method in islanding detection in grid-connected photovoltaic system. The proposed method utilized 31 features generated from 46 different cases to classify and detect the islanding. The proposed method succeeded in detecting islanding with a high accuracy of 98.1% and a rapid detection time of 0.28 second.

Keywords: Convolutional neural networks; deep learning; passive islanding detection, photovoltaic systems; smart distribution systems.

AUTHOR'S DECLARATION

I hereby declare that this thesis consists of original work of which I have authored. This is a true copy of the thesis, including any required final revisions, as accepted by my examiners.

I authorize the University of Ontario Institute of Technology (Ontario Tech University) to lend this thesis to other institutions or individuals for the purpose of scholarly research. I further authorize University of Ontario Institute of Technology (Ontario Tech University) to reproduce this thesis by photocopying or by other means, in total or in part, at the request of other institutions or individuals for the purpose of scholarly research. I understand that my thesis will be made electronically available to the public.

Omar Allan

STATEMENT OF CONTRIBUTIONS

The work demonstrated in this thesis was performed to enhance the islanding detection in smart grids. The work includes the following main contributions:

- Introducing smart grids and their advantage over other traditional electrical power systems as shown in chapter 1.
- A literature review for the various methods and techniques used for islanding detection as presented in chapter 2.
- Improving passive islanding detection and minimizing non-detection zones (NDZs) by using artificial intelligence (AI) techniques as presented in chapter 3.
- Presenting deep learning (DL) as one of the most advanced artificial intelligence techniques and its role in passive islanding detection as discussed in chapter 3.
- Studying smart grid system consisting of grid-connected PV system (D-RER) with various islanding and non-islanding events presented as discussed in chapter 4.
- Applying one of the popular deep learning networks called convolutional neural networks (CNN) to train a model to build classifier capable to classify the islanding and non-islanding events as discussed in chapter 4.
- Part of the work presented in the thesis has been submitted for publication and is currently under review:

O. A. Allan, W. G. Morsi, "A New Passive Islanding Detection Approach Using Wavelets and Deep Learning for Grid-Connected Photovoltaic Systems in Microgrids," International Journal of Electrical Power and Energy Systems, In Review.

ACKNOWLEDGEMENT

I would like to extend my sincere appreciation to the continuous support of Dr. Walid Morsi Ibrahim throughout my study and my research work. His guidance, patience, and deep knowledge has driven me to completing the MASc program and thesis work.

Special thanks to all the research team members within Dr. Morsi's research group in the Smart Grid & Electric Vehicles Research Laboratory who facilitated and removed any barriers throughout my study.

I would like to thank my parents for their motivation and remembering me in their prayers. Also, I would like to thank my wife Rawan for her days and nights support during any difficult time I went through. I appreciate her sacrifices and motivation throughout my studies. I cannot forget my kids, Nada, Ezz-Eddine, and Hamza for being around and keeping it up.

TABLE OF CONTENTS

LIST OF TABLES

Chapter 2

Chapter 4

LIST OF FIGURES

Chapter 1

Chapter 2

Chapter 3

Chapter 4

LIST OF ABBREVIATIONS AND UNITS

LIST OF ABBREVIATIONS

AI	Artificial Intelligence
AFD	Active Frequency Drift
CNN	Convolutional Neural Networks
CPU	Central Processing Unit
CWT	Continuous Wavelet Transform
DC	Direct Current
DER	Distributed Energy Resource
D-RER	Distributed Renewable Energy Resource
DFT	Discrete Fourier Transform
DL	Deep Learning
DQIVF	DQ Implementation Voltage Feedback
DVS	Deferential level Voltage Shift
DWT	Discrete Wavelet Transform
EPS	Electric Power System
F	Frequency
FN	False Negative
FP	False Positive
Fs	Sampling Frequency
GB	Gigabyte
GHz	Giga Hertz
Hz	Hertz
I	Current
IEEE	Institute of Electrical and Electronics Engineers
Imp	Current at Maximum Power Point
Isc	Short Circuit Current
L	Inductance
LSTM	Long short-term memory
MLP	Multilayer Perceptron
MPPT	Maximum power point tracking
NDZ	Non-detection Zone
OF	Over Frequency
OV	Overvolt
P	Active Power
PCC	Point of Common Coupling
PG	Generated Power
PL	Load Power
PLL	Phase Lock Loop
Pmp	Maximum Power
PV	Photovoltaic
Q	Reactive Power
QF	Quality Factor
QL	Inductive Reactive Power

RAM	Random Access Memory
ReLU	Rectified Linear Unit
RNN	Recurrent Neural Network
ROCOF	Rate of Change of Frequency
ROCOP	Rate of Change of Power
ROCOV	Rate of Change of Voltage
S	Apparent Power
SCADA	Supervisory Control and Data Acquisition
SFS	Sandia Frequency Shift
SMS	Slip Mode Frequency Shift
STC	Standard Test Conditions
STFT	Short-Time Fourier Transform
SVS	Sandia Voltage Shift
TN	True Negative
TP	True Positive
UF	Under Frequency
UV	Under Voltage
V	Voltage
VAC	Alternating Voltage
VDC	Direct Current Voltage
Vmp	Voltage at Maximum Power Point
Voc	Open Circuit Voltage
VSC	Voltage Source Converter
WPT	Wavelet Packet Transform

LIST OF UNITS

A	Ampere
kHz	KiloHertz
km	Kilometer
kV	KiloVolt
kVA	KiloVolt-Ampere
kVAr	KiloVolt-Ampere Reactive
kW	KiloWatt
mH	Millihenry
MW	Megawatt
W	Watt

Chapter 1. Introduction

1.1 Background

1.1.1 Legacy Electric Power Distribution Systems

Traditional electric power systems utilize centralized generations that feed through step up transformers an interconnected high voltage network known as the transmission grid. The transmission grid is used to deliver the electrical power from the generation stations, through long distance transmission lines, to the distribution system. The legacy electric power distribution system consists of step-down distribution transformers, primary circuits, and secondary circuits to deliver the power to end users with a unidirectional power flow from the substation to the end user customers who are only consumers.

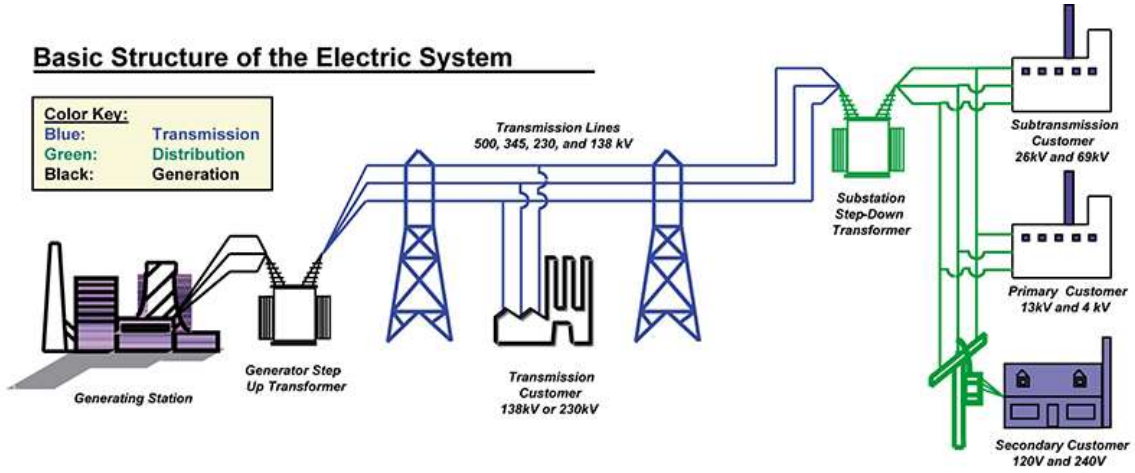

Figure1.1: Legacy Electric Power System [1]

While the world's demand load has been increasing in the recent decades, the generation has been following the growing load demand, the transmission lines have extended into new lands, and the operation of the electrical power system have become more complicated [2]. Therefore, the construction of new power plants or upgrading the existing power plants have economical and environmental constraints, which has led the researches to find alternative ways to optimize the electric power system's operation [3]. Designing electric power systems that are capable to integrate renewable energy resources and use the digital technology to improve the reliability, the security, and the efficiency,

have become known as smart electric grids, which are the most important topics in the electricity market.

1.1.2 Smart Electric Power Distribution Systems

Recently, the use of the distributed renewable energy resources (D-RERs) is dramatically increased in the existing electrical power systems due to its environmental and economical benefits. D-RERs are type of Distributed Energy Resources (DERs), but they are of renewable resource type, such as photovoltaics, biomass, and wind turbines. Typically, the D-RERs are connected to the distribution systems and are located within the electric power distribution systems through a power electronic interface, as well as the microgrids, that may contain energy storage systems and loads. As a result, the power flow in the smart distribution systems is not unidirectional as the D-RERs can generate power and feed it back to the grid. There are many benefits of integrating D-RERs into the electric power distribution systems such as reducing the system energy losses, reducing the transmission congestion, improving the system efficiency, improving the electric power quality, minimizing the peak load, reducing the energy prices and reducing greenhouse gas emissions. On the other hand, the increased penetration of such D-RERs gives rise to a wide range of operational issues such as intermittent power supply, system stability, supply security and reliability, protection coordination, and hence complex protection to protect the network. Besides, other problems may arise in the networks when integrating D-RERs, such as the reverse power flow and the islanding problem that will be discussed in the next section.

Therefore, there is a need to enhance the electrical power systems by using the technology (sensing, embedded processing and digital communication) in the electric power grids to intelligentially integrate all D-RERs and all users' actions in order to deliver sustainable, economic, and secure electricity supplies [4].

1.1.3 Islanding Problem

One of the most serious issues in the operation of the smart electric power distribution systems is the unintentional islanding and its consequences on the smart grid operation. Islanding is a situation in which a distributed energy resource continues to

energize a portion of an Area EPS through the PCC while this portion is electrically disconnected from the rest of the Area EPS [5]. Failure to detect the islanding will not only create risk to electric power system, but also it will create risk to the line workers and the electric equipment. According to the IEEE standard 1547-2018 [5], the distributed renewable energy resource must detect the island and trip within 2 seconds of occurrence of islanding. The island can occur in any part of the electric power system that consists of one or more distributed renewable energy resources as shown in Fig. 1.2. The Fig. 1.2 depicts different islands that may occur within the electric grid. When any breaker trips due to any fault or an unscheduled maintenance, then the distributed renewable energy resource downstream this breaker will be part of the island and must trip within 2 seconds. If the upstream breakers trip, then this will form another larger island, so in this case all distributed renewable energy resources located within this island must trip. The IEEE 1547 in [5] categorized the islanding into two types: intentional and unintentional islanding. In this thesis, only the unintentional (undesirable) islanding will be discussed since in case of intentional islanding, proper measures are usually taken to avoid any operational issue.

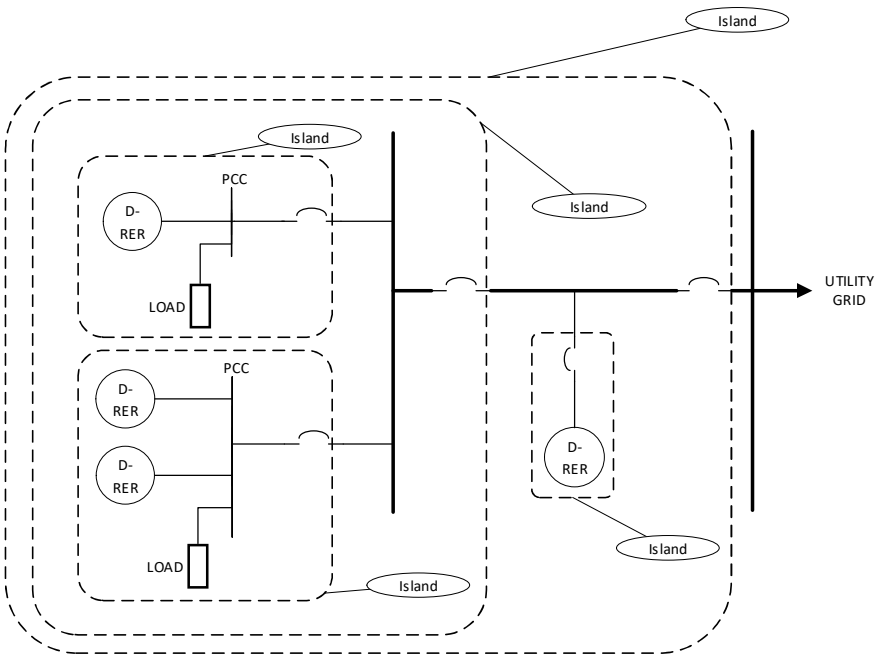

Figure1.2: Potential Island within EPS

1.1.4 Islanding Detection Methods

There have been several proposed methods in the literature to develop an efficient, fast, and accurate islanding detection in the smart distribution systems considering the integration of distributed energy resources. The methods can be classified into active, remote (communication-based), hybrid, and passive detection techniques as shown in Fig. 1.3.

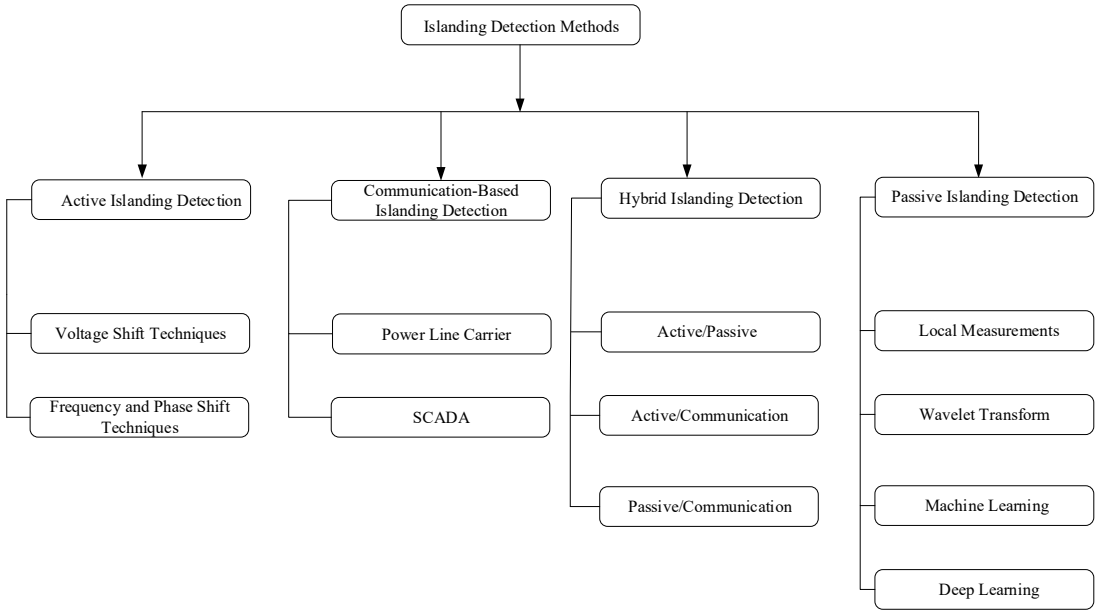

Figure1.3: Islands Detection Methods

1.1.4.1 Active Islanding Techniques

Active methods inject disturbances to the grid and constantly monitor the utility grid response to determine if it is still connected [6]–[11]. The active methods are classified into two main groups [12] and each group is divided into techniques as shown in Fig. 1.4.

Regardless of the technique used in active methods, these techniques increase harmonic distortion and lead to several power quality issues. These methods have small NDZ, but they usually cause disturbance and compromise system's power quality as well as creating noise in the grid [13]. Some active methods have failed to detect islanding when there are multiple DERs within the island [12]. Therefore, the active methods are not appropriate for use in smart grids which are designed to enhance power quality.

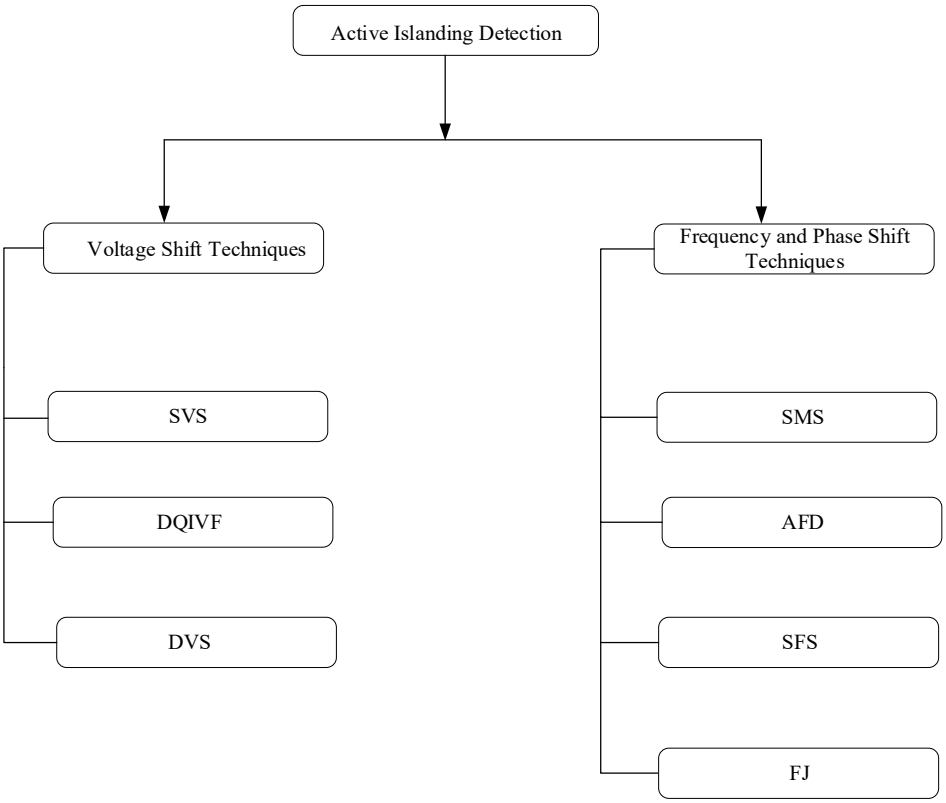

Figure1.4: Active Islanding Detection Techniques

1.1.4.2 Communication-Based (Remote) Islanding Detection Methods

Communication-based detection methods transmit communication signals from the area EPS to the DERs in the island to trip when the islanding occurs [14], [15]. The communication-based islanding detection are classified into power line carrier and the Supervisory Control and Data Acquisition (SCADA)-based techniques. In power line carrier communication, the utility sends signals through power line to the DERs. This requires transmitters to be installed on the utility side and the receiver on the DERs side and once the signal is lost, then the islanding is detected [3]. The SCADA is also used in the islanding detection through measuring the voltage at the DER, which is then sent to the utility through SCADA system and when the islanding occurs, the utility can determine if the DER is still connected and sends trip signal to disconnect the DER [3]. Although the remote islanding methods do not have NDZs, but these methods are expensive and require high speed communication [16], [17], which may not be reliable in rural areas where the signals may be attenuated due to long run of power lines carrier communications (PLCC).

Furthermore, a complex and expensive SCADA infrastructure may be required to connect microgrids in remote areas to the utility central control units, which leads to high cost, and tremendous infrastructure work and redesign [18]. Besides, the islanding detection can be exposed to cyber-attack when communication detection methods are used, which may cause false detection in normal situations or no detection in case of islanding [19], [20].

1.1.4.3 Hybrid Islanding Detection Methods

A combination of two or three detection methods are used to enhance the system's response to islanding. If one method fails, the other will function and properly detect the islanding upon occurrence [16]-[21] . However, the hybrid methods may be expensive and complex to implement [22].

1.1.4.4 Passive Islanding Detection Methods

The passive methods do not affect the systems' power quality and are not expensive to implement since they utilize the grid's local measurements for the islanding detection. The only drawback for using the traditional passive detection is the large NDZ. If the NDZ can be minimized or eliminated, then the passive islanding detection will be the most cost-effective method to use for islanding detection. Therefore, there have been several research works and attempts to enhance the passive islanding to minimize the non-detection zones. However, there is still some research gaps that this thesis aims to fulfill in order to detect the islanding efficiently whenever it occurs. Different passive islanding methods will be discussed in detail in chapter 2. In addition, a literature review of the previous work will be presented as well.

1.2 Statement of the Problem

As the penetration of DERs has increased in the smart grids, the islanding problem has been analyzed and further studied in many papers and research works in order to find practical and efficient solutions that are able to detect islanding upon occurrence. The D-RERs are usually integrated with the smart electric power distribution systems through power electronic-based inverters. Such power electronic interface has added complexities to the problem of islanding detection compared to the non-inverter-based DERs. The DC/AC inverters produce distorted waveforms and inject harmonic-polluted currents to the

grid, which leads to poor power quality. In addition, the D-RERs have fluctuating characteristic that causes power quality problems, such as voltage variation, frequency variation, transients, and harmonics distortion that affect the performance of islanding detection [12]. The previous work used several passive methods, such as local measurements, signal processing, machine learning, whereas other methods used active methods and remote methods. However, the active and remote detection methods do have drawbacks in islanding detection associated with poor power quality and high cost issues respectively as presented in the previous sections. Therefore, the islanding issue remains a chronic issue in the smart grids that integrate various types of D-RERs and generate massive data.

As a result, there is a need to find a cost-effective technique while maintaining a high level of power quality at the same time. Furthermore, the technique should also be able to deal with the raw/unclassified data measured from the smart grids. The machine learning techniques have been used in many studies, but they failed when dealing with unclassified data, which require human interference during the model training and when building the events classifiers. Therefore, there is a necessity to find a technique that can process and extract the features from the data, and automatically learn the features to accurately predict the events.

This thesis proposes the use of the Continuous Wavelet Transform (CWT) to get the time-frequency coefficients from the local measurements of the inverter-based DER (D-RER), which are very challenging to detect within the island, and pass these coefficients to the Convolution Neural Network (CNN). Such CNN is considered as one of the advanced deep learning tool that consists of deep hidden layers which can learn the features and classify the events with a high accuracy and rapid detection time. The proposed work aims to address all the above issues and work efficiently in smart grids to detect the islanding in different operating conditions.

1.3 Statements of The Objectives

The work introduced in this thesis aims to:

- Minimize non-detection zones (NDZs) and improve passive islanding detection.

- Introduce effective islanding detection that can work efficiently in smart distribution systems containing inverter-based DERs (D-RERs).
- Deal with raw and massive data received from smart distribution systems and automatically detect, extract, and learn the features to build the classifiers.

1.4 Contribution

The work presented in this thesis aims to address the islanding detection in smart electric power distribution systems by introducing a novel approach that combines the deep learning and the signal processing to minimize the NDZ and improve the passive islanding detection, which does not affect the system power quality. The continuous wavelet transform (CWT) is one of the signal processing methods that is used in this thesis to obtain time-frequency coefficients/features from the local measurements generated from numerous cases and different loading conditions, including zero power mismatch cases, applied to grid-connected Photovoltaic system (D-RER). Deep learning is an approach that uses artificial intelligence to develop the mathematical models without the need to determine the signal features a priori. In fact, the features are identified by the neural networks during the deep learning process. A deep learning architecture consists of hidden layers to process the features obtained from the wavelet transform (CWT). The features pass through each of the deep layers, where the output from each previous layer is passed as input to successor layer and then classifies the events as islanding or non-islanding.

This approach was simulated and tested and has successfully detected islanding under various conditions and different cases with a high accuracy of 98.1% and rapid detection time of 0.28 second which is acceptable by the respective standards.

1.5 Thesis Organization

The work is organized as follows:

Chapter 1 presents comparison between legacy power system and the smart grid. This chapter also discusses the islanding problem as well as the operational challenges associated with it. The main islanding detection methods are presented, and a comparison between the existing detection methods is discussed. The statement of problem and the thesis contribution are demonstrated at the end of this chapter.

Chapter 2 presents the existing passive islanding detection methods previously published in the literature. A review of the advantages and disadvantages of each method is presented in this chapter. Finally, the main research gap of the existing methods is discussed, and the research objectives of the proposed passive islanding method are highlighted.

Chapter 3 demonstrates the different methods used in the signal processing and the deep learning methodology. The advantages and the drawbacks of each method are presented, and a comparison of the various methods is discussed. The evaluation metrics and the method of calculating the accuracy of the proposed method is presented.

Chapter 4 describes the system study characteristics, the signals and measurements used in the analysis. This chapter presents the islanding and the non-islanding cases under various operating conditions. Also, the model's training and testing, and the computed detection time are presented in this chapter. A comparison with other studies results is discussed at the end of this chapter.

Chapter 5 introduces the conclusion of the work, the thesis recommendations, and the proposed future work.

Chapter 2. Literature Review

2.1 Introduction

Due to the increased penetration of DERs in smart electric power distribution systems in particular the D-RERs, which are inverter-based DERs, islanding has become a challenge and there has been a need to detect it and isolate the DERs within the time specified in the respective standards. The main goal of this chapter is to present a literature review of the existing passive islanding detection methods used to detect islanding in the distribution systems. Besides, this chapter reviews the previously published work in the passive islanding detection, which are classified into four main groups: local measurements, wavelet-based methods, machine learning, and deep learning. A summary of the existing methods' advantages, disadvantages, and limitations in the passive islanding detection will be presented. Moreover, this chapter presents the research gaps in the previous work in literature and delivers the main contributions of the research work introduced in this thesis.

2.2 Previous Work on Passive Islanding Detection

This section presents the existing passive islanding methods that were proposed to detect islanding. The previous work studied local measurements, wavelet-based methods, machine learning-based methods, and deep learning-based methods that will be presented hereafter.

2.2.1 Local Measurements

Passive islanding methods use the system's parameters measured at the point of common coupling (PCC) between the DER system and the grid. In case of any variance in the parameters beyond the threshold, these techniques will detect islanding upon occurrence [13], [17], [23]–[26]. Different islanding detection relays are employed to monitor the parameters at the PCC to trip the DER when the threshold values are exceeded. Some relays use voltage measurements and are called OV/UV relays, where other relays use frequency (OF/UF relays), or rate of change of frequency (ROCOF). The voltage/frequency relays fail to detect islanding when the local load matches the local generation, which typically leads to a large NDZ particularly for inverter-based D-RER

integrated systems [12]. On the other hand, the ROCOF relays are sensitive to the network disturbance and leads to a nuisance tripping. Also, selecting the right settings of the ROCOF relays is still complicated [12]. Fig. 2.1 shows some indices that are used in passive islanding detection.

In general, when using the local measurements only, it is difficult to set the thresholds to prevent the islanding and the nuisance tripping at the same time. The thresholds are set experimentally, so selecting the lower thresholds causes nuisance tripping while selecting the higher thresholds will prevent the detection [27]. Also, other non-islanding events, such as faults, load switching, and different loading conditions especially when the local generation is equal to the local load (zero power mismatch) affect the islanding detection and lead to high NDZs [3]. Therefore, using the local measurements only is not reliable for islanding detection and other techniques shall be used.

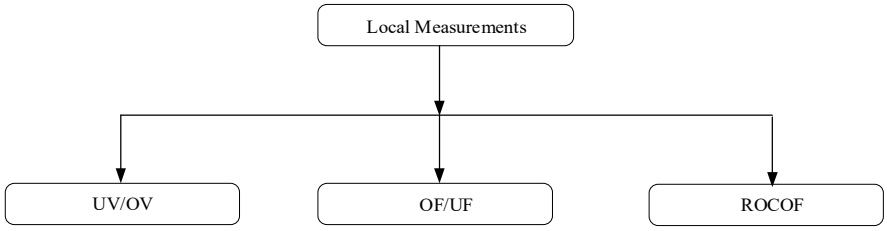

Figure 2.1: Local Measurements

2.2.2 Wavelet Transform

Some approaches used signal processing techniques for passive islanding detection. These approaches used different wavelet-transform techniques (STFT, DWT, CWT) to extract all signal features and frequency components from the local measurements [21], [22]. This is achieved by dividing the signals into variable time windows while using the scaled or the time-shifted wavelets (baby wavelets) to get the similarities with the analyzed signals. The works in [28] used the short-time discrete Fourier transform (STFT) for passive islanding detection. The STFT localizes the transients by using the fixed frequency time window, which does not operate in a multiresolution analysis. Several passive islanding methods in [29]–[32] implemented the discrete wavelet transform (DWT) to overcome the fixed resolution issue associated with the STFT. The passive islanding

detection using the DWT is divided into non-energy and energy-based indices. In non-energy-based, the voltage and frequency DWT coefficients were compared to arbitrary thresholds [31]. The direct use of arbitrary thresholds leads to misdetection and nuisance tripping. Therefore, the energy-based methods were proposed to implement the energy of the wavelet coefficient of the voltage and the current in islanding detection [33], [34]. However, the DWT considers only a dyadic scale, which may not provide detailed representations of the signal at every frequency and time sample. The continuous wavelet transform (CWT) is also used in passive islanding detection. The work in [35] used the CWT for implementing a wavelet-based hybrid islanding detection scheme and the study utilized the transient detection scheme to mitigate the implementation of the injected disturbances by the active islanding techniques.

Although using the signal processing can be useful, it requires a selection of the filters' parameters to accurately extract the features and hence achieving accurate classification. The feature extraction requires the human intervention and therefore require substantial efforts and it is considered a time-consuming process [36]. Also, using conventional wavelet transform is vulnerable to noise caused by the power electronics equipment [37].

2.2.3 Machine Learning

Machine learning techniques have been used in many studies for passive islanding detection [27], [38]–[40]. These methods combine feature extraction and classification to reduce the non-detection zone (NDZ). The extracted features are used to train the classifiers that are used to classify the events into islanding and non-islanding events. The classifiers are trained models (algorithms) using large data set of parameters. Fig. 2.2 shows the main machine learning techniques used in passive islanding detection.

Artificial neural network (ANN) classifiers create a set of neurons capable to learn from pattern and recognize them. A function weighs the input data and then transforms them. The neurons are activated by the transformed input data and this process is repeated until the output neuron is activated and the pattern is identified [41]. ANN classifiers were

used in [42] to classify the events from the input data features. Also, the work in [43] used ANN with 7 neurons in a hexagonal to detect islanding for synchronous DER.

Decision tree (DT) classifiers contain root nodes, each branch of the nodes represents YES or NO decision. The initial classification problem is divided into internal nodes that check the parameters against respective methods and branch out. The work in [44] used 11 features from 54 events to detect islanding events. The work in [38] used DT for islanding detection by training and testing the model using two different sets of features. The DT is used in [45] for classifying islanding and non-islanding events and achieved an accuracy of 98%.

The Bayesian classifiers learn the conditional probability of each feature of a given set of training data set. To estimate the probability of a given input data with respect to a certain class (e.g. c), where the features expressed as xi:

$$P(C = c|X = x) = \frac{P(X = x|C = c)P(C = c)}{P(X = x)} \tag{2.1}$$

Bayesian classifiers have been used in [46] for islanding detection. The work in [38] used 21 features and 4 important features to classify events for three different scenarios.

Support Vector Machine (SVM) classifiers use labeled training data for supervised learning in order to classify the events. The classifiers use kernel function K(xi, xj) that links the training vector x_i to testing vector x_j. The work in [47], [48], and [38] used SVM classifiers in passive islanding detection.

Although machine learning techniques have been used widely in islanding detection, these methods deal with structured/labeled data and require human intervention during the models training to build the classifiers. Selecting the relevant features from the data in these methods is typically performed manually [49], which represents a major drawback in particular when dealing with inverter-based D-RER that adds complexities by making the features extraction process not trivial.

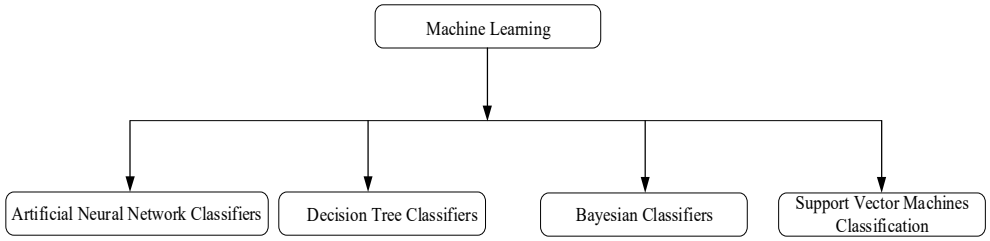

Figure 2.2: Machine Learning Techniques

2.2.4 Deep Learning

Recently, advanced AI (Artificial Intelligence) deep learning techniques have been proposed. The neural network sends the input data (raw data) through multi-layer artificial neural networks (deep layers) defining the features and classifying the events into the islanding and non-islanding events. There are different architectures [36] of deep learning as shown in Fig. 2.3.

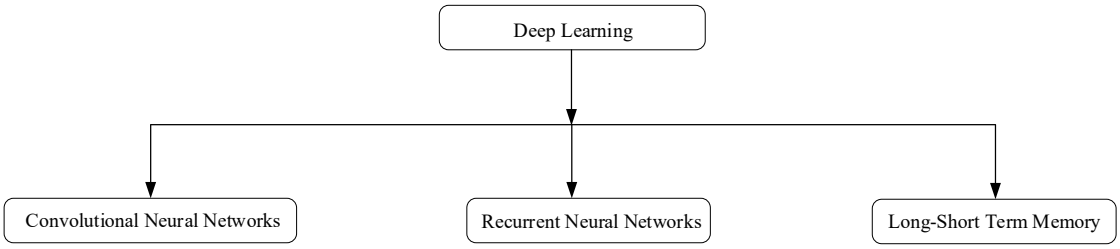

Figure 2.3: Common Types of Deep Learning Techniques

The RNN is a type of feed-forward networks, which feed the information in one direction. RNN deals with data in sequential form and uses short memory to save the information in the network and transfers the output from the previous state to the next state [36]. The RNN requires built-in memory to save and update the state from previous calculations [50]. The long short-term memory (LSTM) consists of blocks known as memory cells with adaptive multiplicative gates input, output and forget outputs. The LSTM handles long-term temporal dependencies, requires hardware accelerators, and produces memory-intensive workload [51].

On the other hand, a Convolutional neural network (CNN) is one of the most popular deep learning structures. The CNN is composed of input layer, convolution layers, and

classification layers. The CNN overcomes the limitation of the RNN and LSTM and stands out from other techniques due to its ease of training and less requirements in terms of memory and hardware requirements.

The work in [37] used an auto-encoder of a three layers neural networks to extract features, generated from two islanding voltage rise and voltage drop cases, to train the model and to classify the islanding and non-islanding events. The method achieved an accuracy of 98.3% and a detection time of 0.18 second. However, this approach used a neural network consisting of three layers only while the increasing amount of data in smart grids requires advanced AI algorithms with deeper layers of neural networks [52], such as CNN, RNN, and LSTM that will be presented in chapter 3. Besides, the frequency used in [37] is 30 kHz which is not a standard relay frequency. Furthermore, the work dealt with only two cases, whereas there are many other real cases may happen in any smart distribution system, which were not considered in the testing phase.

The work in [22] used Multi-Layer Perceptron (MLP) neural networks and used the input data to train the model and build the classifier to detect the islanding in a power system consisting of a synchronous generator as the DER. The accuracy achieved using this method is 99.88%, but it requires a lengthy computational time of 2 seconds to detect the islanding. This method applied deep learning on traditional power system of synchronous generators only which is not applicable to the inverter based DERs (D-RER). Deep learning techniques will be discussed thoroughly in chapter 3.

2.2.5 Deep Learning Vs Machine Learning

Unlike machine learning, deep learning networks automatically learn the optimal features from the raw data and do not necessarily need to deal with structured/labeled data for classification. Also, deep learning algorithms can reduce the human intervention in the signal processing and the classification processes as the features identification and extraction are implemented automatically during the model training by deep learning layers.

2.3 Research Gaps

According to the literature review and table 2.1, the research gaps can be summarized as follows:

- The lack of AI application in previous studies that used local measurements only or wavelet-based methods.
- The lack of automatic features learning from input data in methods used local measurements, wavelet-based, and machine learning techniques.
- Despite few studies have used deep learning, these methods lack the rapid detection time, insufficient studied cases, and less number of hidden layers.
- The lack of investigation of islanding detection for inverter-based DERs (D-RERs) penetrating smart distribution systems.

In summary, there are research gaps in finding a passive islanding method that use AI techniques, such as deep learning to automatically learn the features in smart distribution system containing inverter-based D-RER.

Table 2.1: Literature Review of Existing Passive Islanding Methods

Ref.	Passive Islanding Detection	AI Techniques			Signal Processing		Inverter-based DER
		Machine Learning	Basic Deep Learning	DL w/ deep layers	Wavelet	Local measurements only	
[34]	✓	×	×	×	✓	×	×
[53]	✓	×	×	×	✓	×	×
[38]	✓	✓	×	×	×	×	✓
[27]	✓	✓	×	×	×	×	✓
[39]	✓	✓	×	×	×	×	✓
[40]	✓	✓	×	×	×	×	×
[37]	✓	×	✓	×	×	×	✓
[22]	✓	×	✓	×	×	×	×

2.4 Research Objective

The work introduced in this thesis aims to present an effective passive islanding detection method that can be used in smart distribution systems embedded with D-RER, which are inverter-based resources. The work adopted deep learning as one of the most advanced AI techniques. Deep learning techniques can best work with raw massive data generated in smart grids, by extracting the features, automatically learning them and classifying the events successfully.

2.5 Summary

This chapter presented the previously published work in the literature pertaining to passive islanding detection in electric power distribution systems. The advantages, disadvantages, and limitations of each existing methods have been presented. An insight about the local measurements' methods, their advantages, disadvantages, and their limitations in setting the thresholds that may lead to nuisance tripping or no response upon islanding occurrence is provided. Also, the chapter investigated the highly possible NDZs especially at zero power mismatch. Besides, a review of the wavelet-based methods and their advantage and disadvantages in passive islanding detection was presented. The filter selection challenge, the need for human intervention, and the high sensitivity to noise have been addressed. Machine learning methods have been also discussed. The manual adjustment to the features and the human interface in the model learning limits the use of the machine learning method in passive islanding methods in smart grids that generate massive data and need efficient and intelligent methods to be adopted and used.

This chapter also introduced the research gaps and what was missing in the previous work. It also presented the research objectives and how the proposed work will contribute to enhancing the passive islanding detection in smart grids. The next chapter will demonstrate the methodology of the proposed deep learning and how it can be applied to the smart distribution systems to effectively detect the islanding in high accuracy and short detection time.

Chapter 3. Wavelet Transform and Deep Learning: The Methodology

In this chapter the fundamentals of the continuous wavelet transform (CWT) is presented in the context of the islanding detection, as well as a comparison with other transform analysis technique followed by a detailed explanation of the use of different methods of deep learning. The chapter concludes with an in-depth discussion on different types of deep learning and signal processing technique when applied to passive islanding detection.

3.1 Wavelet Transform

This section introduces the wavelet transform in order to choose the most suitable wavelet function that can be best used with deep learning techniques for passive islanding detection and classification in smart grids.

3.1.1 Discrete Wavelet Transform

In discrete wavelet transform (DWT), the signal important features are represented in both time and frequency domain using the multi-resolution analysis (MRA) [54]. The Multi-resolution analysis applies successive decomposition to the approximation with no further decomposition to the details. In MRA, the original signal $x(t)$ is decomposed into low frequency and high frequency components, where the approximation represents the low frequency components and the details represent the high frequency components.

3.1.2 Wavelet Packet Transform

Wavelet Packet decomposition is a general representation of the wavelet decomposition that provides the approximation and the details in tree sort structure where level k represents the breadth, i represents the time location at the tree [55]. Moreover, the WPT has an additional factor m, which is interpreted differently. In WPT is organized as a tree for positive values of integers k and m where the level/scale k defines the breadth, frequency m defines node position in the tree, and i is the number of samples at the different nodes of level k. The total retained energy in the approximation coefficients for a decomposition level k is defined as:

$$\varepsilon_a(k) = \sum_{m=1} \sum_{i \in Z} \left| W_{k,m,i} \right| \qquad (3.1)$$

Where k is levels, m is node index, i is the number of samples at different nodes. An example of tree structure generated by wavelet packet is shown below in Fig. 3.1.

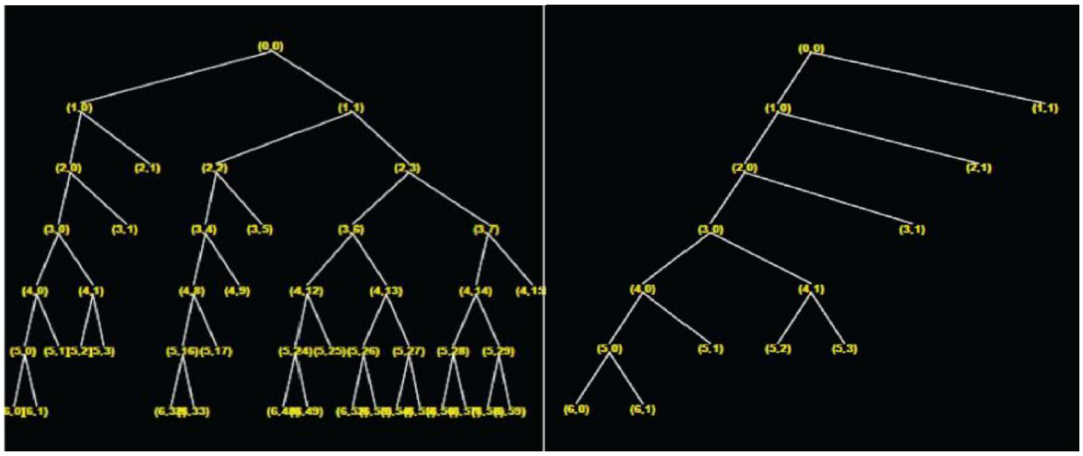

Figure 3. 1: Example of Wavelet Packet Tree Structure [56]

3.1.3 Continuous Wavelet Transform

The continuous wavelet transforms the signal into different time and scales [57], which provides time-scale characteristics contained within the islanding signal. In Continuous Wavelet Transform (CWT), the time-scale property allows good time-frequency resolution representation, which helps in identifying the unique features of the islands. The use of CWT is advantageous over other time frequency transforms such as short-time Fourier Transform (STFT) since the latter suffers fixed window width and hence a trade-off must always be made between time and frequency resolution. The Continuous wavelet transform of voltage signal $v(t)$ at scale a and time b is represented as:

$$C(a,b) = \frac{1}{\sqrt{a}} \int_{-\infty}^{\infty} v(t)\omega(\frac{t-b}{a}).dt \qquad (3.2)$$

Where ω(t) is the mother wavelet, a is the scale while b is the time shift. In this work, the mother wavelet used in CWT is Morse wavelet. Morse wavelets are useful for analyzing transient signals whose amplitude and frequency varying with time [58]–[60]. Local features are usually extracted using the wavelet analysis that can provide an in-depth view of the time and frequency variations of the analyzed signals and therefore the CWT is best used for islanding detection. The magnitude of the coefficient obtained from the continuous wavelet transform is represented using the scalogram, which can help

visualizing the abrupt changes in any signal. The Scalogram of the CWT is a 2D plot showing the time on the horizonal axis and the scales on the vertical axis. Fig. 3.3 depicts the scalogram of applying the CWT to an islanding voltage signal "Va" and it clearly shows the time-scale features of the signal when the islanding occurs at 0.6 second until the end of 1.5 second duration or to the range of samples from sample no. 2304 to 5770. The time-frequency representation of the scalograms are used as input data to the deep learning layers to extract and learn the features for further classification.

The CWT employs filter banks to extract the frequency contents of the islanding signal by passing it through various filters to obtain time-frequency representation/coefficients. The filter bank used by CWT are normalized so that the peak magnitude for all passbands are equal to 1. Therefore, the CWT coefficients are the output of the original signal (e.g. $v(t)$) passing through the filter bank with impulse response ($\frac{1}{\sqrt{a}}\omega(-t/a)$) at constant scale, a:

$$v(t) \longrightarrow \boxed{\omega\left(-\frac{t}{a}\right)/\sqrt{a}} \longrightarrow CWT\ (a,b)$$

Figure 3. 2: CWT Filter Bank and output coefficients of original signal $v(t)$

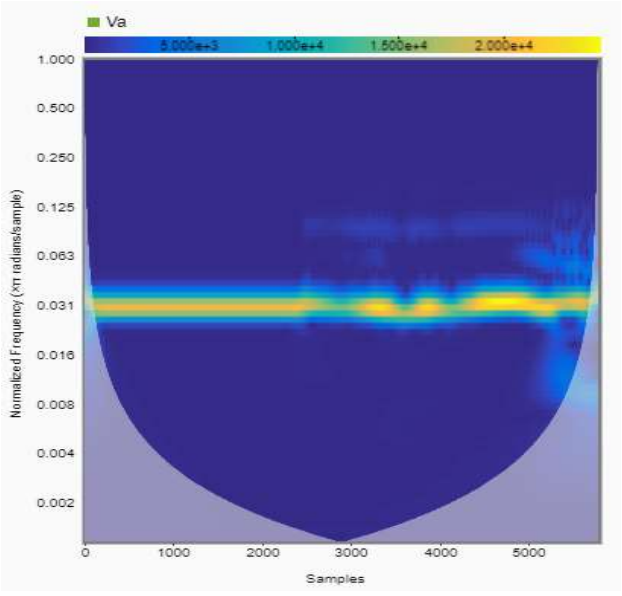

Figure 3. 3: Scalogram showing the time-frequency spectrum of islanding voltage signal "Va"

3.2 Other Non-Wavelet Transforms

In this section, a short overview of Discrete Fourier transforms and Short-term Fourier transform is discussed [57]. Discrete Fourier transform can be mathematically described as:

$$x[f] = \frac{1}{N}\sum_{t=1}^{N-1} v()e^{-\frac{i2\pi ft}{N}} \qquad (3.3)$$

where, $v(t)$ is the original voltage signal (or any islanding signal), $e^{-\frac{i2\pi ft}{N}}$ is the function to perform the Fourier transform, and $x(f)$ is the frequency representation with t is time, f is frequency and N is the total length of the signal. There are some drawbacks of the Fourier transform in signal processing that is the window size is always fixed, since the DFT window is computed assuming that there is no change in the signal outside of this window, this further creates different issues for non-stationary signals. Furthermore, The DFT only provides an amplitude-frequency spectrum of the signal and the time information of the signal is totally lost. The STFT [61] is mathematically expressed as:

$$X[f,\tau] = \sum_{n=-\infty}^{\infty} v[n]g[n-\tau]e^{-i2\pi f} \qquad (3.4)$$

The advantage of using the STFT is that it uses a moving window function $g[n-\tau]$ where τ is the amount in which the shifts occur at one time, v[n] is a time domain representation of original voltage signal (or any islanding signal), x[f] is frequency domain representation of the original targeted signal and g[n] is a window function with a fixed window size of τ. At the same time, this moving window in the time domain might create problems, as the moving window decreases, the frequency resolution increases, but at the expense of the time resolution. In order to address these drawbacks, the wavelet transform was introduced and it was adopted in islanding detection.

3.3 Comparison of Different Transform Analysis Techniques

The main drawback of using the DFT and the STFT is that they have fixed width frequency and hence fixed window with limited resolution, whereas the CWT overcomes the limitation of the DFT and STFT regarding the time-frequency resolution. On the other

hand, the DWT (Discrete wavelet transform) consider a dyadic scale, which may not provide detailed representations of the signal at every frequency and time sample [53], whereas in the continuous wavelet transform, the signal can be represented at every scale and time, which leads to higher detailed representation. The wavelet packet on the top of tree created, during the decomposition, the time resolution of the WPT components is good but at the expense of poor frequency resolution. Moreover, due to its tree sort of structure, it requires more processing time in determining the optimal tree composition [62].

3.4 Deep Learning

Deep learning is an approach used in artificial intelligence applications. Deep learning is a family of advanced machine learning. Traditional machine learning techniques deal only with structured/labeled data and requires human intervention during the models training, whereas deep learning can deal with unstructured data. For instance, in the machine learning the features sets are pre-defined before simulations, whereas in deep learning this step is not required. Those features are themselves automatically extracted and identified by the network during the deep learning process.

A deep learning architecture consists of hidden layers to process the features received from wavelet transform (CWT). The features pass through each of the deep layers, where the output from each previous layer is passed as input to the successor layer and then classifies the events as islanding or non-islanding. Fig. 3.4 depicts the structure of the deep learning algorithm with input features passing through 25 hidden layers and eventually reach the output layer classifying the events as islanding or non-islanding.

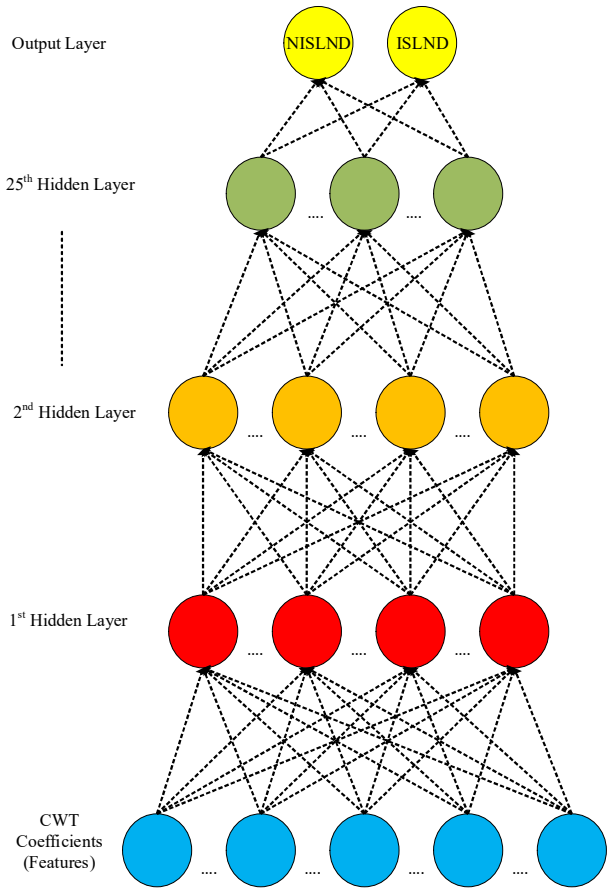

Figure 3. 4: Deep Learning Algorithm

3.2.1 CNN (Convolutional Neural Network)

A Convolutional neural network (CNN) is one of the most popular deep learning structures [63]. To the best knowledge of the authors, this thesis is the first that uses CNN networks for passive islanding detection. In this work, a pretrained CNN models called AlexNet is used for passive islanding detection. The AlexNet is a pretrained CNN networks that has been trained on more than one million of images in 1,000 categories [64]. The features created by CWT are used to transfer the learning to the AlexNet to classify new set of images (Scalograms) and detect the islanding cases [64].

The AlexNet is composed of input layer, 25 hidden layers (defined as convolution layers, subsampling layers of max pooling & ReLU), classification layers (fully connected layers, Softmax layers), and output layers. The Convolution is performed by sliding the features/coefficients produced by the CWT wavelet transform on CNN filters to create

initial features map (output of filters). The processed features produced by the convolution layer is followed by subsampling layer or Pooling layer to further reduce the dimensionality while preserving the important information. The same process is repeated among the deeper layers of convolution and the subsampling layers. The features are further classified by giving the features map to a fully connected layer or dense layer to calculate the scores for each category/class that the high-level features correspond to. Lastly a Softmax layer is implemented over the features to turn the scores into probabilities and predicting the output class labels as islanding or non-islanding [65] as depicted in Fig. 3.5. The deep learning framework is shown in Fig. 3.6.

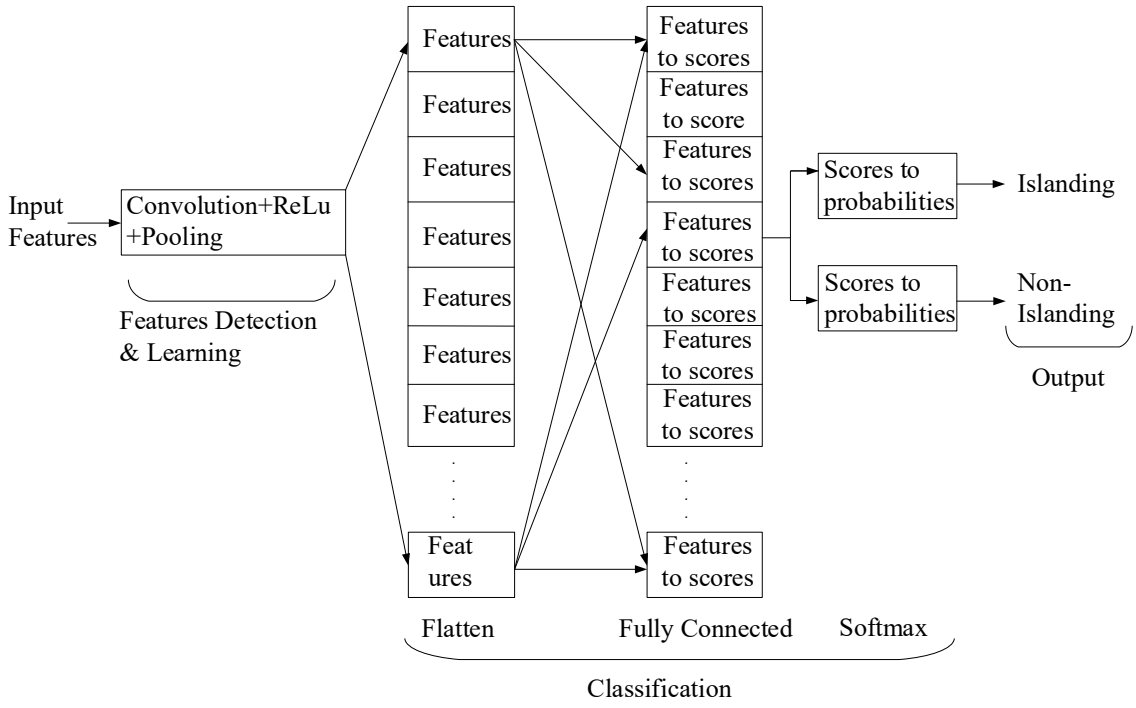

Figure 3. 5: Classification Output [65]

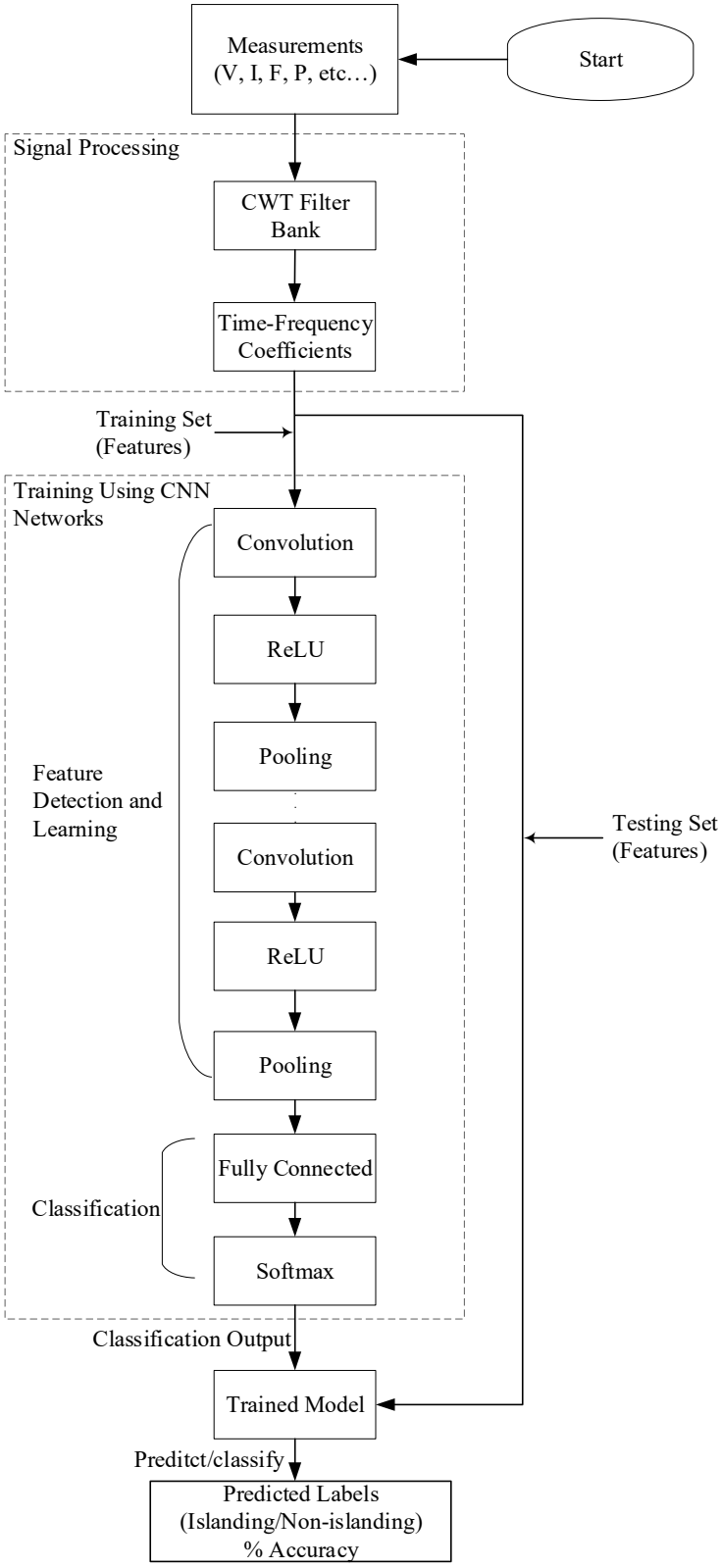

Figure 3. 6: Signal Processing and Deep Learning Work Flow

3.2.2 Recurrent Neural Network (RNN)

The RNN is a sequential data neural network process due to its internal memory to update each neuron in the network with the previous one's states and is usually the extension of the feed-forward network. Backpropagation is used while training the RNN. The output from one state in RNN is taken back as the feedback input to the same state through a loop structure. The RNN holds the information in the network as short memory through the feedback loop. In a given time instant, the information from the previous states are held in the hidden state [66]. The computational graph of the RNN has N sequential x^i is the input and y^i is the output whereas t to τ is time. The following mathematical calculation [66] represents RNN computational model where the number of layers is denoted by l from 1 to N with activation function denoted to l as $h1$.

$$a_1(t) = b_1 + W_1 \times h^{(t-1)}{}_1 + U_1 \times x^{(t)} \qquad (3.5)$$

$$a_1(t) = b_1 + W_1 \times h^{(t-1)}{}_1 + U_1 \times h^{(t)} \qquad (3.6)$$

$$y(t) = b_N + W_N \times h^{(t-1)}{}_N + U_N \times h_N{}^{(t)} \qquad (3.7)$$

Where $x(t)$ is input and $y(t)$ is output.

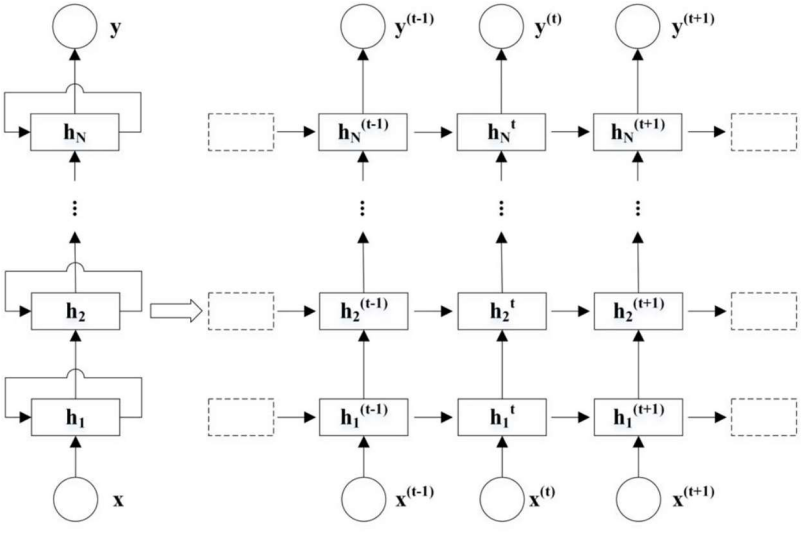

Figure 3. 7: Mathematical process of RNN [66]

The RNN networks are sequential data networks that require built-in memory to save and update the state from previous calculations. The RNN networks fail due to vanishing gradient descent [50].

3.2.3 Long Short-Term Memory (LSTM)

The LSTM is a further modification of the RNN developed to avoid any failure on some vanishing gradient decent. The LSTM is designed in a way that the long-term member is provided. In a Basic LSTM internal self-looping system is used for storing information. The LSTM computational graph consists of five different steps as shown in Fig. 3.8. The basic and important elements of the LSTM is the input gate, the output gate, the forget gate cell and the state output. The following equations shows the mathematical process of LSTM computation [50]:

$$v_i = \sigma(v_t W_{vin} + h_{(t-1)} W_{vim} + b_i) \tag{3.8}$$

$$v_f = \sigma(v_t W_{vfn} + h_{(t-1)} W_{vfm} + b_f) \tag{3.9}$$

$$v_o = \sigma(v_t W_{von} + h_{(t-1)} W_{vom} + b_{io}) \tag{3.10}$$

$$U = \tanh(v_t W_U n + h(t-1) W_{Um} + B_U) \tag{3.11}$$

$$C_t = v_f \times C_{t-1} + v_i \times U \tag{3.12}$$

$$h_t = v_o \times \tan(U) \tag{3.13}$$

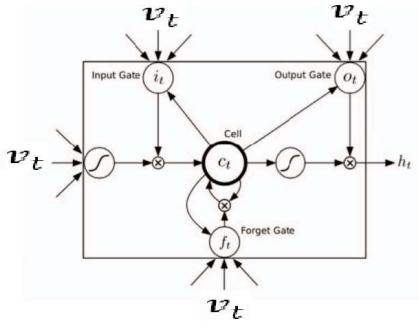

Figure 3. 8: Computational Graph of LSTM [50]

Where, v_i is the input of the input gate, vf is the input of the forget gate, vo is the input of the output gate, U is the update signal, Ct is the state value at the time t and ht is the output of the LSTM cell. However, running the LSTM requires hardware accelerators to overcome the poor performance on the regular processor. Also, the LSTM produces a memory-intensive workload [51].

3.2.4 Comparison of different Deep Learning Techniques

The main drawback of using the RNN is that it requires a built-in memory to save and update the state from previous calculations. In addition, the RNN networks fail due to the vanishing gradient descent [50]. As previously mentioned, the LSTM requires hardware accelerators and produces a memory-intensive workload [51]. On the other hand, CNN overcomes the limitation of the RNN and LSTM and stands out for its ease of training and less requirements in terms of memory and hardware requirements.

3.5 Evaluation Metrics

Since the occurrence of islanding events is rare compared to other non-islanding events (such as faults, load switching), so this creates class imbalance in the input data set. Therefore, islanding detection is classified as an imbalance type problem. Besides, the classification's accuracy "τ", the ratio between the tested data set that is properly classified by the trained model and the total number of tested data as depicted in equation 3.14, is not sufficient to assess the performance of classifiers. Therefore, other metrics such as precision (p), recall (r), and F-measure are used to assess the performance of DL classifiers used for passive islanding detection [39]:

$$\tau = \frac{(TP + TN)}{(TP + FN + TN)} \tag{3.14}$$

$$p = \frac{TP}{TP + FP}, r = \frac{TP}{TP + FN}, F - measure = \frac{2rp}{(r + p)} \tag{3.15}$$

Where (TP) is the number of islanding events that are correctly classified by the model, (TN) is the number of non-islanding events that are correctly classified by the model, false positive *(FP)* is the number of non-islanding cases misclassified by the model, and false negative *(FN)* is the number of islanding cases misclassified as non-islanding events by the model.

3.6 Summary

In this chapter, a comparison of different transform analysis techniques is presented. It was observed that both STFT and DFT suffer due to the fixed window size and hence the trade-off between the time and frequency resolution. The CWT method overcome such limitations by introducing the variable window size and hence the CWT is selected due to its capability of resolving time and frequency resolution better than other techniques. On the other hand, the CNN is selected for this research because of its ease of training that requires few parameters without compromising on the number of hidden layers involved [67]. The mathematical equations for metrics evaluation have been introduced for imbalance type islanding problem. The equations will be used to compute the trained model accuracy when tested on new data that it has never dealt with.

Chapter 4. Results and Evaluation

4.1 Introduction

In this chapter, the performance of the proposed passive islanding detection approach will be evaluated. The study system's characteristics, the measured signals and different cases will be presented in this chapter. Furthermore, the procedures of obtaining the features using the continuous wavelet transform, as well as applying the features learning and event classification using deep learning will be explained.

In this work, 46 cases are considered and are categorized into islanding and non-islanding events. The islanding cases consider different scenarios of the power flow across the PCC between the island (microgrid) containing the DER and the utility grid. The non-islanding cases consider faulty cases and non-faulty cases that present different loading events. The study system is simulated using SIMSCAPE toolbox and the data set generated from different cases are extracted and are used in MATLAB. The proposed deep learning approach is implemented in MATLAB using the Statistics and Machine learning toolbox to learn the features, and to train and test the model for classification. The detection time and the model's accuracy are computed as well.

4.2 Study System

4.2.1 System's Characteristics

Fig. 4.1 depicts the single-line diagram of a utility grid, which has 120 kV transmission line connected to 120 kV-25 kV transformer to feed 25 kV distribution feeders with a length of 19 km. The feeder is connected at the PCC to a microgrid of 100 kW Photovoltaic (PV) array via a circuit breaker. The utility frequency is 60 Hz. The microgrid includes a 100 kW PV array, which is considered as distributed renewable energy resource (D-RER), a 100-kVA, 0.26 kV-25 kV three-phase transformer, and 100 kVA three phase load.

Fig. 4.2 depicts the model of the system in MATLAB-SIMSCAPE. The figure shows the detailed model of the 100 kW Grid-Connected PV Array (D-RER), which consists of 100kW photovoltaic (PV) array, a dc-dc booster, a Voltage Source Converter (VSC) control system, and the Maximum Power Point Tracking (MPPT) controller [68].

The PV array consists of 330 SunPower modules, where 66 strings of 5 series-connected modules are connected in parallel to deliver a maximum power of 100.7 kW (66 strings × 5 modules × 305.2 W/module) and 273.5 Volts (5 modules × 54.7 Volts/module) at a standard test conditions (STC) of 1000 W/m^2 solar irradiance, 25°C PV module temperature. Table 4.1 lists a summary of the PV system characteristics at the STC [69].

The 5kHz dc-dc boost converter is used at the output of the PV array to boost the dc voltage from 272 Volts (PV voltage at maximum power) to 500 Volts. The MPPT is implemented in the boost converter using a MPPT variant subsystem DC-DC MPPT Boost Control that automatically varies and optimizes the switching duty cycle to generate the required voltage to extract the maximum power using the State flow implementations of the incremental conductance algorithms [69].

A 1.98 kHz three-level three-phase VSC controller as shown in Fig. 4.3. The controller is connected to the three-level inverter to convert the 500 Volts DC to 260 Volts AC and maintains a unity power factor. A filter that contains the 25 μH inductor L and the 10 kVAr capacitor bank C is used to filter the harmonics produced by the VSC. A 100 kVA, 0.26 kV-25 kV transformer is used to step the voltage to 25 kV and connect to 25 kV distribution system.

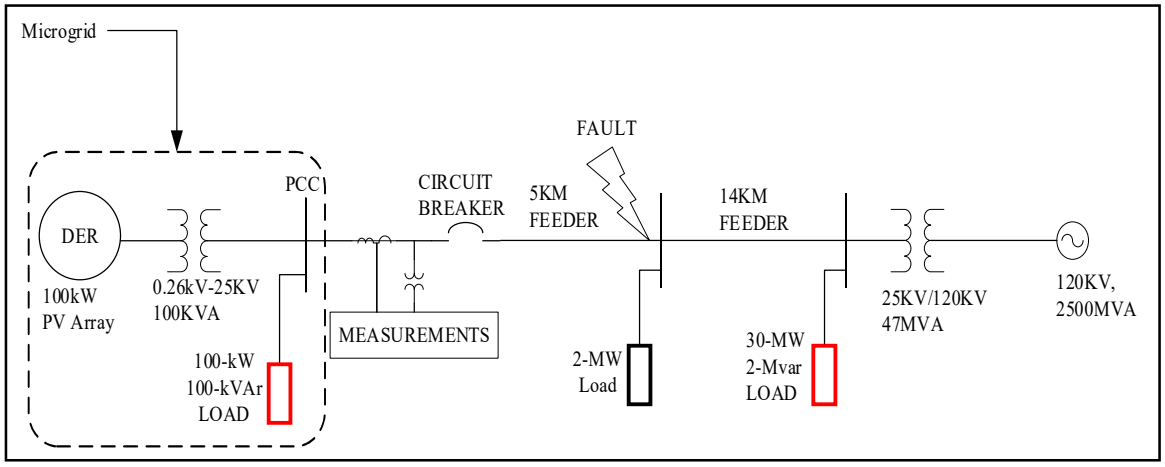

Figure 4. 1: Single Line Diagram of Grid-Connected Photovoltaic System

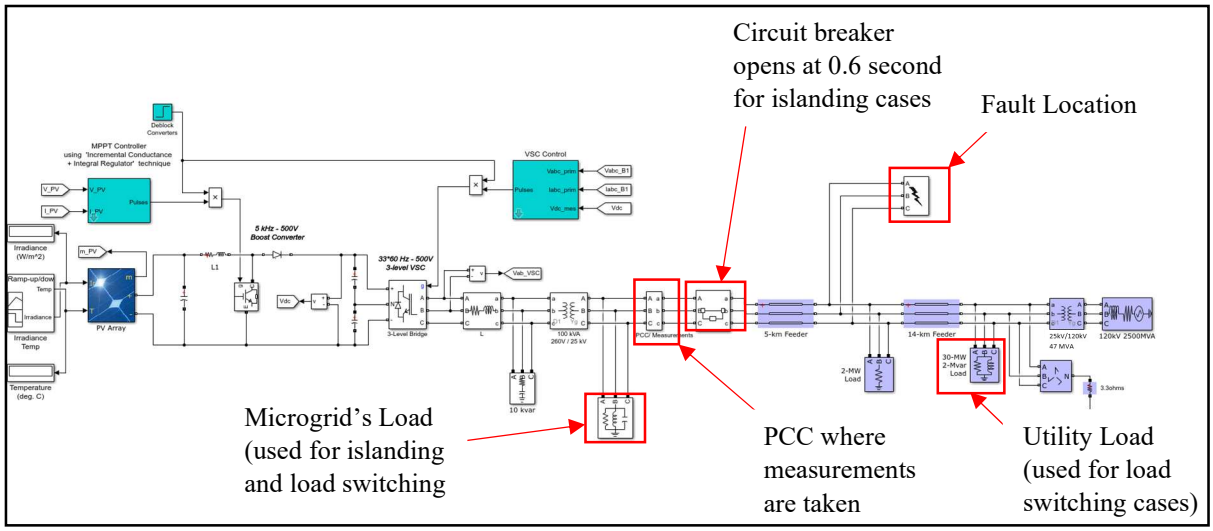

Figure 4. 2: Simulink Model of Grid-Connected Photovoltaic System

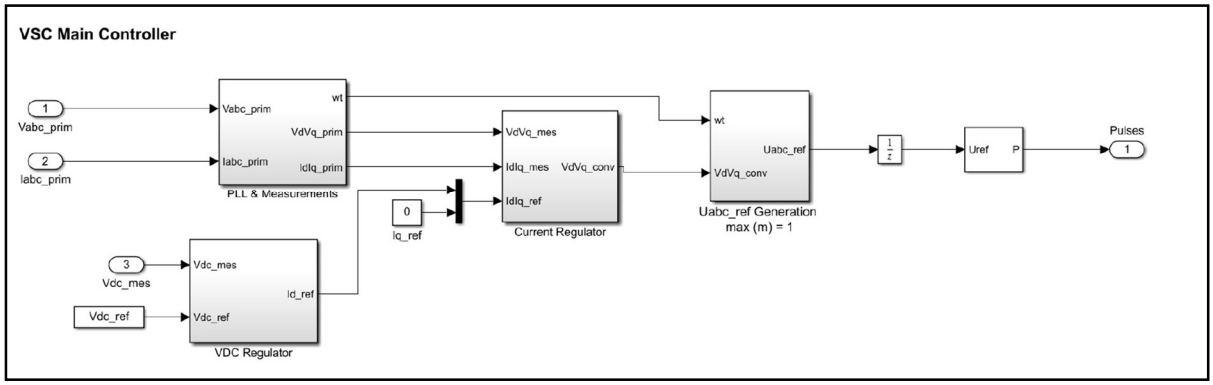

Figure 4. 3: Simulink Model of VSC Main Controller

Table 4.1: PV Module Specifications

330 SunPower modules (SPR-305E-WHT-D)	
Module's specifications	Value
Number of cells in series per module	96
Open circuit voltage, Voc	64.2 Volts
Short circuit current, Isc	5.96 A
Voltage at maximum power point, Vmp	54.7 Volts
Current at maximum power point, Imp	5.58 A
Maximum power, Pmp	305.2 W

4.2.2 Signals & Measurements

The node for measuring the basic system's parameters were added to the model to obtain various measurements [38] at the PCC (utility grid side). A simulation for a duration of 1.5 second is performed to consider the transient states of all the signals considering many possible cases of islanding and non-islanding cases, which will be discussed in the next section. The signals are sampled at a sampling rate of 64 samples per cycle, which represents the sampling rate used in most digital protective relays [70]. The corresponding sampling frequency is 3.84 kHz (64 samples/cycle×60 cycles=3.84 kHz) [70]. Table 4.2 shows 31 signals and indices used for the passive islanding detection.

Table 4.2: Signals & Measurements

Measurements @ PCC	
Signal	Symbol
Phase A Voltage	Va
Phase B Voltage	Vb
Phase C Voltage	Vc
A-B (line to line) Voltage	Vab
B-C (line to line) Voltage	Vbc
C-A (line to line) Voltage	Vca
Phase A Current	Ia
Phase B Current	Ib
Phase C Current	Ic
Zero Sequence Voltage	$V0$
Negative Sequence Voltage	$V1$
Positive Sequence Voltage	$V2$
Zero Sequence Current	$I0$
Negative Sequence Current	$I1$
Positive Sequence Current	$I2$

Phase A Impedance	*Za*
Phase B Impedance	*Zb*
Phase C Impedance	*Zc*
Phase A Apparent Power	*Sa*
Phase B Apparent Power	*Sb*
Phase C Apparent Power	*Sc*
Direct Component of Voltage, axis-d	*Vd*
Quadrature Component of Voltage, axis-q	*Vq*
DC Voltage	*Vdc*
Frequency	*F*
Power	*P*
Rate of Change of Frequency	*ROCOF*
Rate of Change of Power	*ROCOP*
Rate of Change of Voltage (a, b, c phases)	*ROCOVabc*

The simulation models of the voltage and the current signals are depicted in Fig. 4.4 to Fig. 4.7. These models/blocks were built to measure the phase voltages, line-line voltages, and phase currents at the PCC.

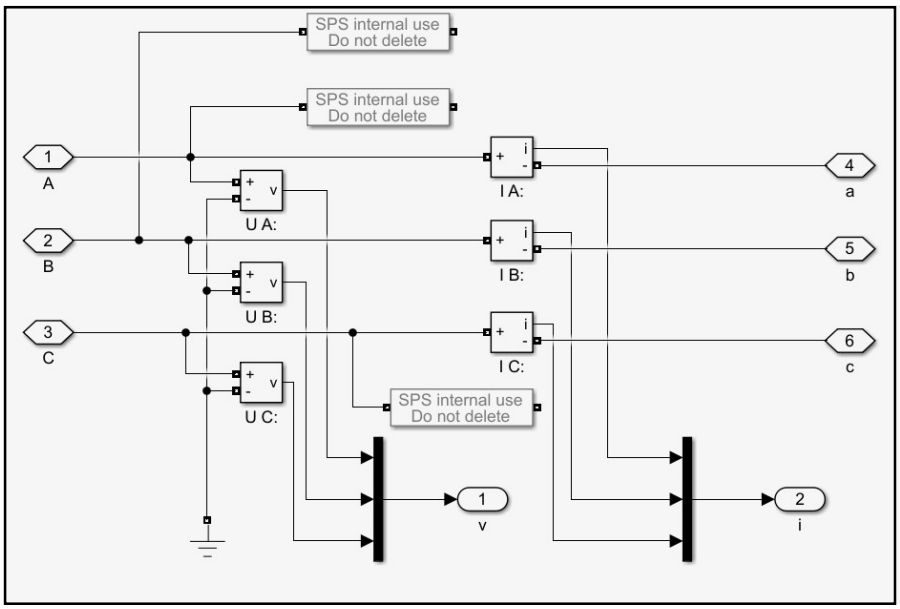

Figure 4.*4*: Simulink Model of $Vabc$ and $Iabc$ at PCC

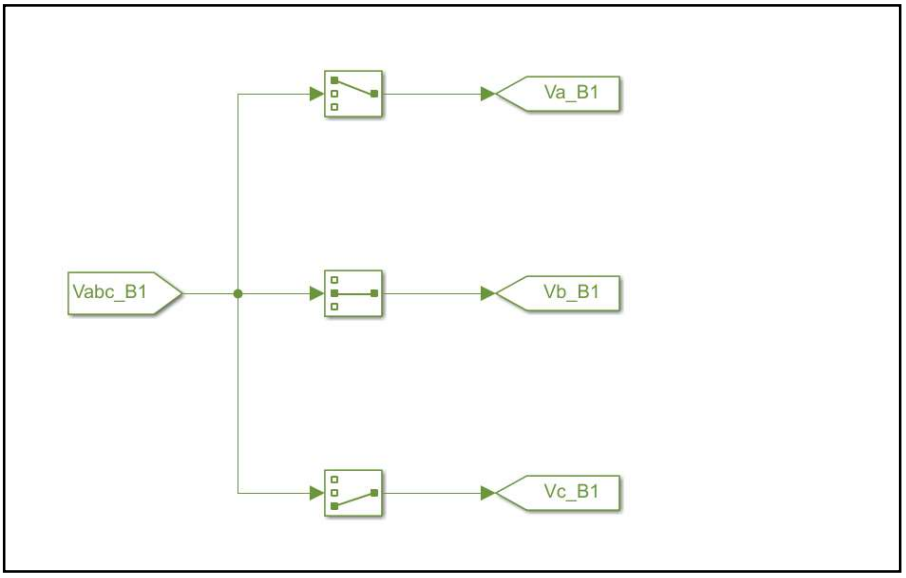

Figure 4.5: Simulink Model of Va, Vb, and Vc signals at PCC

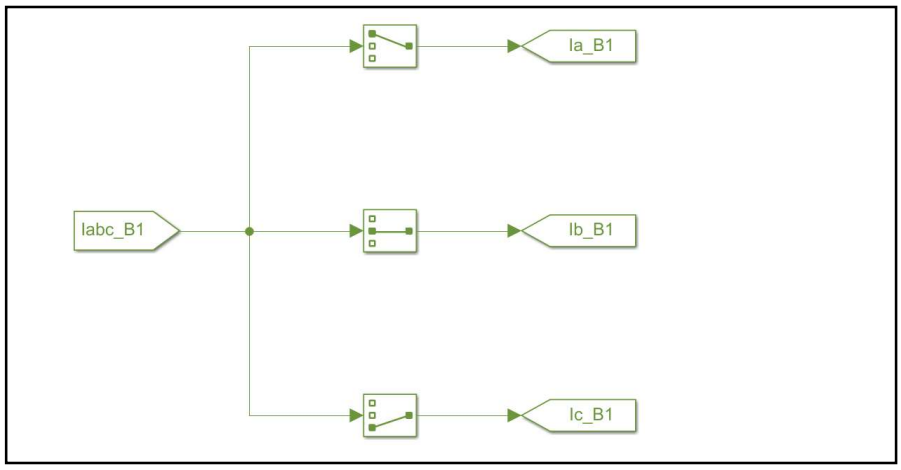

Figure 4.6: Simulink Model of $Ia, Ib,$ and Ic signals at PCC

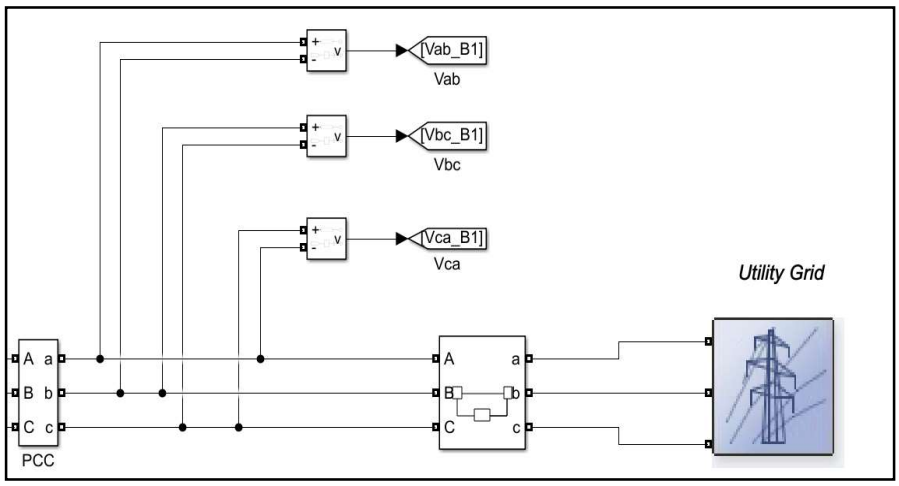

Figure 4.7: Simulink Model of $Vab, Vbc,$ and Vca signals at PCC

The sequence analyzers have been used to extract the zero, negative, and positive sequences of the voltage and the current signals. The models/blocks were built to compute the indices at the PCC as depicted in Fig. 4.8 and Fig. 4.9.

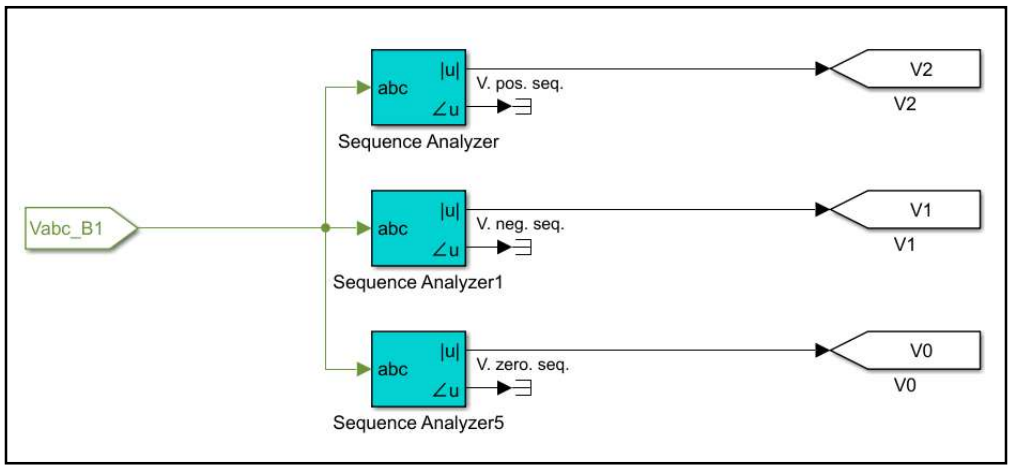

Figure 4. 8: Simulink Model of $V0, V1$, and $V2$ at PCC

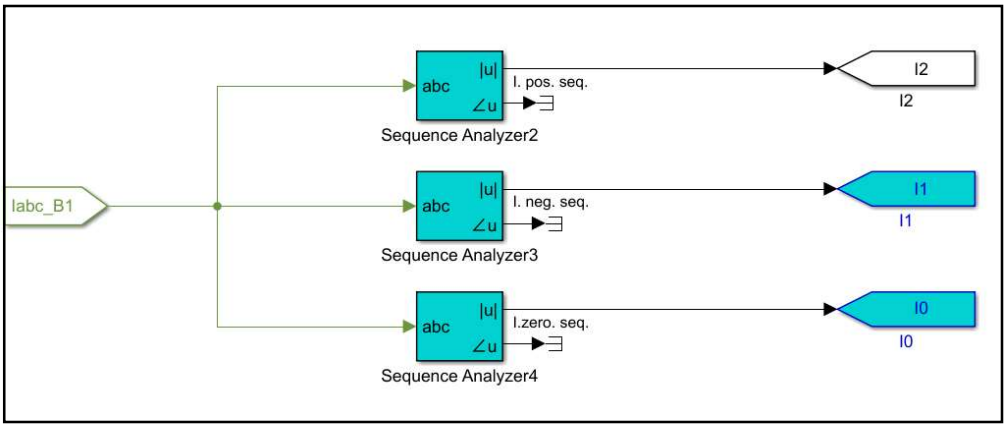

Figure 4. 9: Simulink Model of $I0, I1$, and $I2$ at PCC

The "Array-Vector divide" blocks used the voltage and the current signals to compute all phases' impedances. The models/blocks used to compute the signals at PCC are depicted in Fig. 4.10.

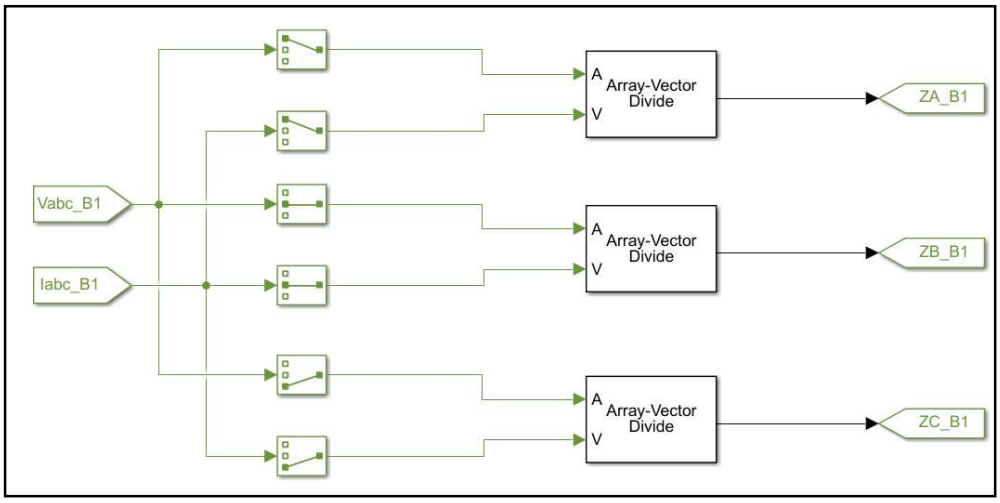

Figure 4. 1*0*: Simulink Model of Za, Zb and Zc at PCC

The "Array-Vector multiply" blocks used the voltage and the current signals to compute all phases' apparent power. The models/blocks used to compute the indices at PCC are depicted in Fig. 4.11.

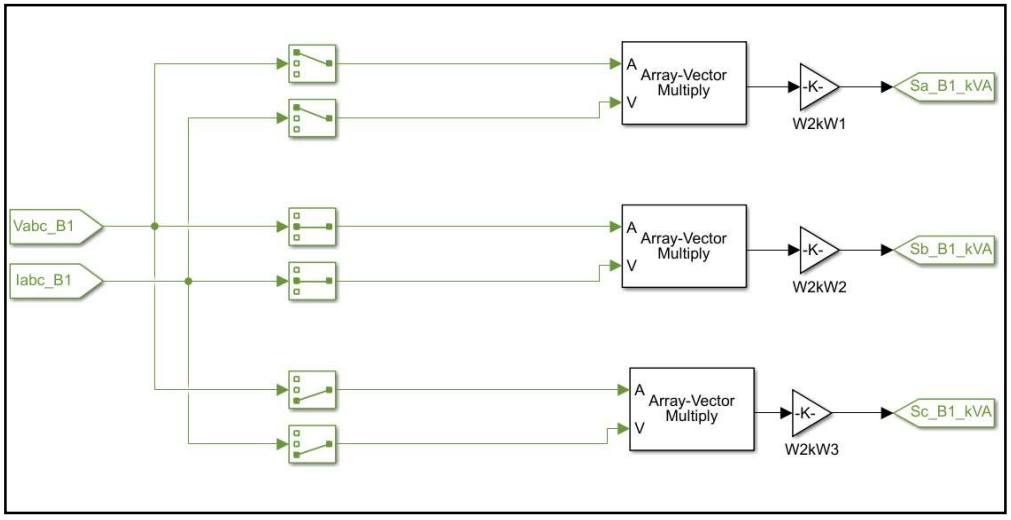

Figure 4.11: Simulink Model of Sa, Sb and Sc at PCC

The "Phase Lock Loop" and the "abc to $dq0$" blocks were used to convert the $Vabc$ (stationary frame) to the dq frame in which the orthogonal components are obtained. The implementation of the direct component of the voltage, the direct d-axis, and the quadrature q-axis components of the voltage at the PCC is depicted in Fig. 4.12.

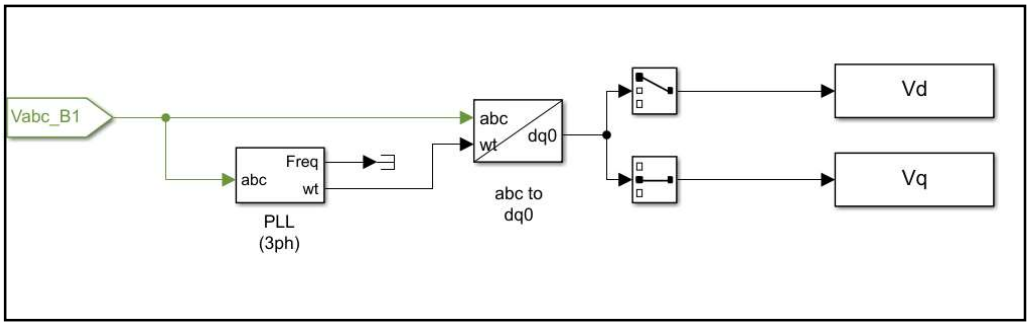

Figure 4.12: Simulink Model of Vd and Vq at PCC

The DC voltage output of the boost converter is measured and is taken as the input data. Fig. 4.13 depicts the measurement of DC voltage at the output of boost inverter.

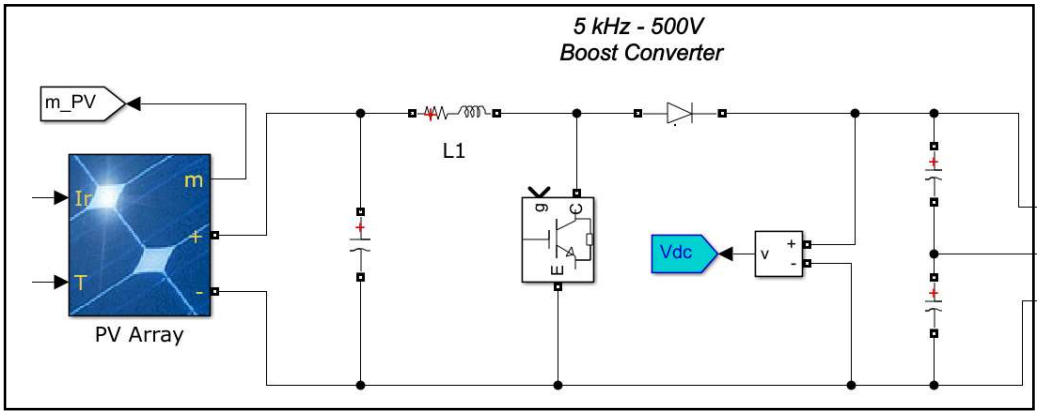

Figure 4. 13: Simulink Model of Vdc at Boost Converter Output

The "Phase Lock Loop" block is used to extract the frequency from the phasor's voltage Vabc. Fig. 4.14 depicts the implementation of the PLL to compute the frequency at the PCC.

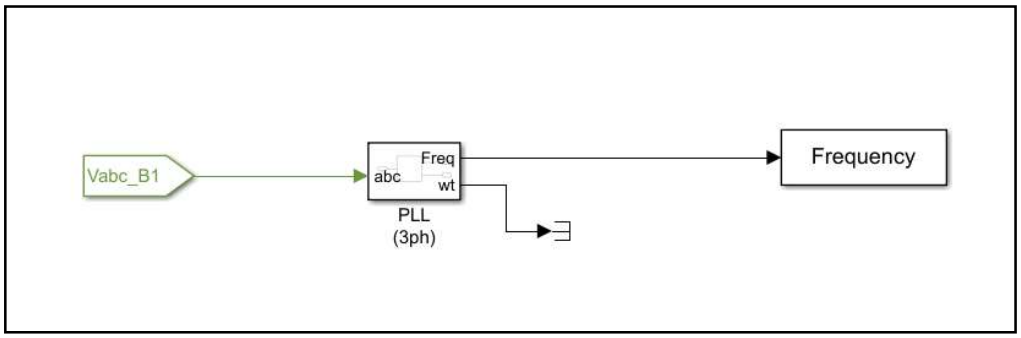

Figure 4. 14: Simulink Model of Frequency at PCC

Fig. 4.15 depicts the measurement of the real power at the PCC. The voltage "$Vabc$" and the current "$Iabc$" are used to compute the real power at the PCC.

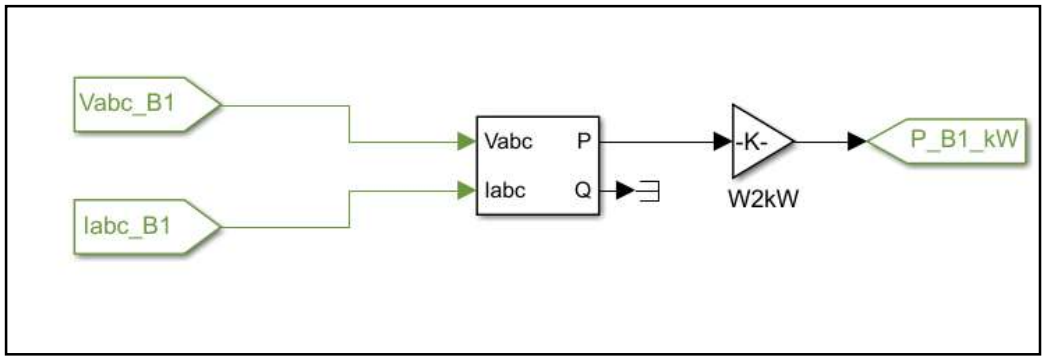

Figure 4.15: Simulink Model of Real Power measurement at PCC

Fig. 4.16 to Fig. 4.18 depict the rate of change of frequency "$ROCOF$" [69], the rate of change of power "$ROCOP$", and the rate of change of voltage "$ROCOVabc$" at PCC.

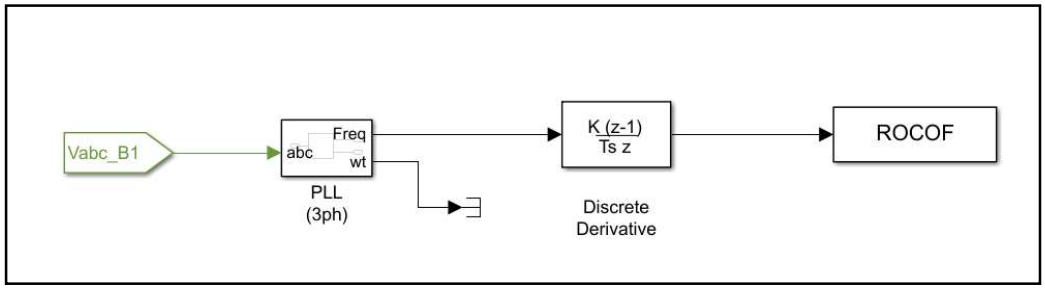

Figure 4. 16: Simulink Model of $ROCOF$ at PCC

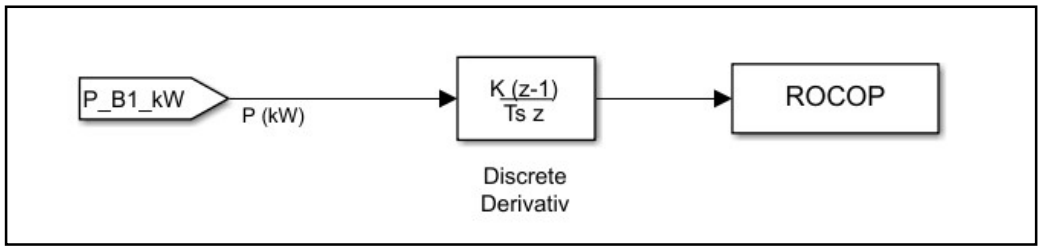

Figure 4.17: Simulink Model of $ROCOP$ at PCC

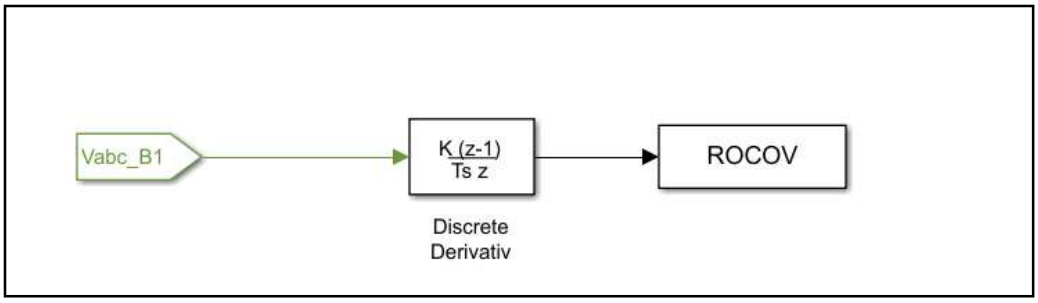

Figure 4.18: Simulink Model of $ROCOV$ at PCC

4.2.3 Islanding and Non-Islanding Cases

A total of 46 cases were simulated including 17 islanding and 29 non-islanding cases using the system shown in Fig. 4.2. The following represents a detailed description of the cases and the results.

4.2.3.1 Islanding Cases

The active and reactive power flowing through the PCC can be categorized into three main scenarios: positive power mismatch, negative power mismatch, and zero power mismatch. The positive active and reactive power means the generated power from the D-RER is greater than the local load's power consumption. On the other side, the negative active and reactive power means that the generated power is less than the local load's power. Lastly, zero power mismatch implies that the generated power by the D-RER is equal to the consumed power by the load within the microgrid and there is no power crossing through the PCC.

The circuit breaker shown in Fig. 4.19 is used to form the islanding cases by tripping at 0.6 second. The microgrid's load, shown in fig. 4.19, is used to generate 17 positive and negative active and reactive power cases to simulate various possible loading conditions that may exist during islanding. As shown in table 4.3, the active power of this load is changed to simulate various loading conditions during islanding (while reactive power is kept at 100%) as follows: 50%, 70%, 90%, 95%, to simulate negative active power scenario, then it is set to 100% to simulate zero power mismatch [3]. The load is increased in steps to simulate the positive active power mismatch, as follows: 105%, 110%, 130% and 150%. In order to simulate the reactive power, the load reactive power is changed (while the active power is kept at 100%) as follows: 96%, 97%, 98% and 99% for the negative reactive power mismatch, while 101%, 102%, 103% and 104% is set for the

positive reactive power mismatch [3]. All loading conditions were at unity power factor and load quality factor of 1 as per IEEE 1547.1 [71].

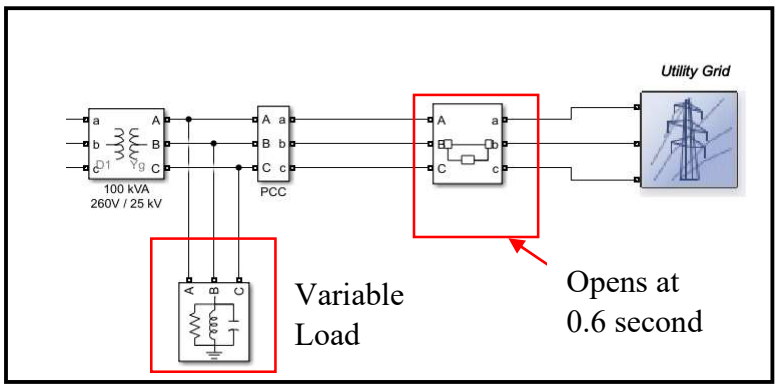

Figure 4. *19*: Islanding Formation at PCC

Table 4.3: Islanding Cases

Islanding Cases		
Case No.	Condition	Classification
01	Active Power Mismatch, P_L = 50 kW (50%)	Islanding Circuit Breaker opens at PCC (@ 0.6 second)
02	Active Power Mismatch, P_L = 70 kW (70%)	
03	Active Power Mismatch, P_L = 90 kW (90%)	
04	Active Power Mismatch, P_L = 95 kW (95%)	
05	**Zero Power Mismatch, P_L = 100 kW (100%)**	
06	Active Power Mismatch, P_L = 105 kW (105%)	
07	Active Power Mismatch, P_L = 110 kW (110%)	
08	Active Power Mismatch, P_L = 130 kW (130%)	
09	Active Power Mismatch, P_L = 150 kW (150%)	
10	Reactive Power Mismatch, Q_L = 96 kVAr (96%)	
11	Reactive Power Mismatch, Q_L = 97 kVAr (97%)	
12	Reactive Power Mismatch, Q_L = 98 kVAr (98%)	
13	Reactive Power Mismatch, Q_L = 99 kVAr (99%)	
14	Reactive Power Mismatch, Q_L = 101 kVAr (101%)	
15	Reactive Power Mismatch, Q_L = 102 kVAr (102%)	

16	Reactive Power Mismatch, Q_L = 103 kVAr (103%)	
17	Reactive Power Mismatch, Q_L = 104 kVAr (104%)	

The signals/indices measured/computed at the PCC, when the breaker opens, are all taken under various power flow cases as input data for the algorithm used for the features learning and the cases classification. Figs. 4.20 to 4.48 present the islanding signals at zero power mismatch case as described in case no. 05 of table 4.3. All shown signals are generated when the islanding occurs at 0.6 second (breaker tripping) and continues until the end of the simulation time (1.5 second) to present the changes in the signals upon islanding occurrence without tripping the D-RER.

Upon applying the proposed method, the D-RER will be isolated following a detection time that will be presented at the end of this chapter. Therefore, the D-RER will not contribute to generate power. The signals will be presented at the end of the chapter to show the changes in the signals when the D-RER trips upon the islanding occurrence.

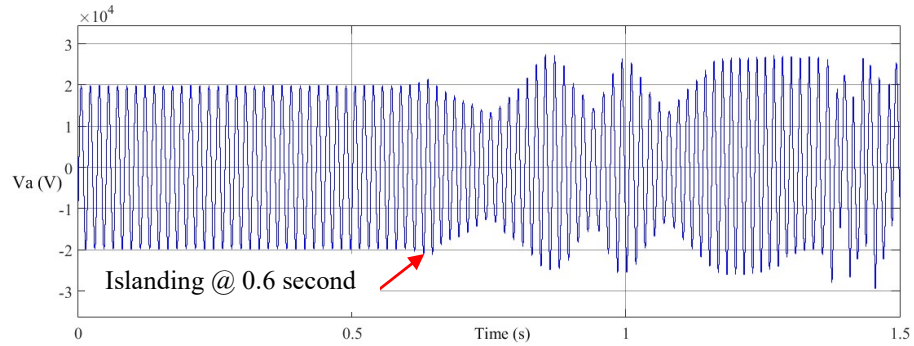

Figure 4.20: Phase A Voltage "Va" at PCC

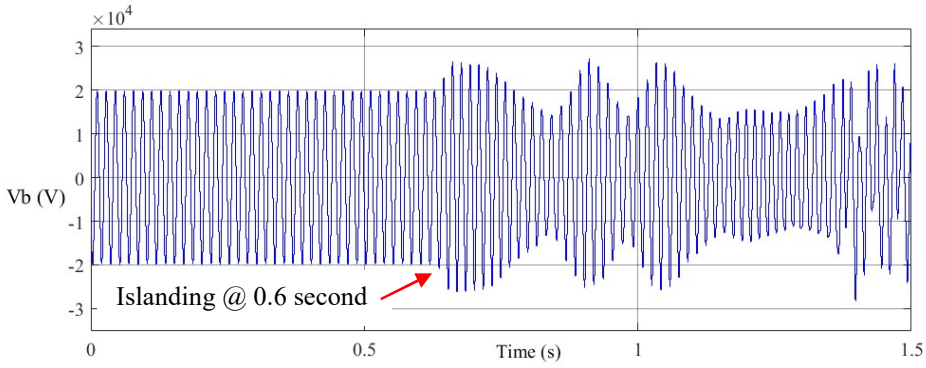

Figure 4.21: Phase B Voltage "Vb" at PCC

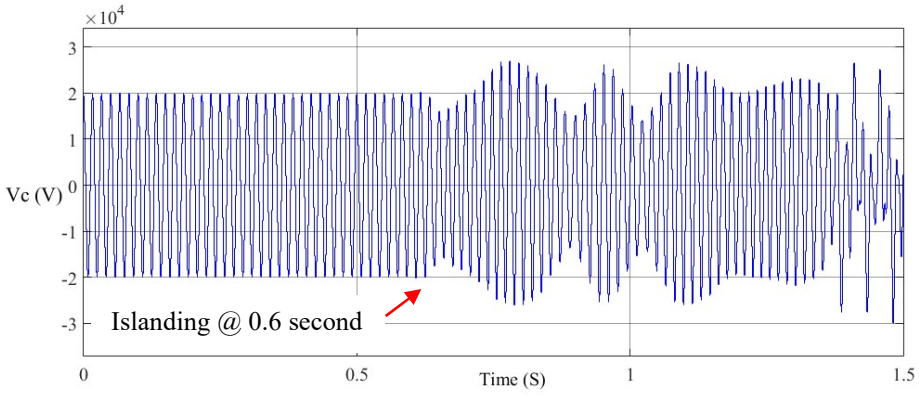

Figure 4.*22*: Phase C Voltage "Vc" at PCC

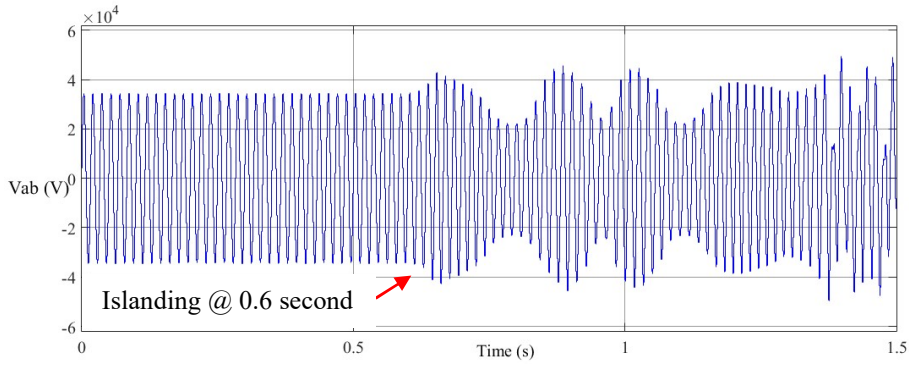

Figure 4.23: Line-Line Voltage "Vab" at PCC

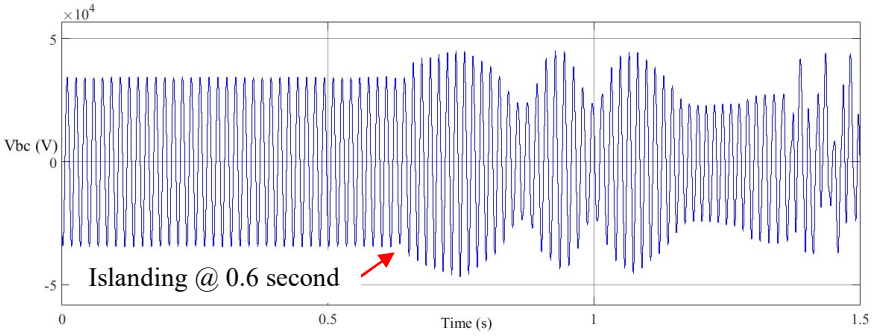

Figure 4. 24: Line-Line Voltage *"*Vbc*"* at PCC

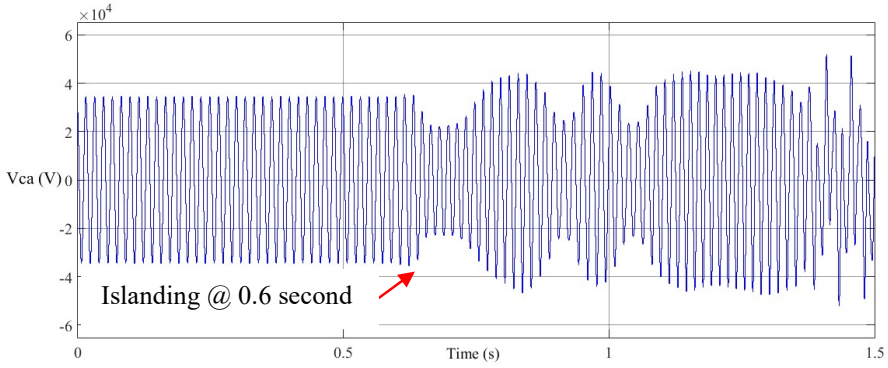

Figure 4.25: Line-Line Voltage "Vca" at PCC

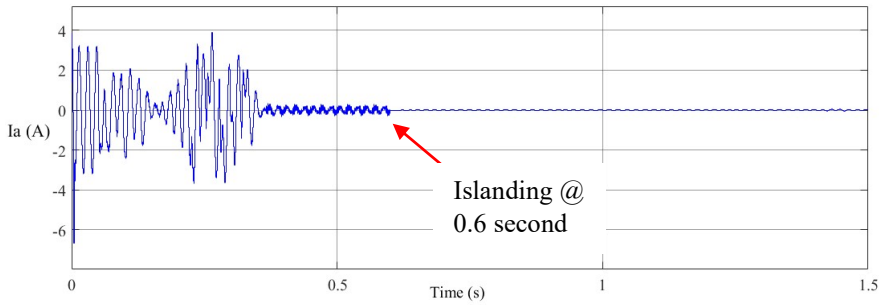

Figure 4. *26*: Phase A Current "Ia" at PCC

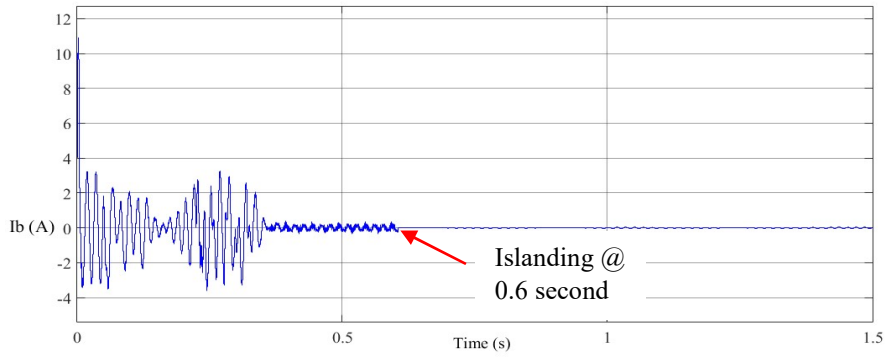

Figure 4.27: Phase A Current "Ib" at PCC

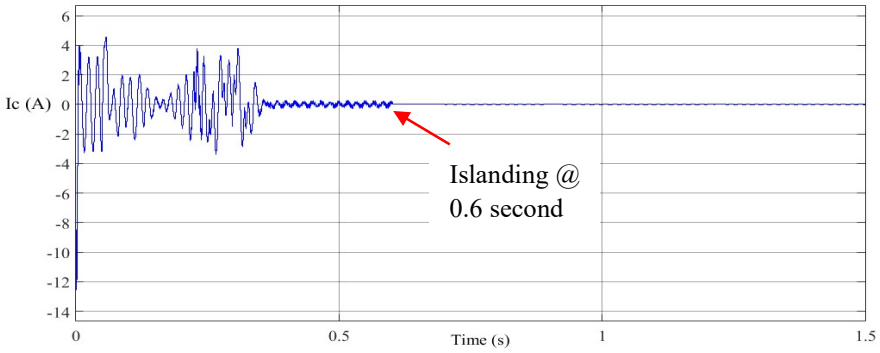

Figure 4.28: Phase A Current "Ic" at PCC

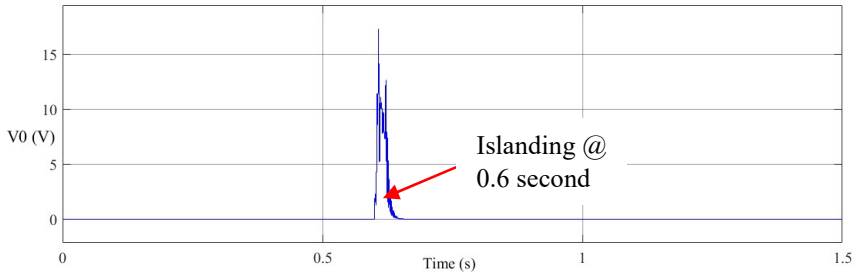

Figure 4.29: Zero Sequence Voltage "$V0$" at PCC

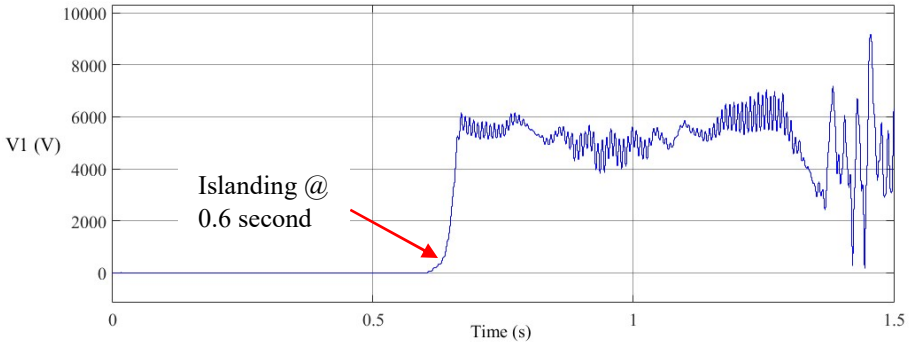

Figure 4.30: Negative Sequence Voltage "$V1$" at PCC

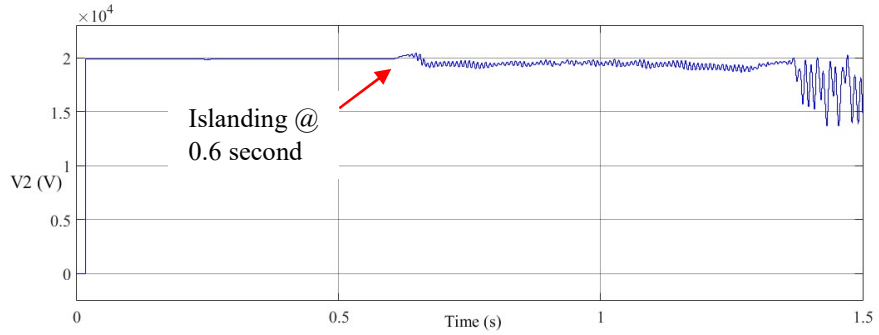

Figure 4. 4: Positive Sequence Voltage "*V*2" at PCC

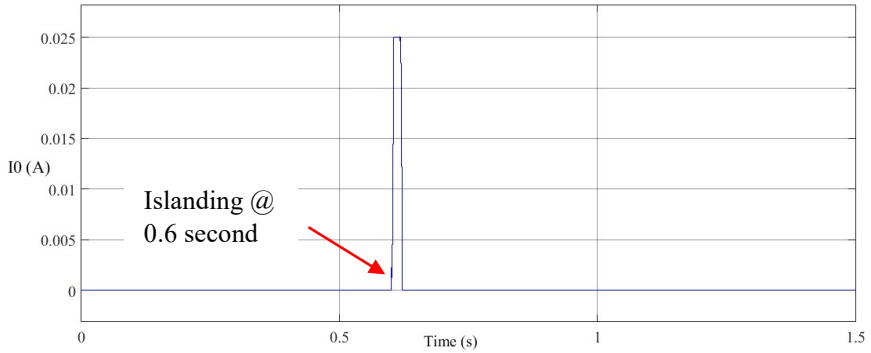

Figure 4.32: Zero Sequence Current "*I*0" at PCC

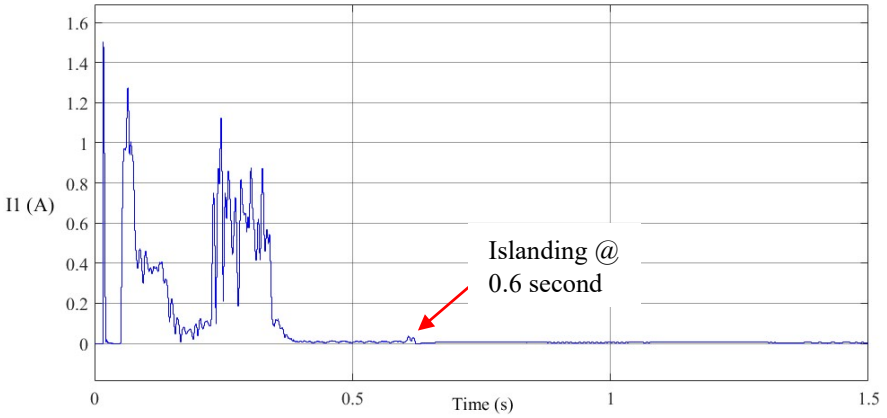

Figure 4.33: Negative Sequence Current "*I*1" at PCC

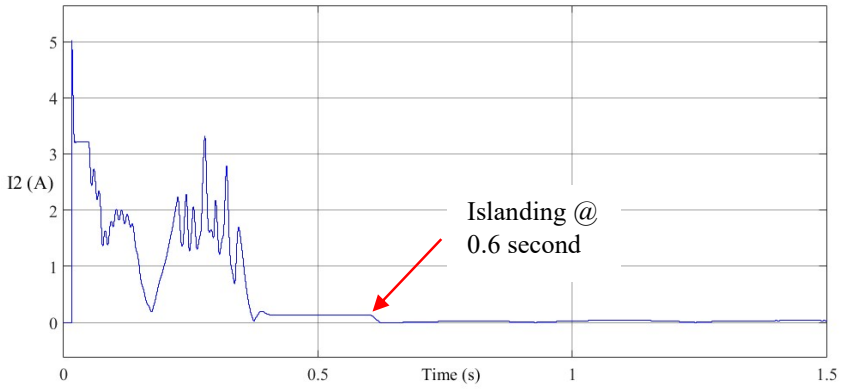

Figure 4.5: Positive Sequence Current "$I2$" at PCC

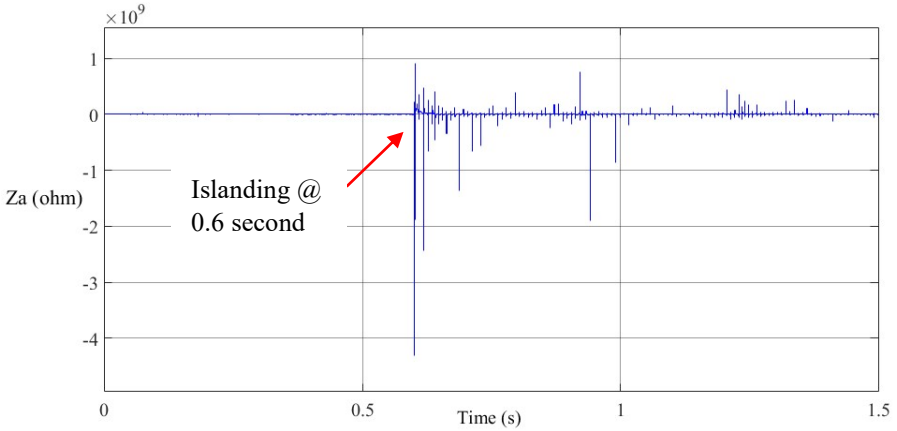

Figure 4.35: Phase A Impedance "Za" at PCC

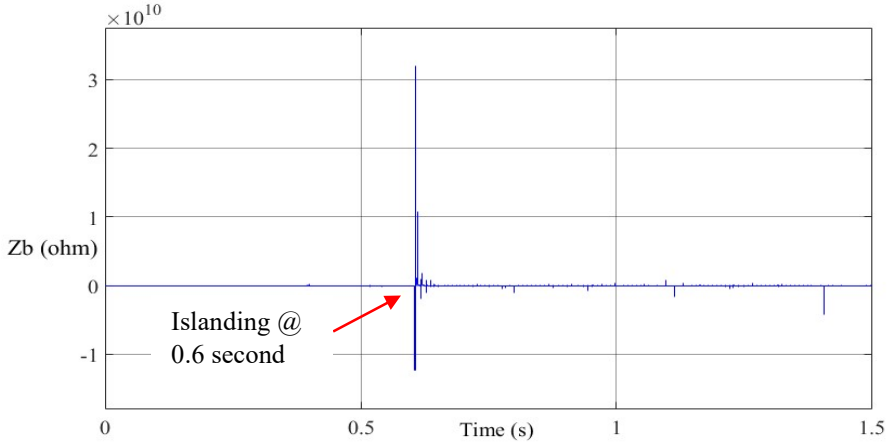

Figure 4.36: Phase B Impedance "Zb" at PCC

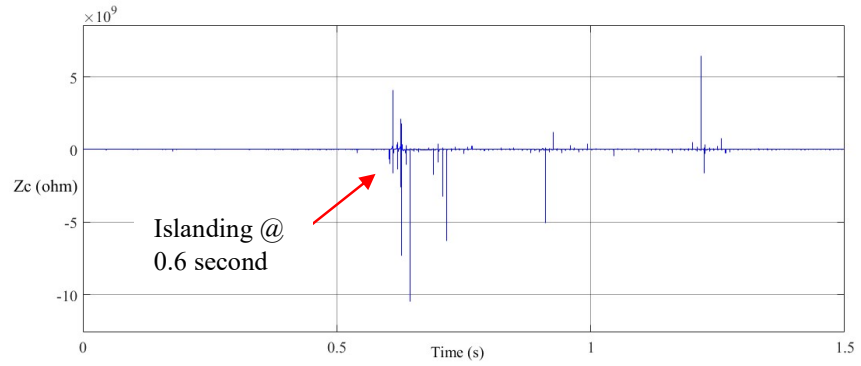

Figure 4.37 Phase C Impedance "Zc" at PCC

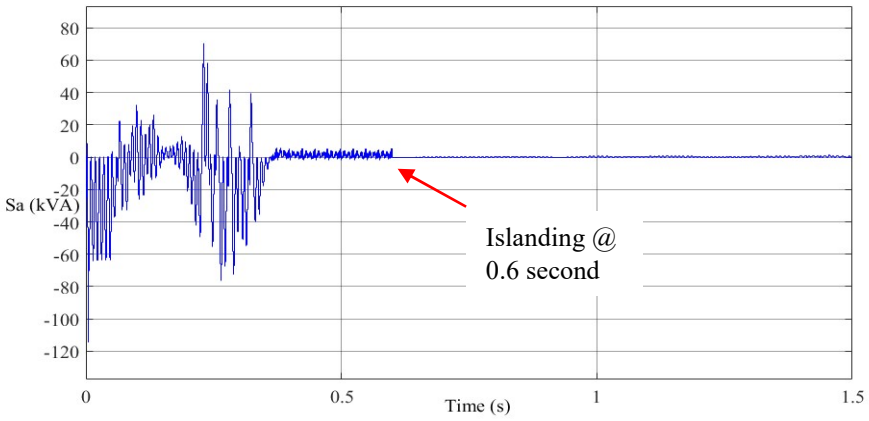

Figure 4.38: Phase A Apparent Power "Sa" at PCC

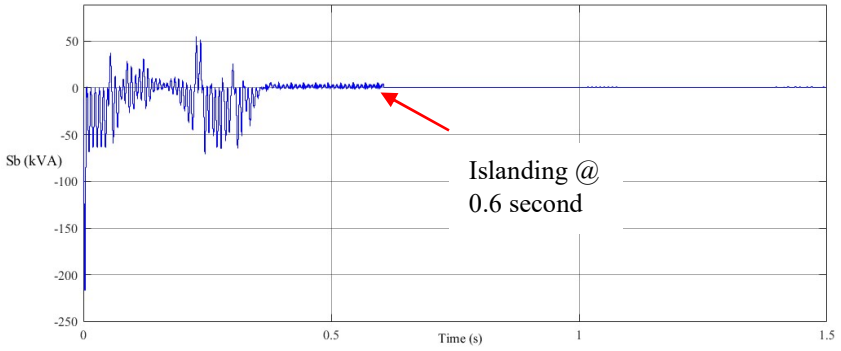

Figure 4.39: Phase B Apparent Power "Sb" at PCC

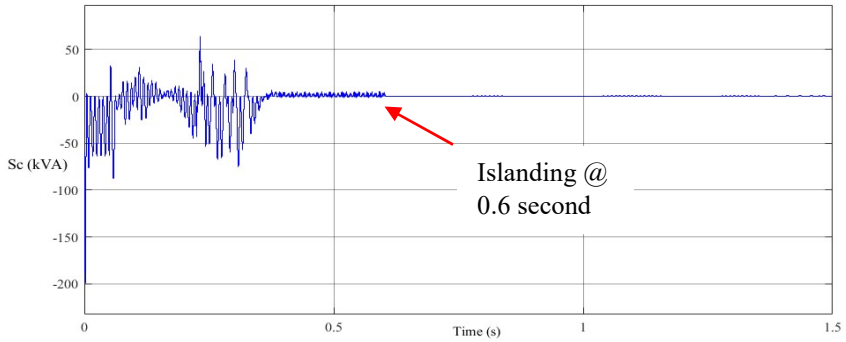

Figure 4.40: Phase C Apparent Power "Sc" at PCC

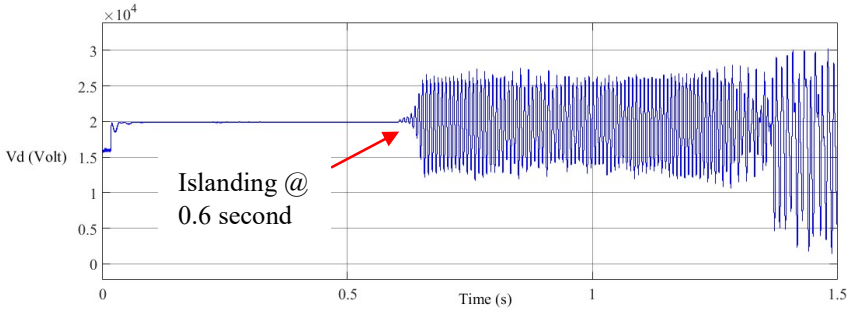

Figure 4.41: Axis-D Voltage "Vd" at PCC

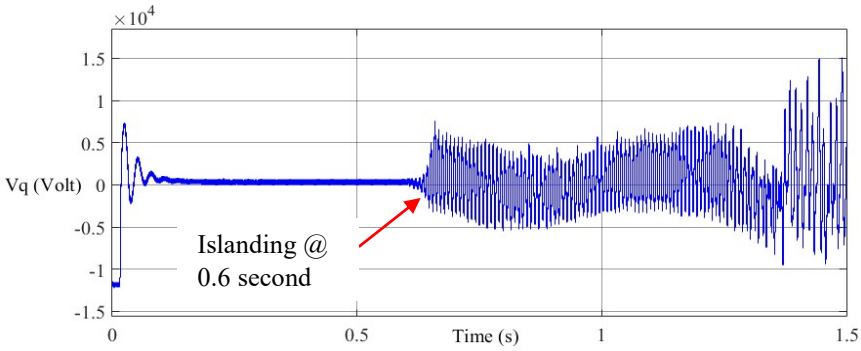

Figure 4. 42: Axis-Q Voltage "Vq" at PCC

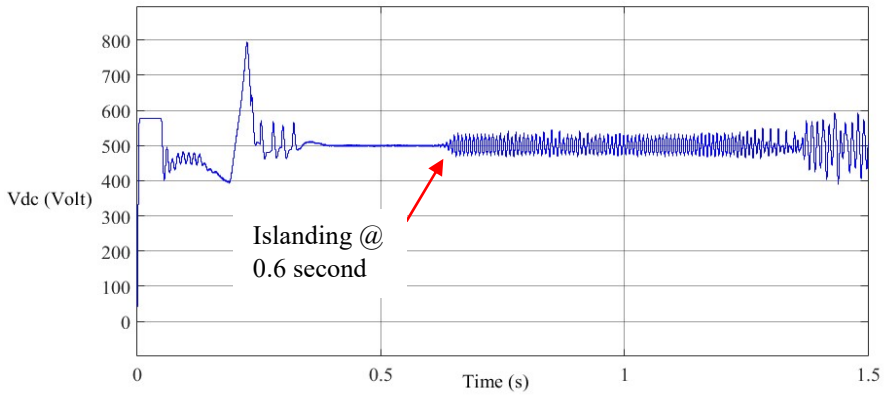

Figure 4.43: DC Voltage "Vdc" at PCC

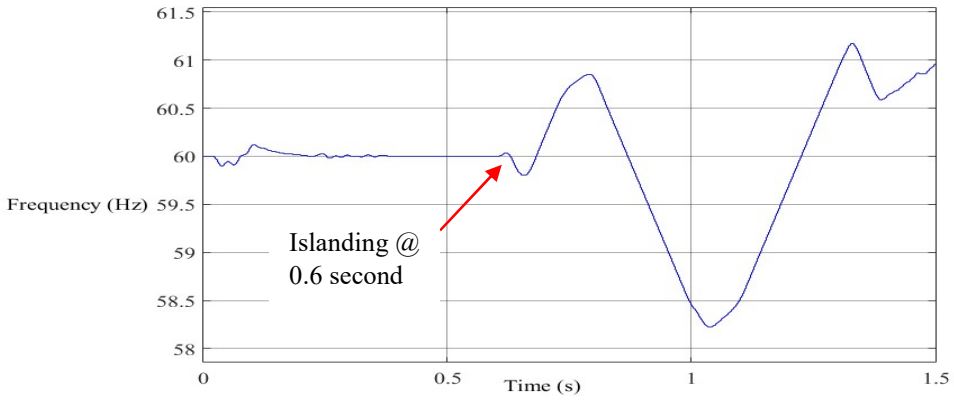

Figure 4.44: Frequency (Hz) at PCC

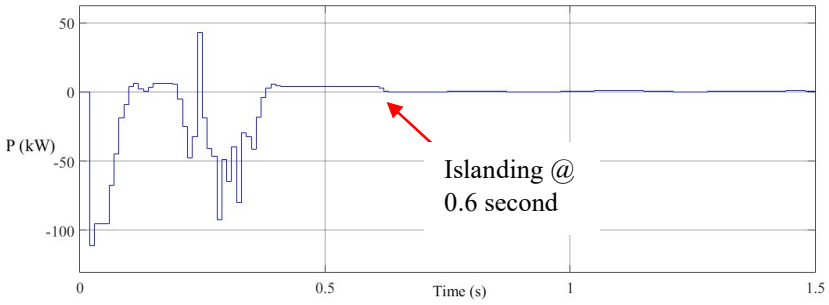

Figure 4.45: Power (kW) at PCC

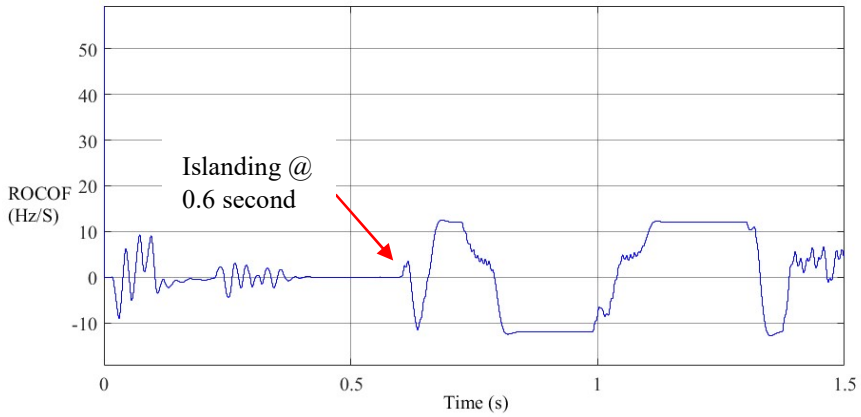

Figure 4.46: Rate of Change of Frequency ($ROCOF$) at PCC

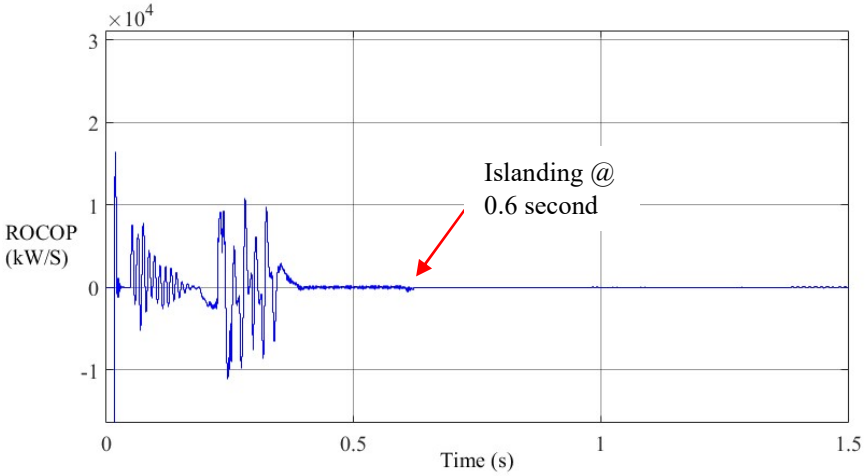

Figure 4.47: Rate of Change of Power ($ROCOP$) at PCC

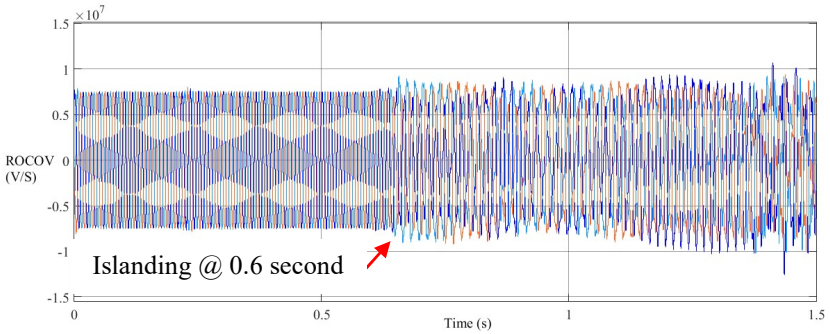

Figure 4.48: Rate of Change of 3 Phase Voltages ($ROCOVabc$) at PCC

Using the CWT transform, the signals shown in Fig. 4.20 to Fig. 4.48 can be seen in the time-frequency representation (Scalogram) that reflects the change in signals' frequencies due to any changes happening in the grid (islanding in this case). These time-frequency representations can later be used as input data for the deep learning techniques. Fig. 4.49 to 4.59 show all scalograms generated when the breaker opens for zero power mismatch case (case no. 05 of table 4.3).

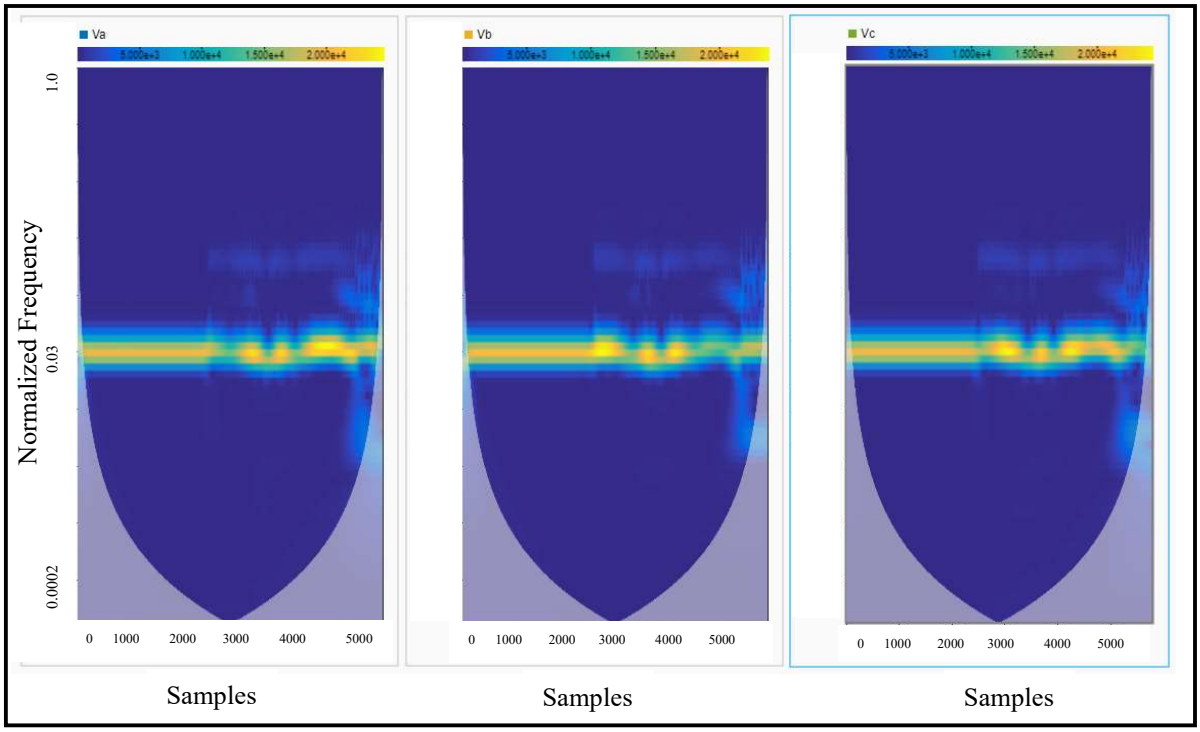

Figure 4. 49: Time-Frequency/Scalogram for Va, Vb, Vc

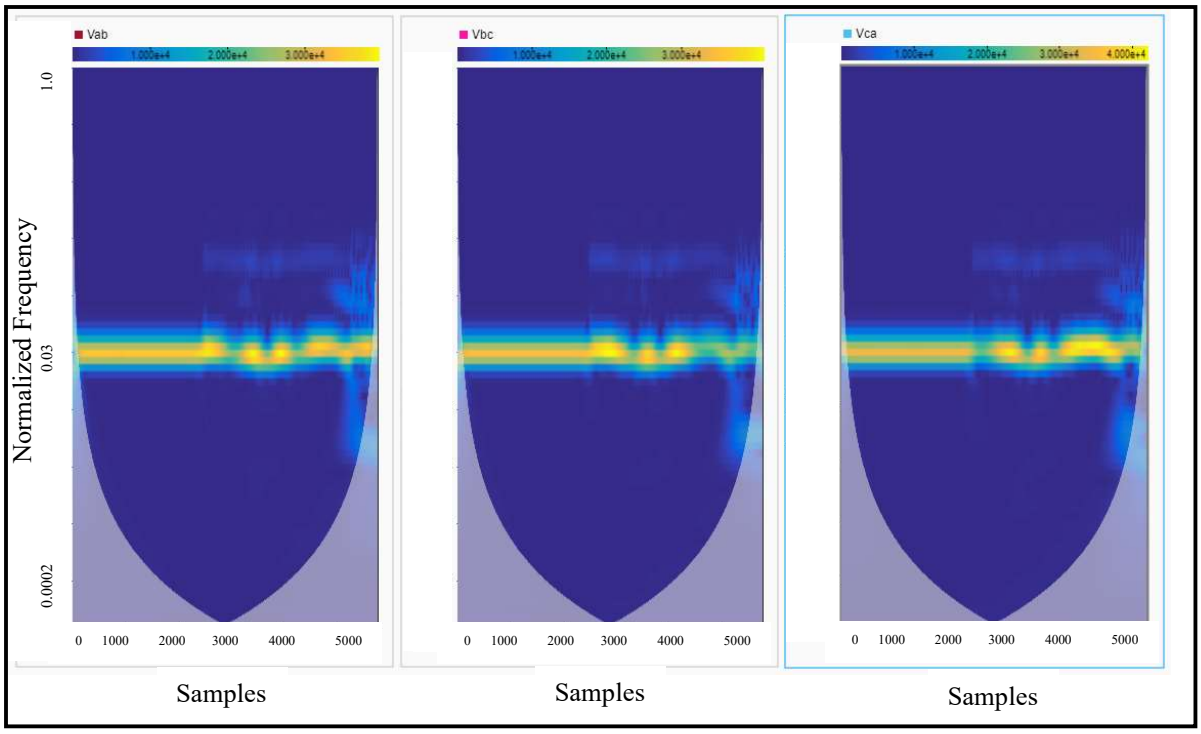

Figure 4.50: Time-Frequency/Scalogram for Vab, Vbc, Vca

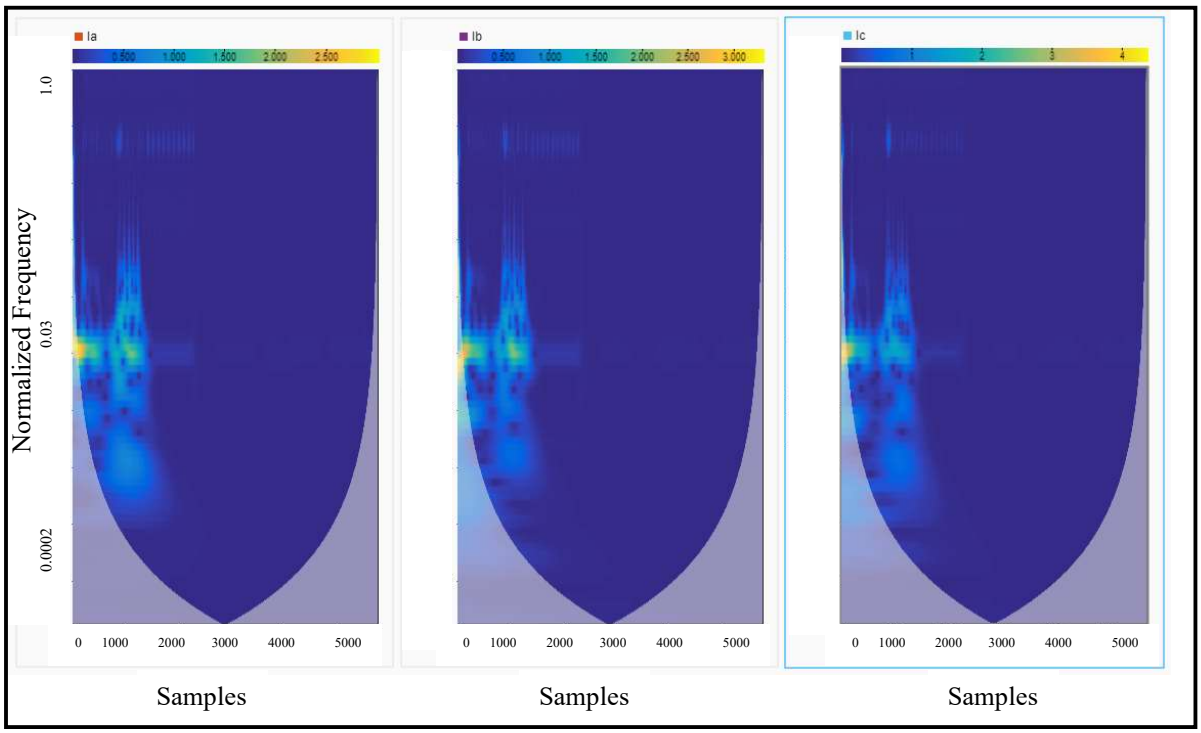

Figure 4.51: Time-Frequency/Scalogram for Ia, Ib, Ic

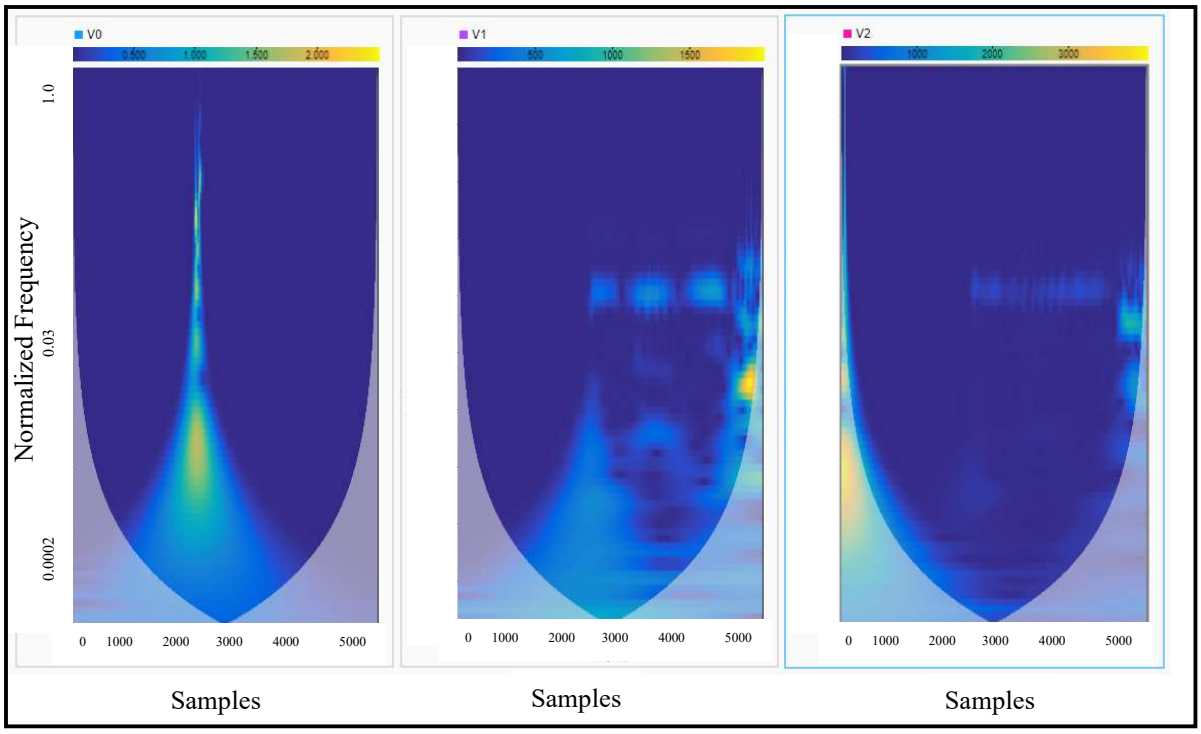

Figure 4.*52*: Time-Frequency/Scalogram for $V0, V1, V2$

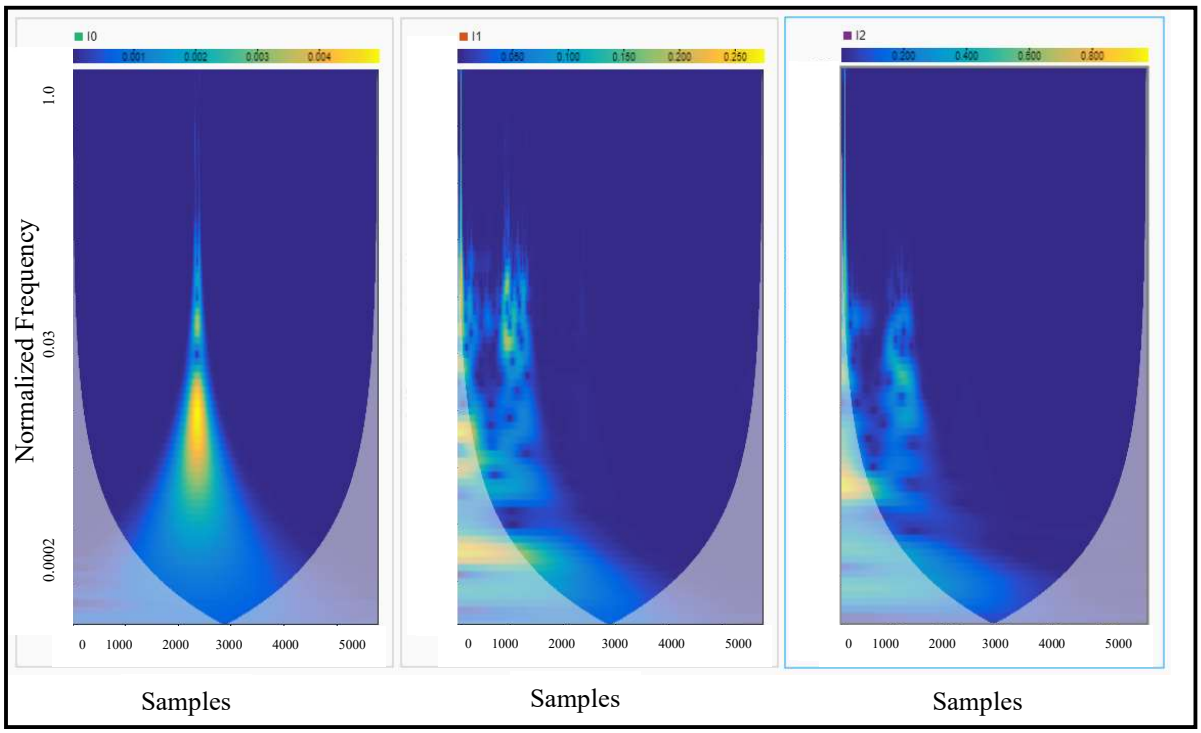

Figure 4.53: Time-Frequency/Scalogram for $I0, I1, I2$

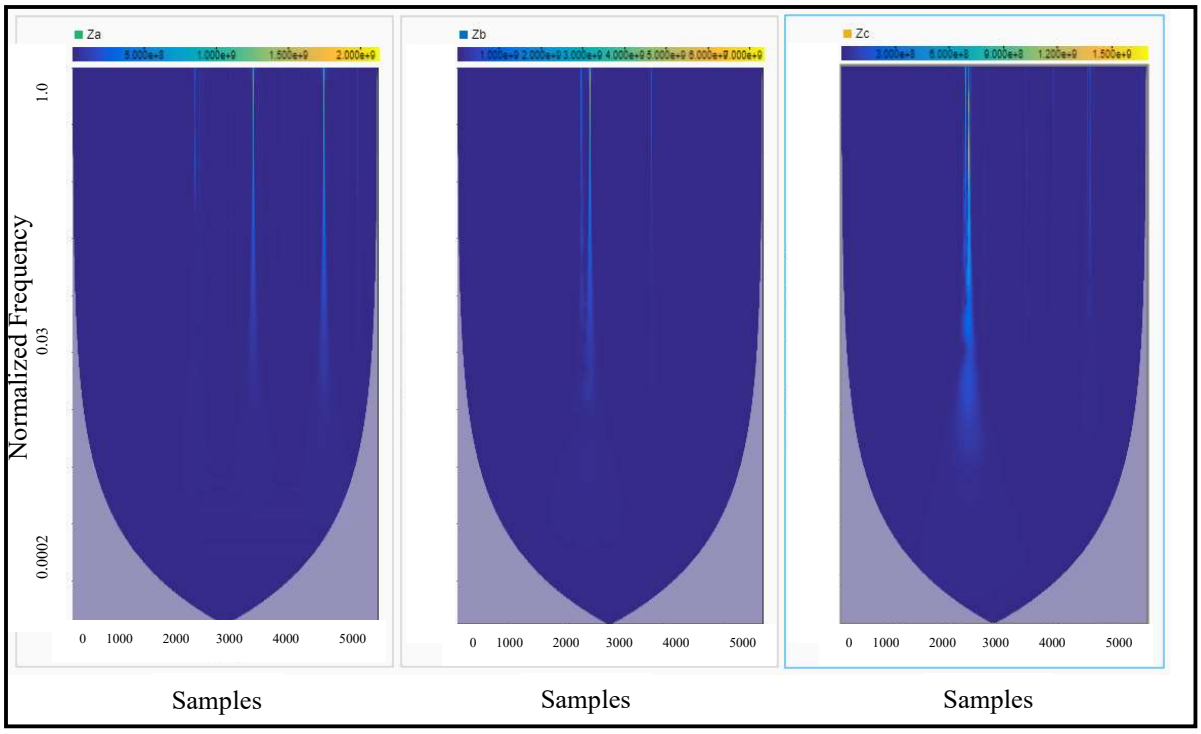

Figure 4.54: Time-Frequency/Scalogram for Za, Zb, Zc

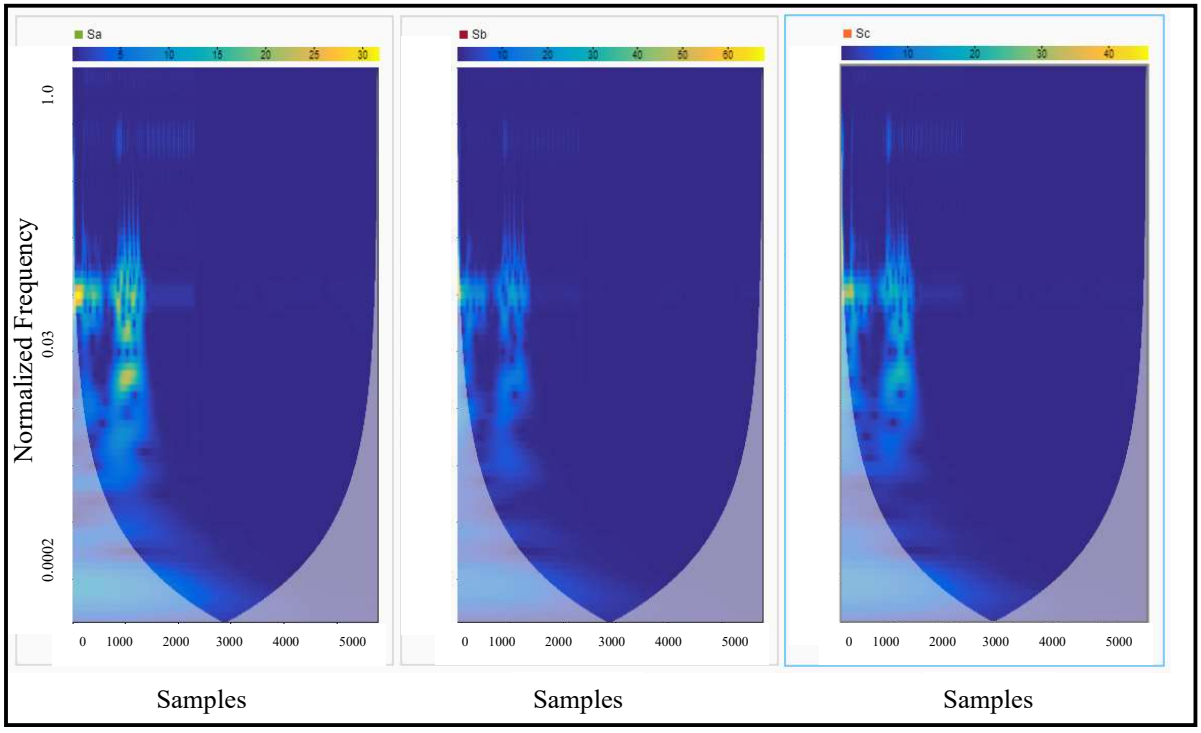

Figure 4.55: Time-Frequency/Scalogram for Sa, Sb, Sc

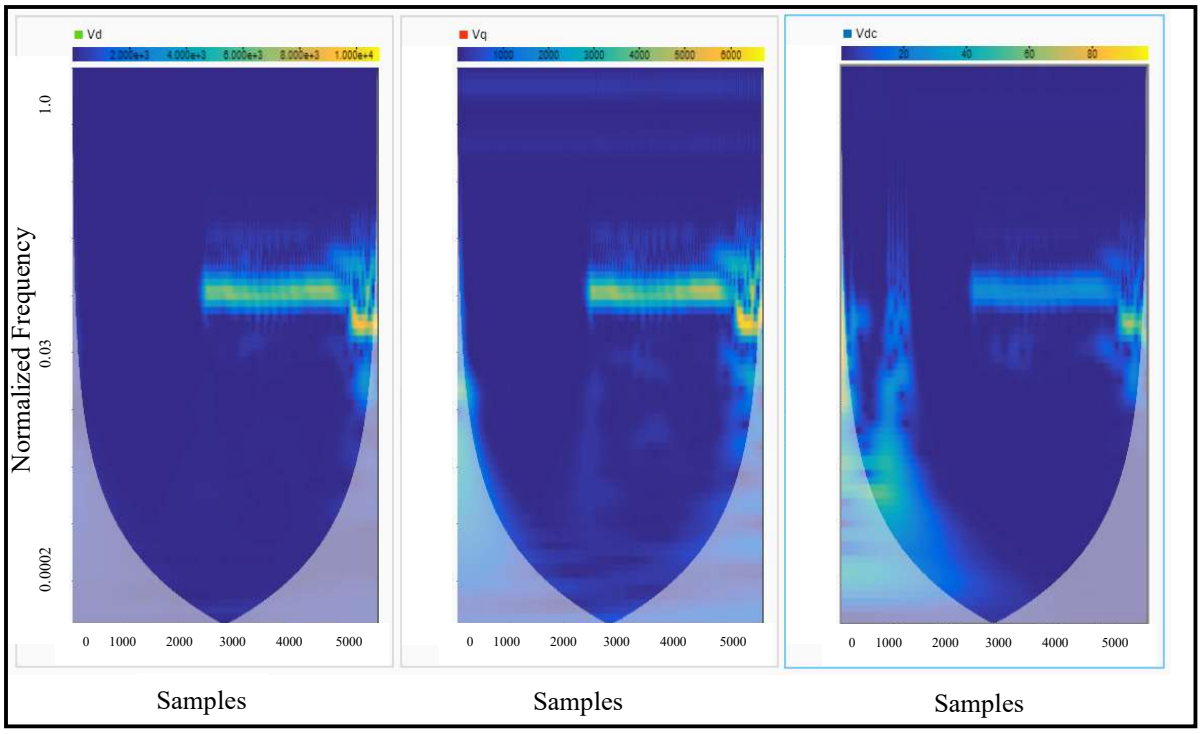

Figure 4.*56*: Time-Frequency/Scalogram for Vd, Vq, Vdc

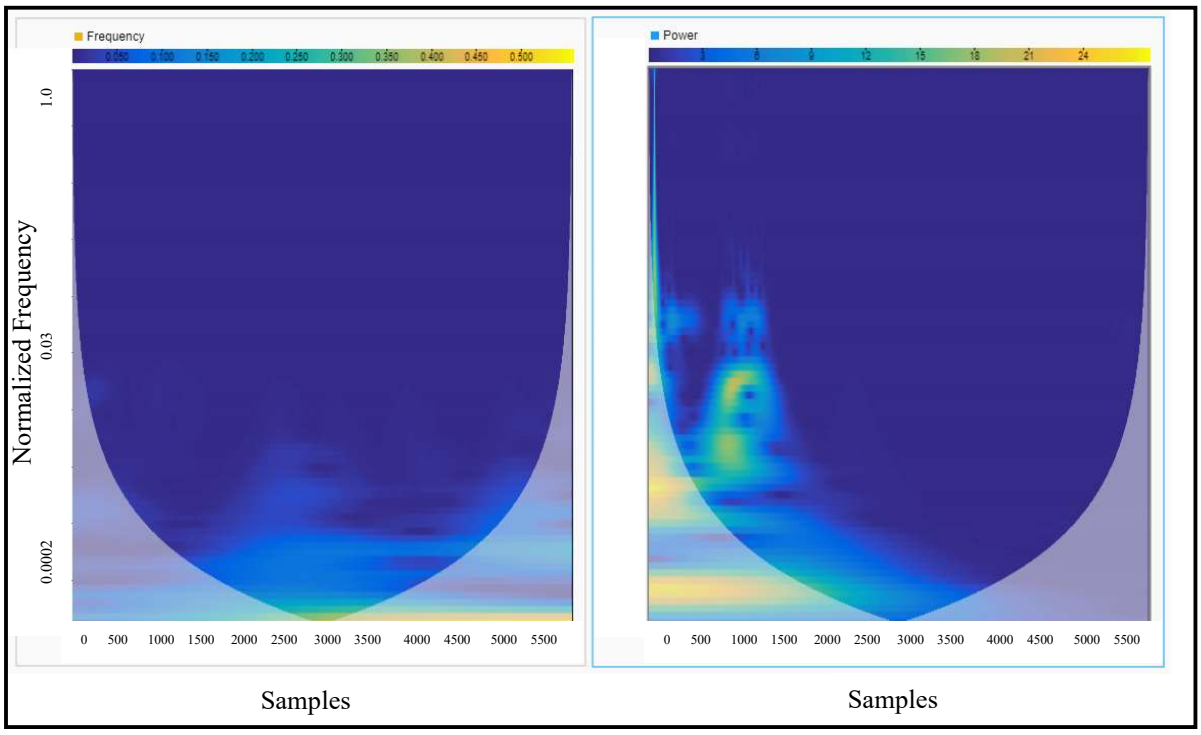

Figure 4.57: Time-Frequency/Scalogram for Frequency, Power

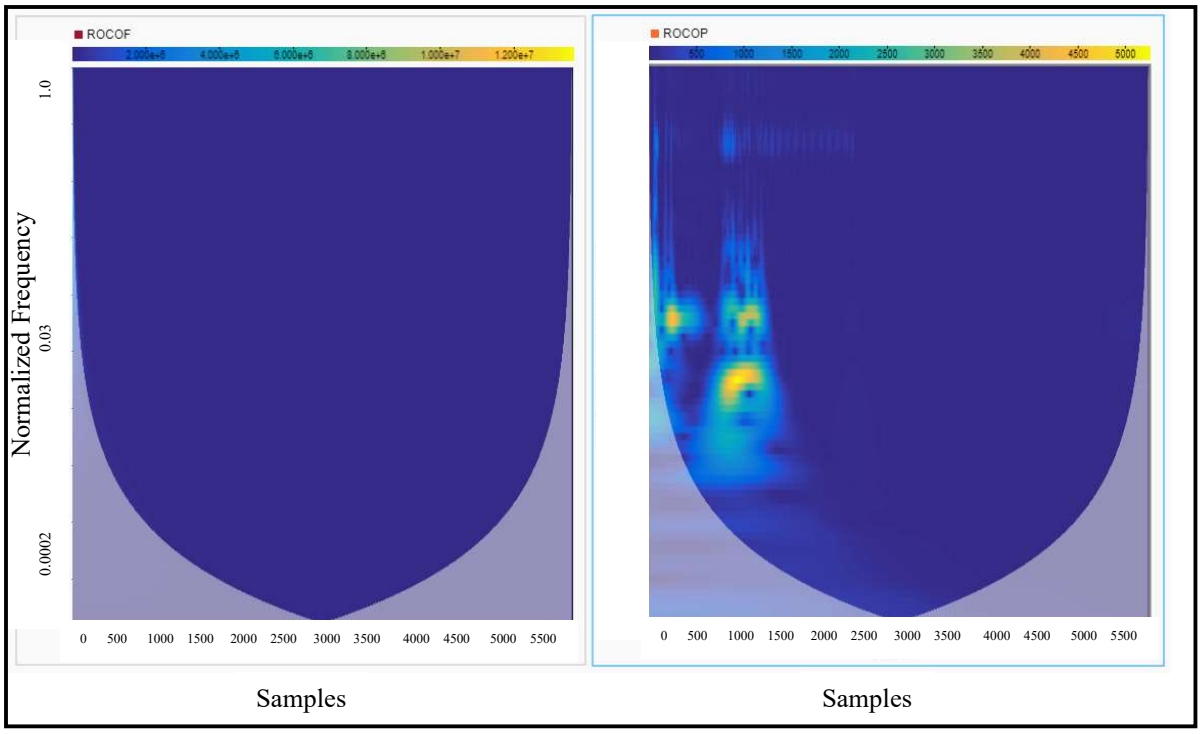

Figure 4.58: Time-Frequency/Scalogram for $ROCOF, ROCOP$

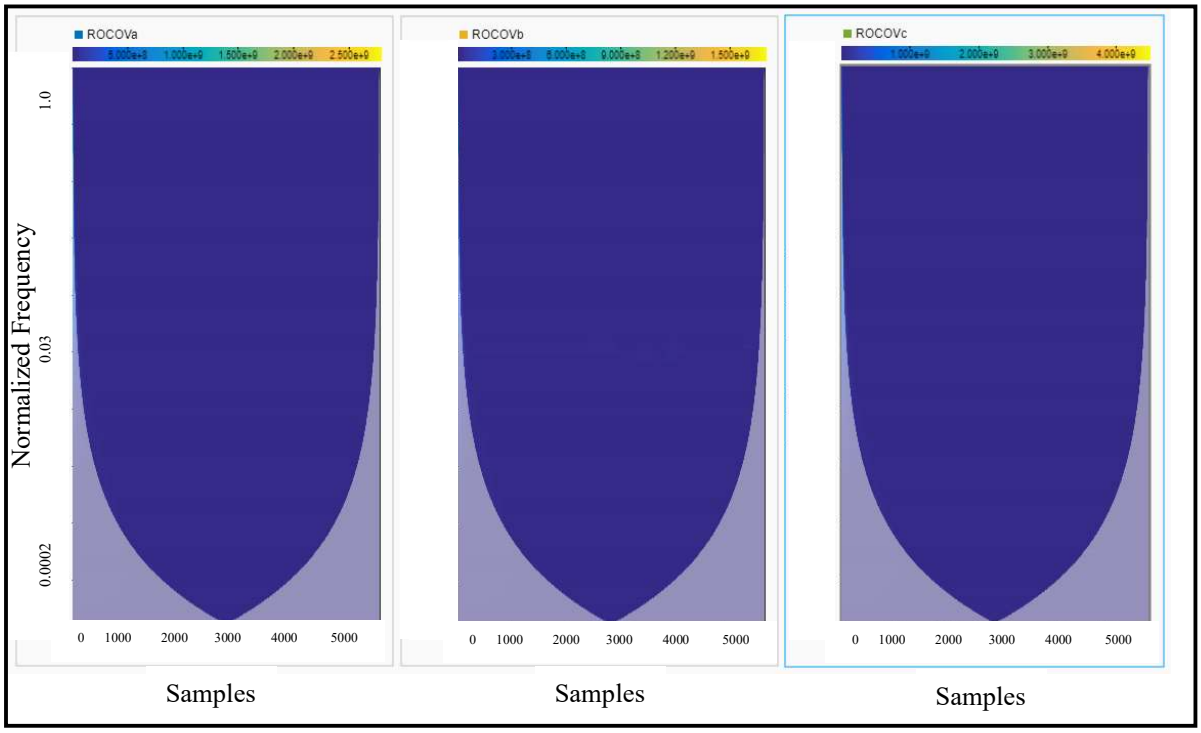

Figure 4.59: Time-Frequency/Scalogram for $ROCOVa, ROCOVb, ROCOVc$

4.2.3.2 Non-islanding Cases

The non-islanding cases represent some faulty and non-faulty events. Table 4.4 shows various types of faulty and non-faulty cases that are considered in this work.

Various types of faults (three-phase, two-phase and single-phase faults) occur at 5 km away from the PCC as shown in Fig. 4.60. Different values of fault resistances were taken to simulate fault events of a total of 24 cases. A three-phase fault occurs at 5 km from the PCC (towards the utility grid side) at 0.6 second and lasts for 20 milliseconds. Each fault is simulated with various possible fault resistance, as follows: 1 ohm, 10 ohms, 20 ohms, 30 ohms, 40 ohms, 50 ohms, 60 ohms and 70 ohms. The same fault resistance values, faults occurrence time, and the clearance time were also used for two phase (A-B) and single phase (A-G) faults [3]. Since the faults occur at the upstream of the breaker and be cleared quickly in 20 milliseconds, therefore, the breaker at the PCC does not trip and hence no islanding occurs, as to why these cases are classified as non-islanding cases. Fig. 4.61 to 4.71 show the scalograms for all measurements and indices when single phase (A-G) happens with 1 ohm ground resistance (case no. 34). However, all other faulty cases are taken into account for further model training via deep learning layers.

A total of five non-faulty cases are included to consider different loading conditions in the microgrid and the utility grid. The loads used to generate the different loading conditions are shown in Fig. 4.60. Three cases were generated due to load switching in the microgrid's load as follows: 10%, 50%, and 100%. Two other cases for load switching in the utility grid were simulated for the utility's load, as follows: 33% and 66% [3]. All loading conditions were at unity power factor and load quality factor (QF) of 1 as per IEEE 1547.1 [71]. The load quality factor is the ratio between load reactive power (Q_L) and the D-RER generated active power (P_G), and it identifies the relative size of the load reactance with respect to the inverter generated power [6]. None of these cases caused breaker tripping, and therefore, they are classified as non-islanding cases. Fig. 4.72 to 4.82 show the scalograms for all measurements and indices for 100% loading condition in both microgrid and utility grid (case no. 44). However, all other loading cases are taken into account for further model training via deep learning layers.

Table 4.4: Non-Islanding Cases

Non-Islanding Cases		
Case No.	Condition	Classification
18-25	Three-phase fault, fault resistance is simulated as follows: 1 ohm, 10 ohms, 20 ohms, 30 ohms, 40 ohms, 50 ohms, 60 ohms, 70 ohms	Faults occur at 0.6 second for 20 milli second
26-33	Two-phase fault, fault resistance is simulated as follows: 1 ohm, 10 ohms, 20 ohms, 30 ohms, 40 ohms, 50 ohms, 60 ohms, 70 ohms	
34-41	Single-phase fault, fault resistance is simulated as follows: 1 ohm, 10 ohms, 20 ohms, 30 ohms, 40 ohms, 50 ohms, 60 ohms, 70 ohms	
42-44	The load in the microgrid was changed and set at different values: 10%, 50%, 100% of nominal load capacity	Loading Conditions in the Microgrid
45-46	The load (active power) in the utility grid was changed and set at different values: 10 Mega Watt, 20 Mega Watt of nominal load capacity	Loading Conditions in the Utility Grid

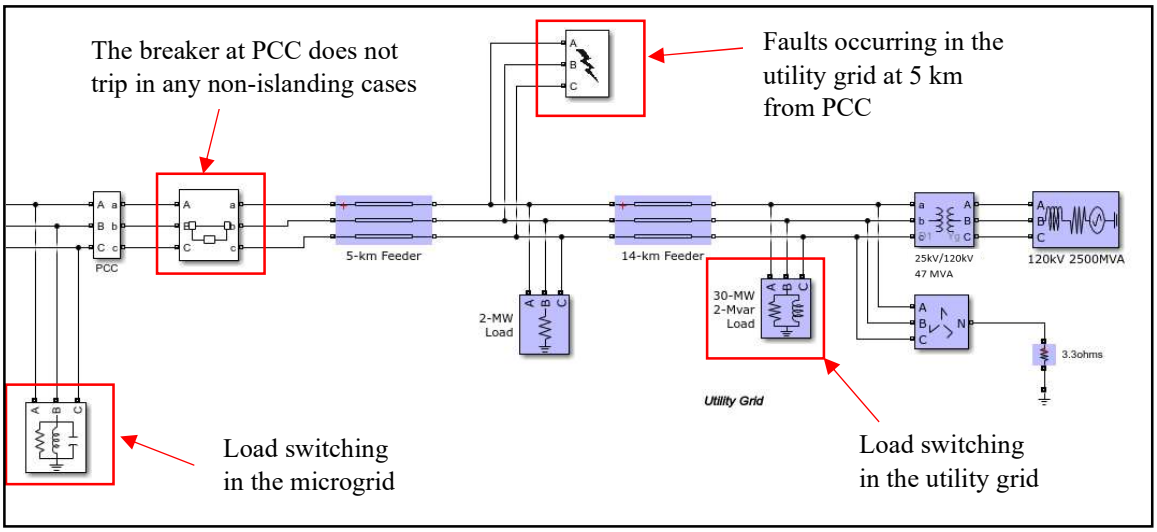

Figure 4.60: Non-islanding cases

The scalograms generated for the non-islanding cases are shown in Fig. 4.61 to 4.82.

- Faulty Cases:

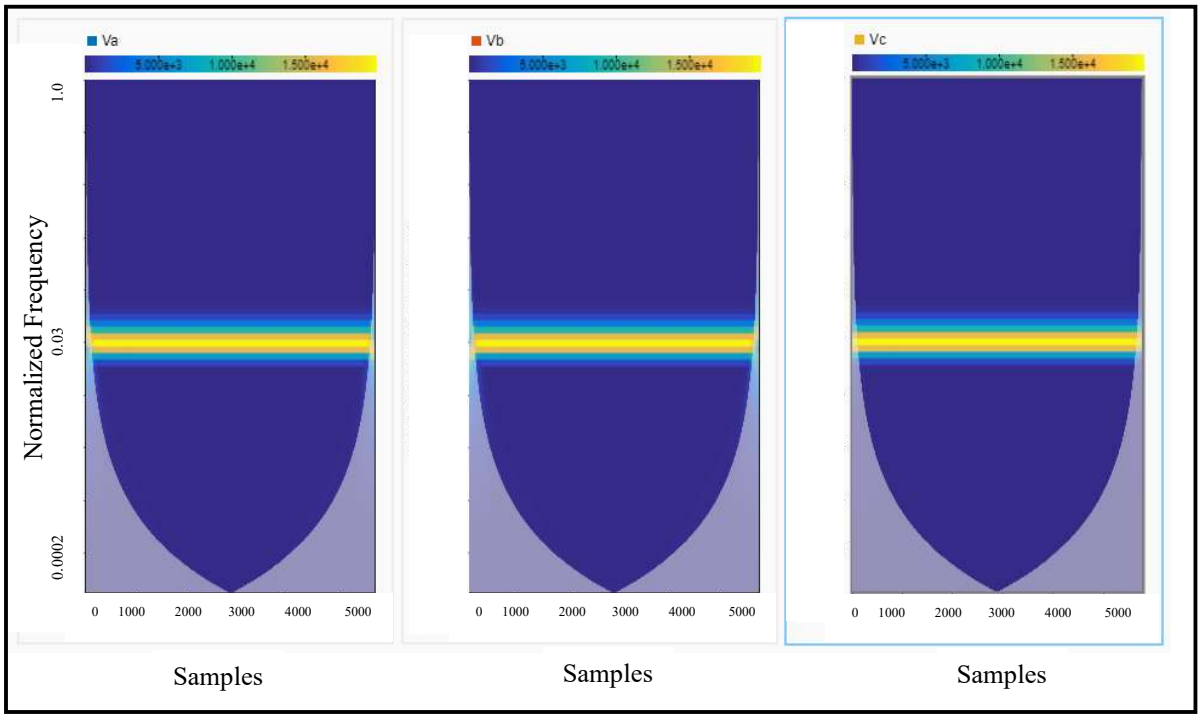

Figure 4.61: Time-Frequency/Scalogram for Va, Vb, Vc

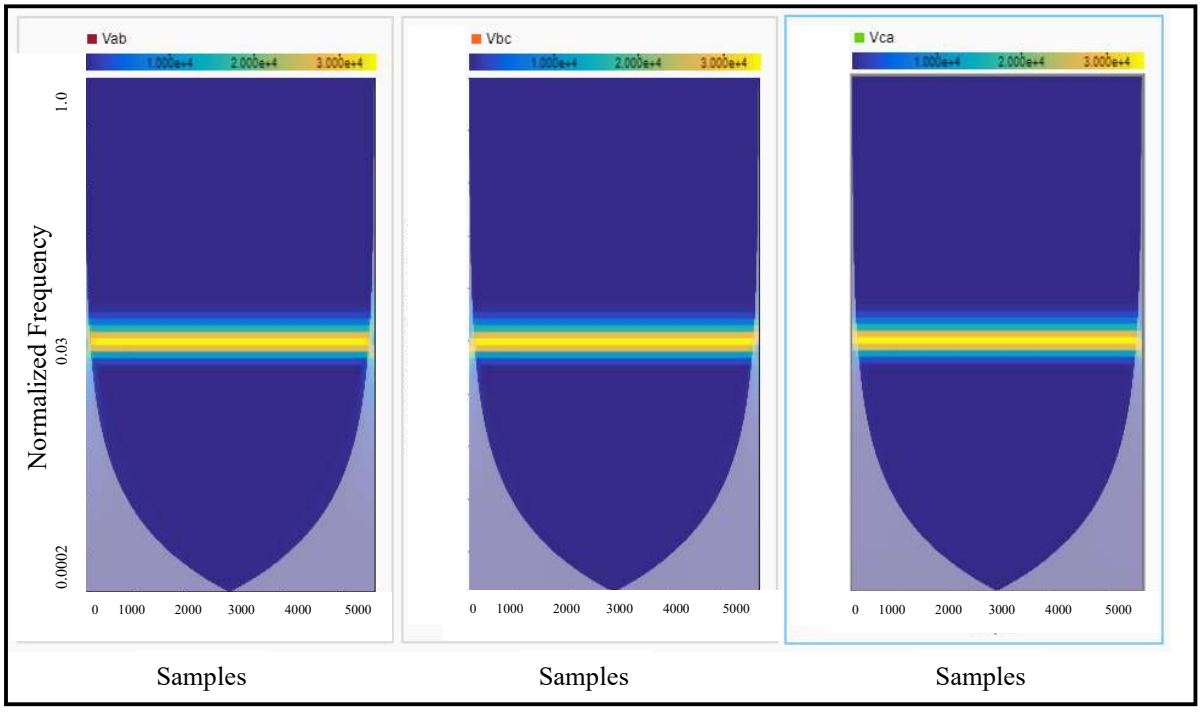

Figure 4.62: Time-Frequency/Scalogram for Vab, Vbc, Vca

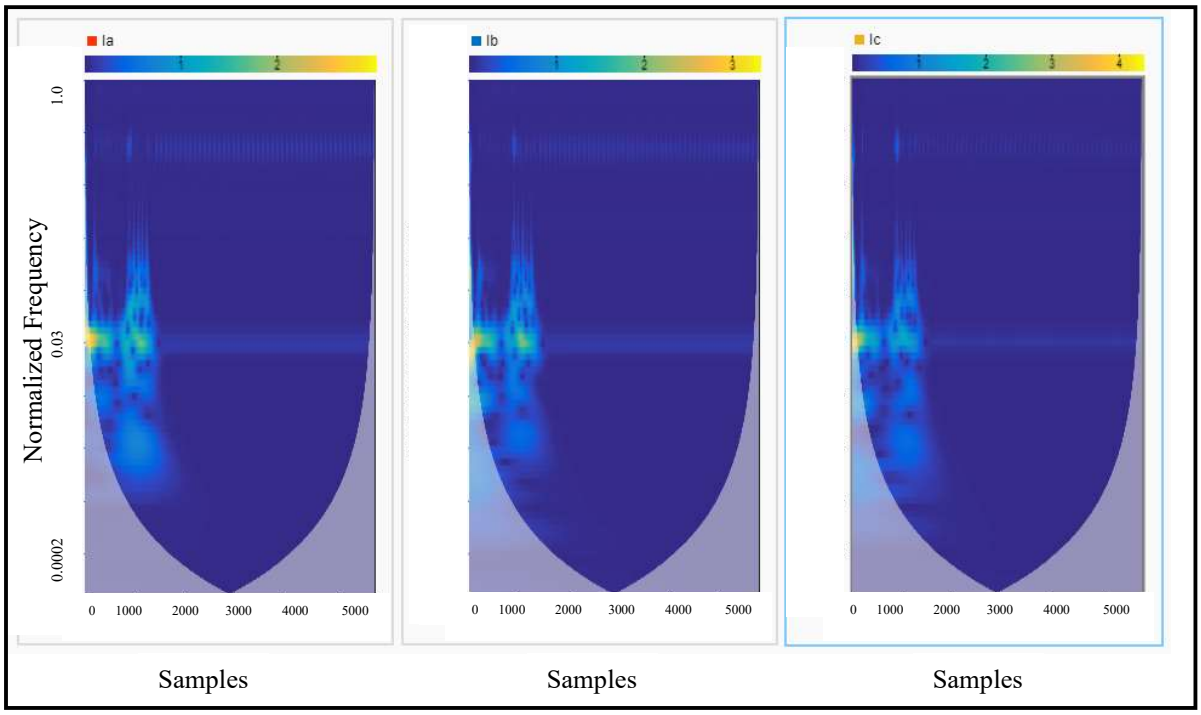

Figure 4.63: Time-Frequency/Scalogram for Ia, Ib, Ic

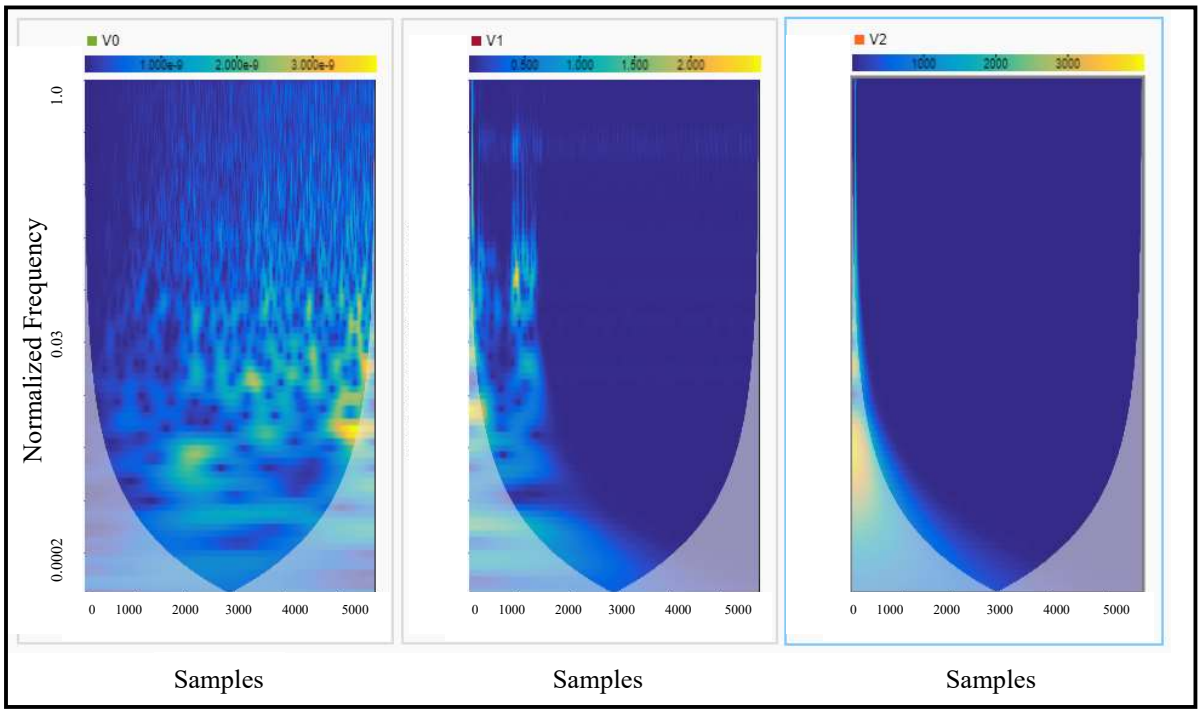

Figure 4.64: Time-Frequency/Scalogram for $V0, V1, V2$

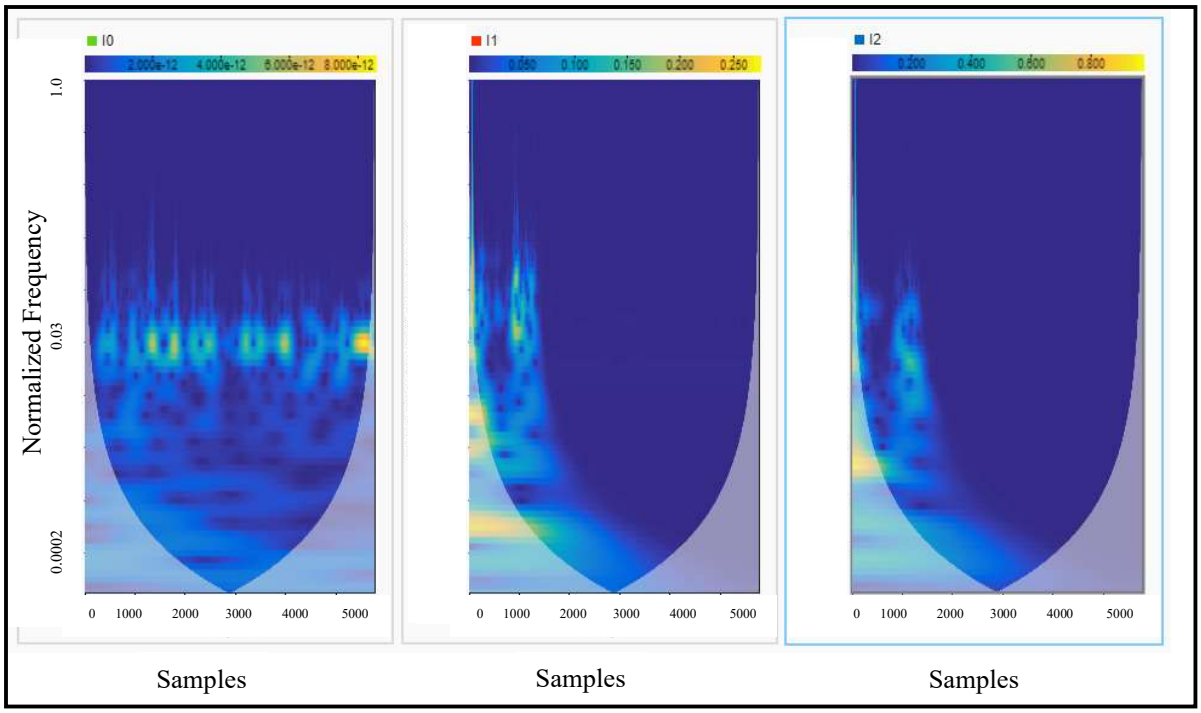

Figure 4.65: Time-Frequency/Scalogram for $I0, I1, I2$

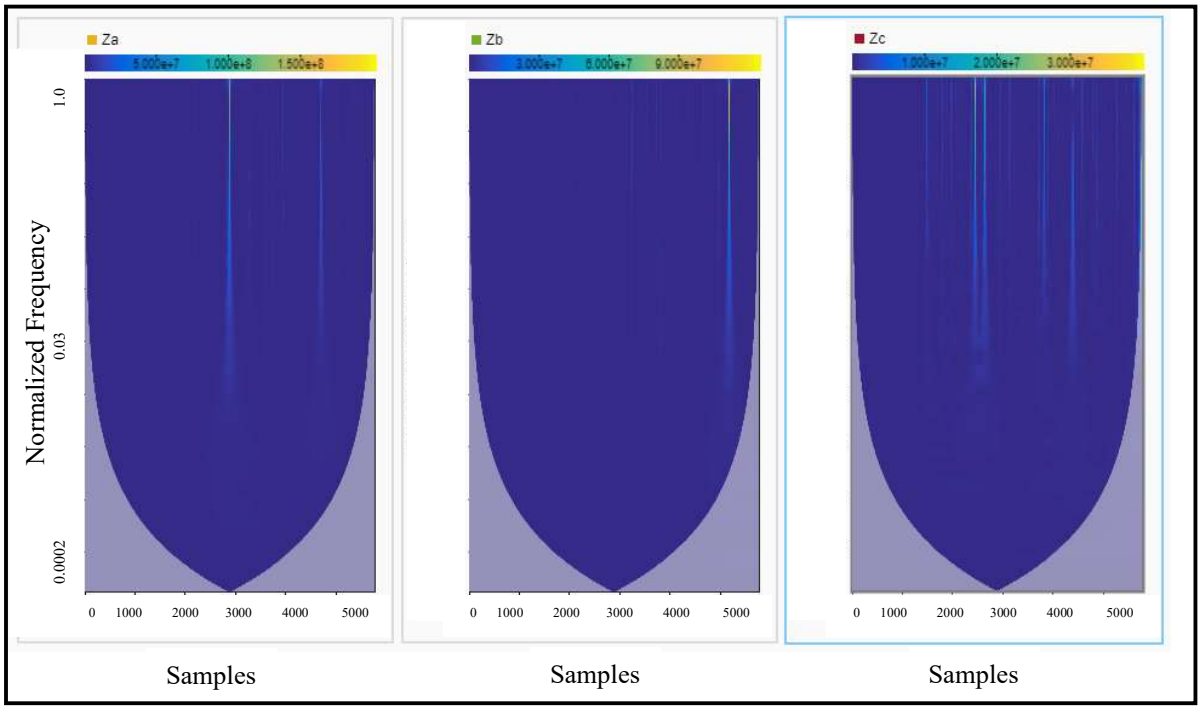

Figure 4.66: Time-Frequency/Scalogram for Za, Zb, Zc

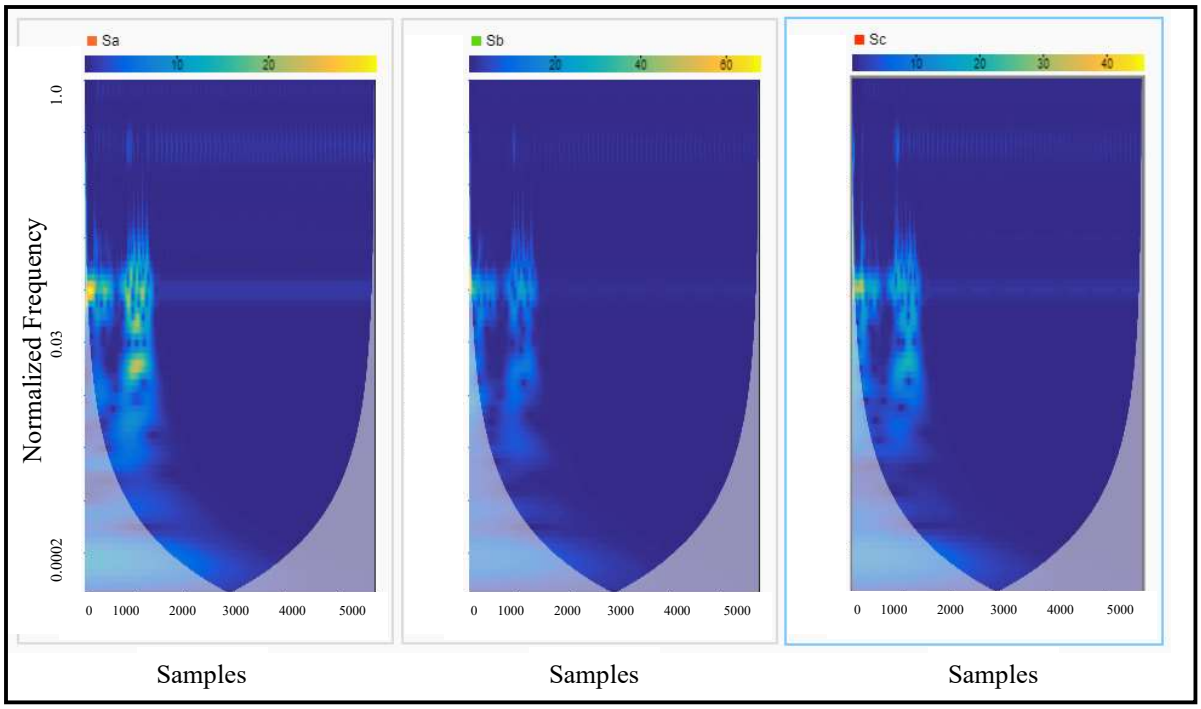

Figure 4.67: Time-Frequency/Scalogram for Sa, Sb, Sc

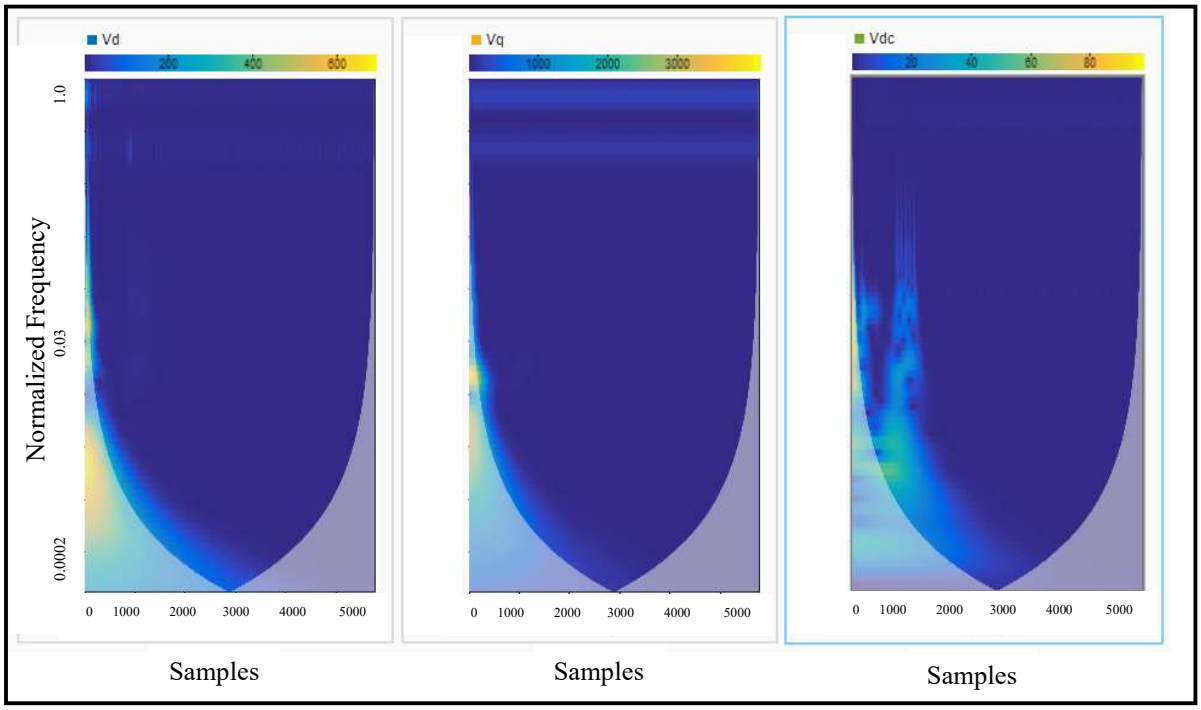

Figure 4.68: Time-Frequency/Scalogram for Vd, Vq, Vdc

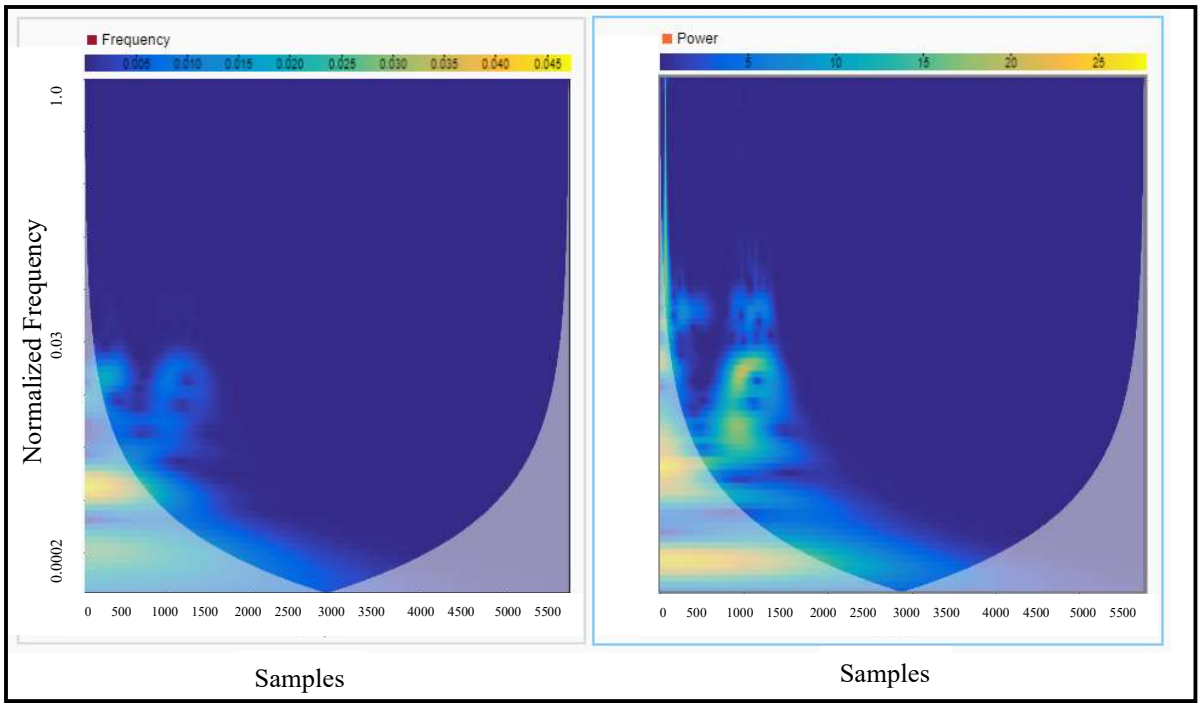

Figure 4.69: Time-Frequency/Scalogram for Frequency, Power

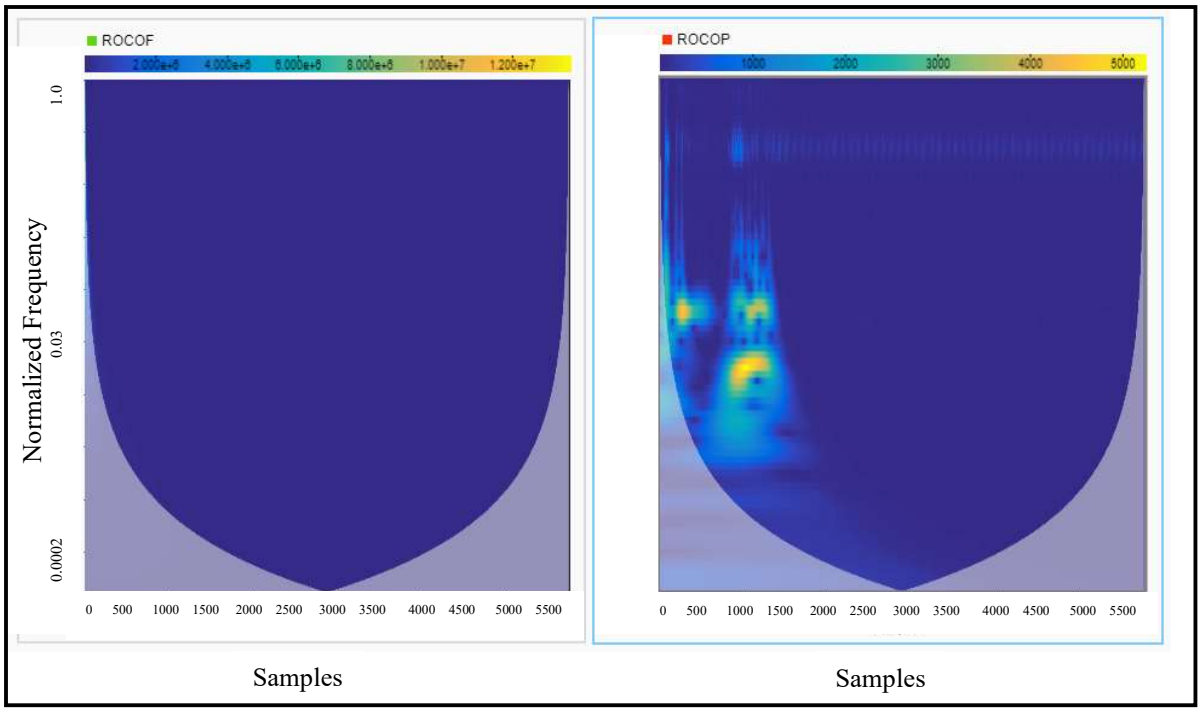

Figure 4.70: Time-Frequency/Scalogram for $ROCOF, ROCOP$

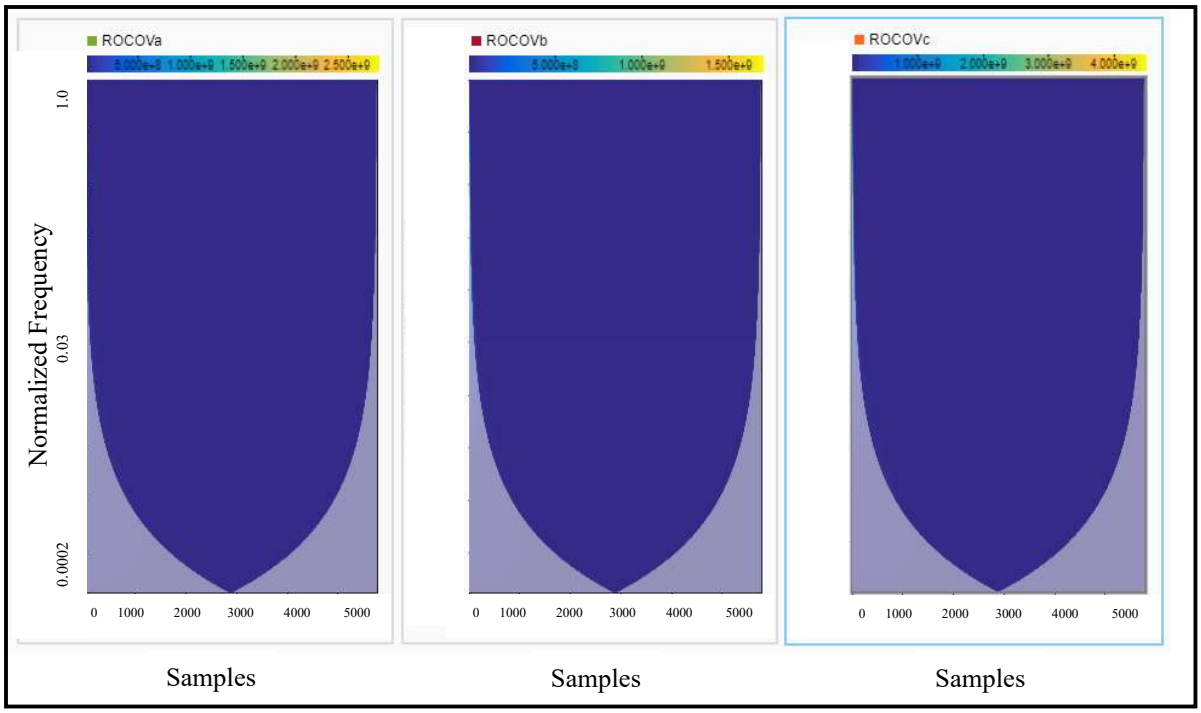

Figure 4.71: Time-Frequency/Scalogram for $ROCOVa, ROCOVb, ROCOVc$

- Load Switching Cases (non-faulty cases):

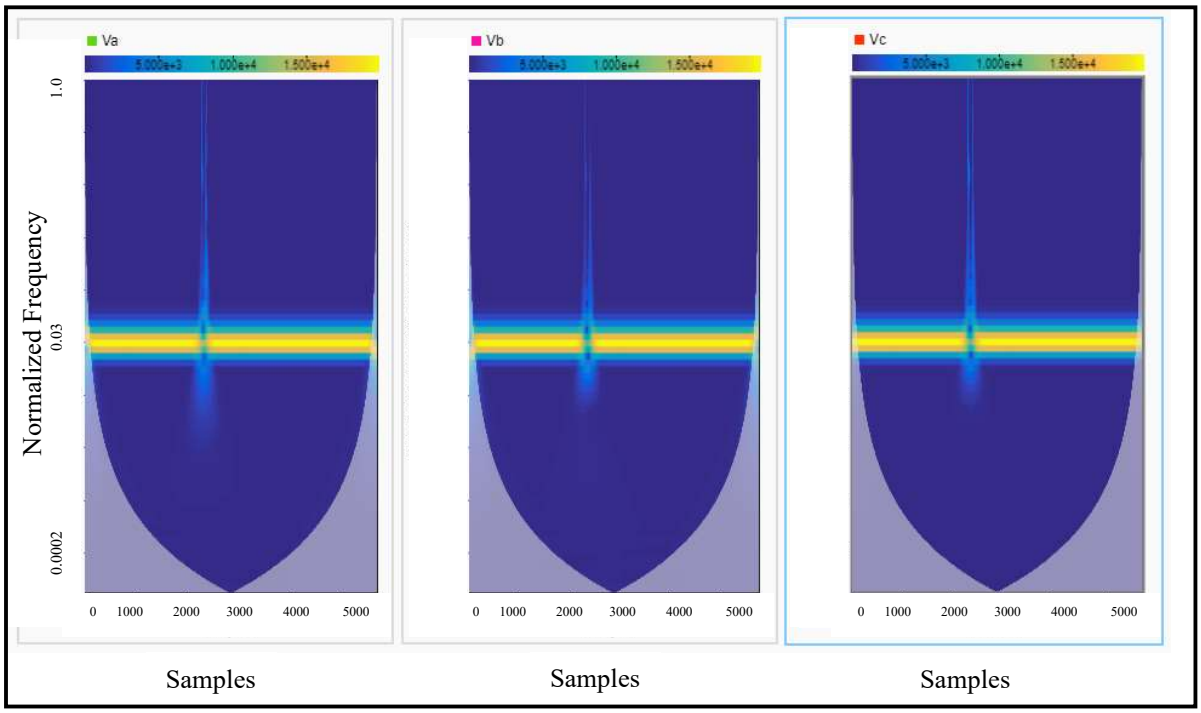

Figure 4.72: Time-Frequency/Scalogram for Va, Vb, Vc

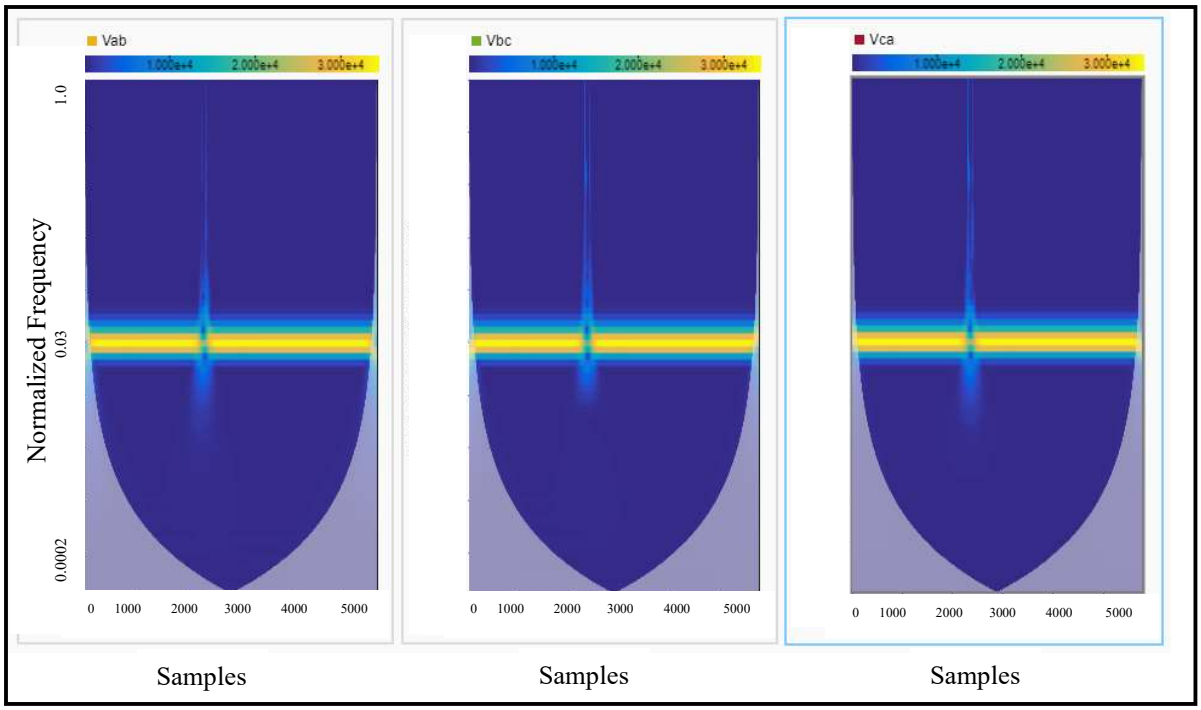

Figure 4.73: Time-Frequency/Scalogram for Vab, Vbc, Vca

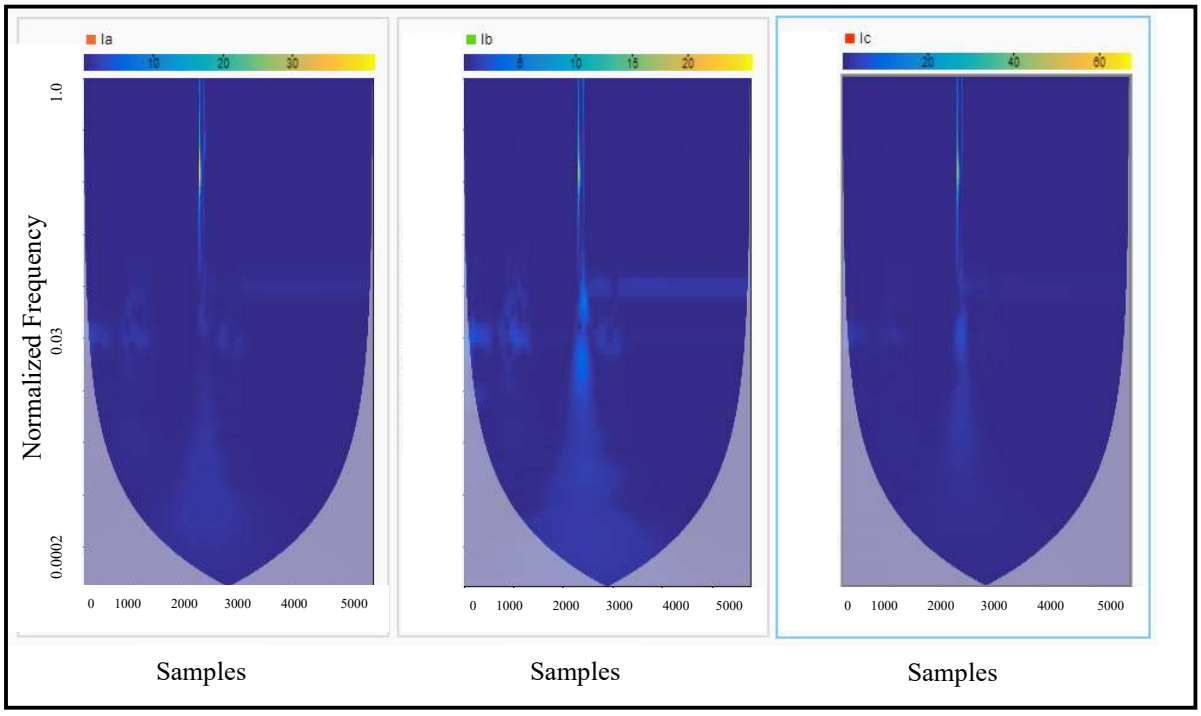

Figure 4.74: Time-Frequency/Scalogram for Ia, Ib, Ic

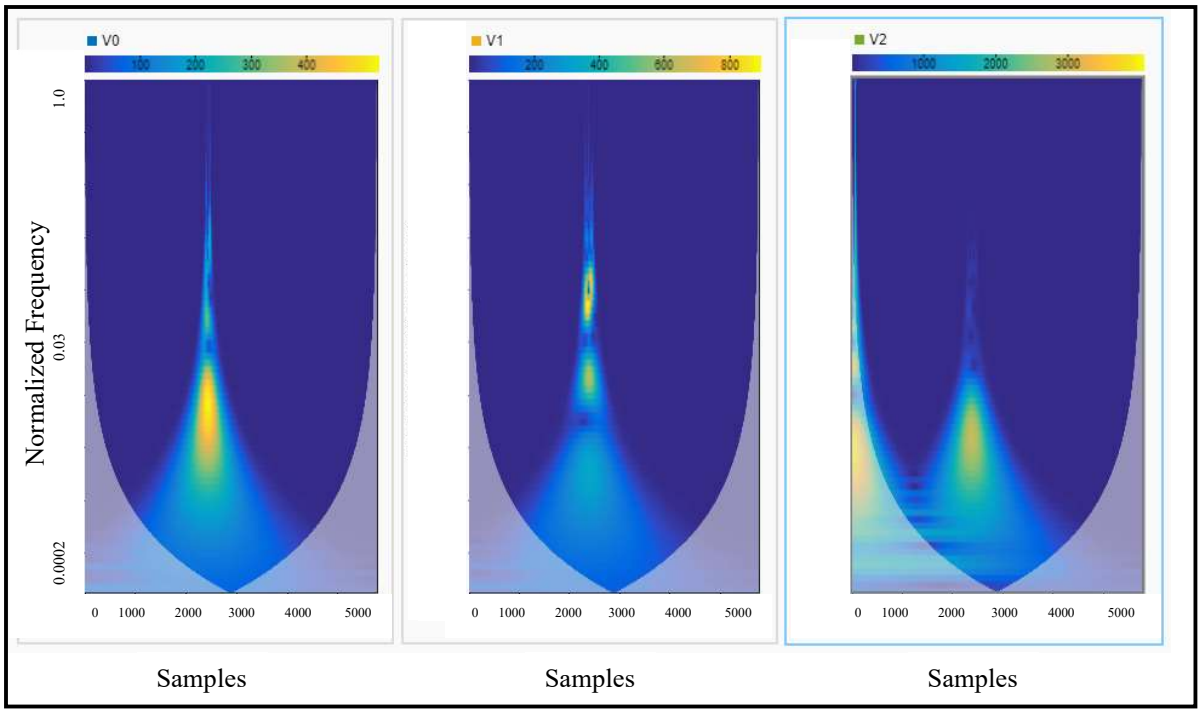

Figure 4.75: Time-Frequency/Scalogram for $V0, V1, V2$

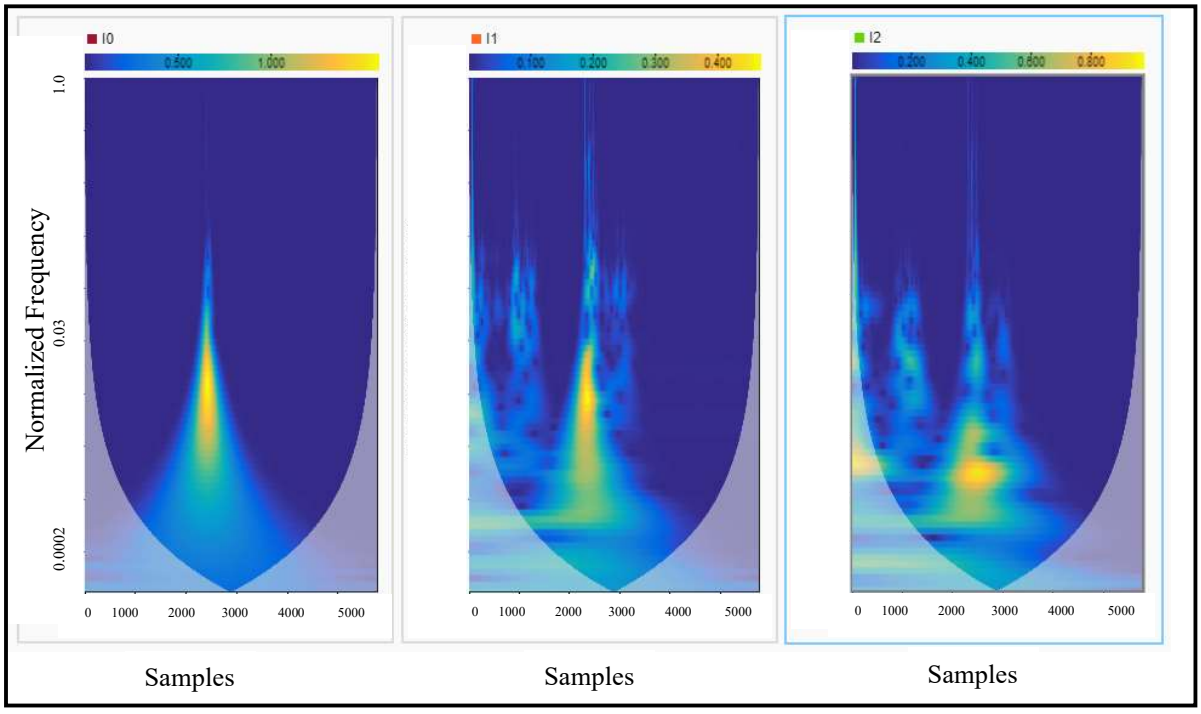

Figure 4.76: Time-Frequency/Scalogram for $I0, I1, I2$

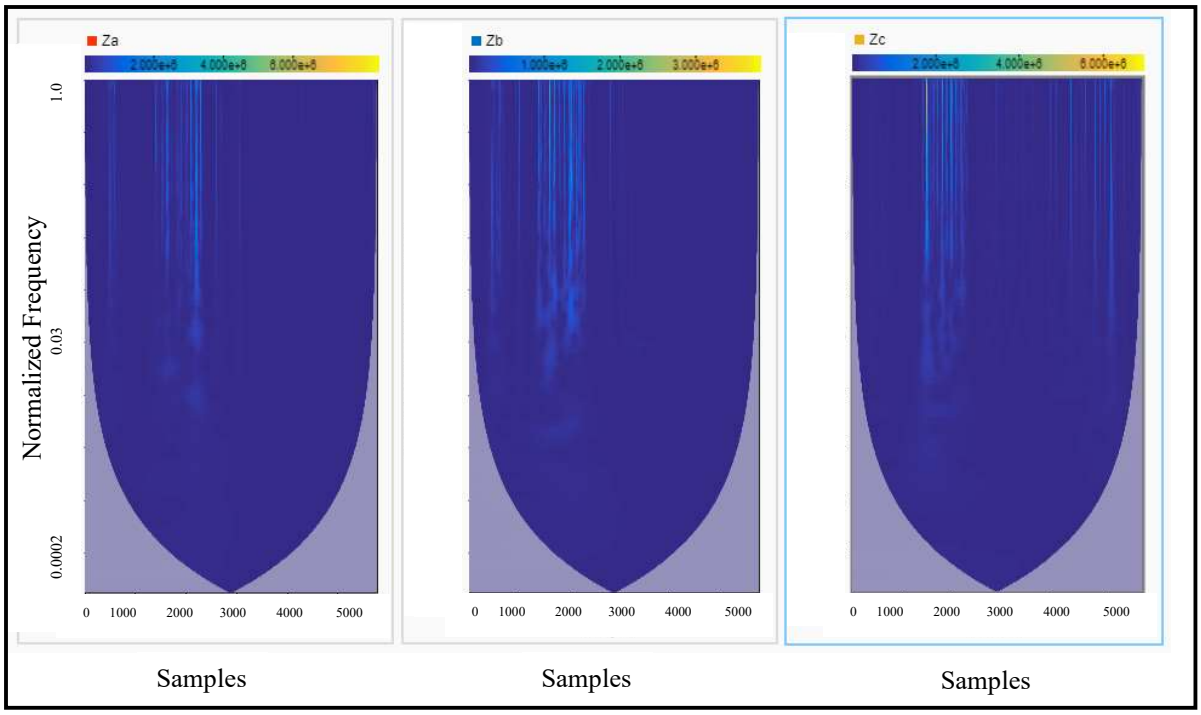

Figure 4. 77: Time-Frequency/Scalogram for Za, Zb, Zc

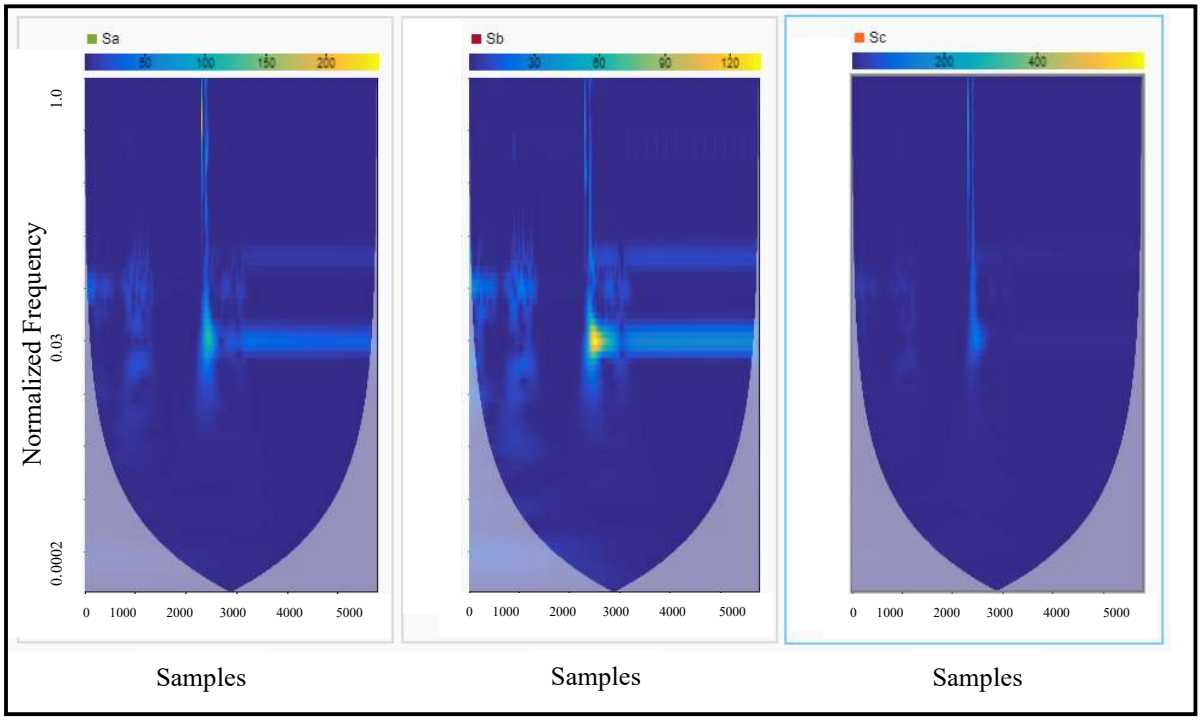

Figure 4.78: Time-Frequency/Scalogram for Sa, Sb, Sc

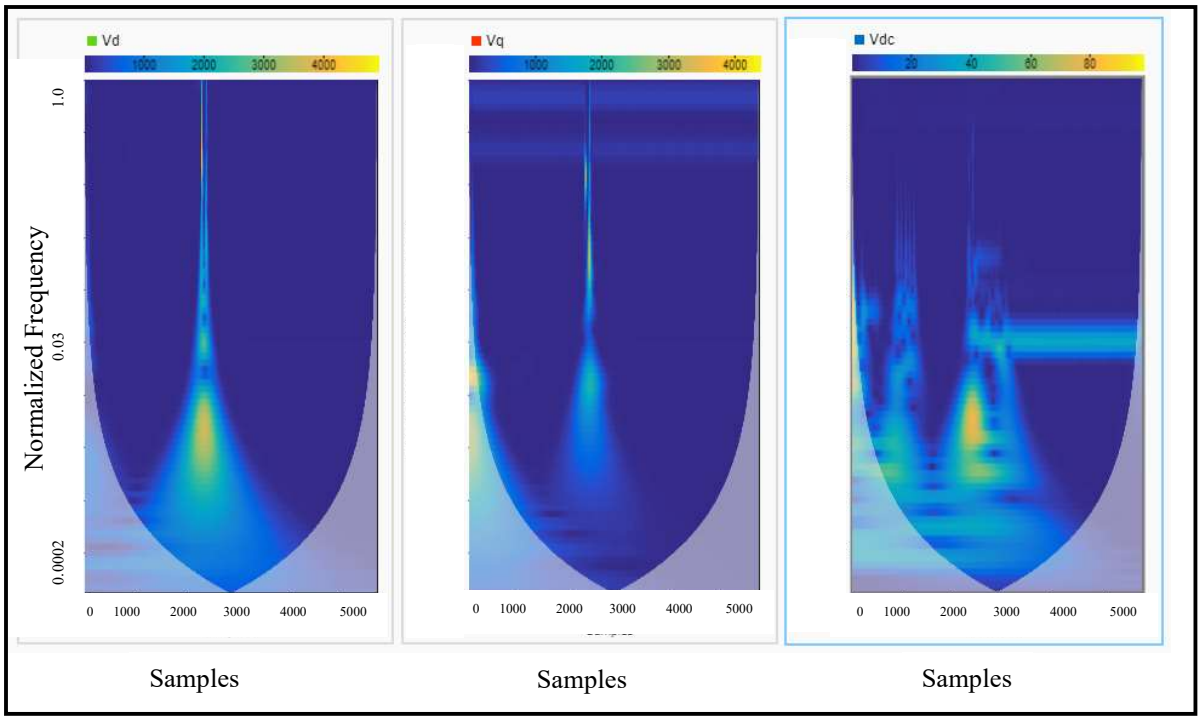

Figure 4.79: Time-Frequency/Scalogram for Vd, Vq, Vdc

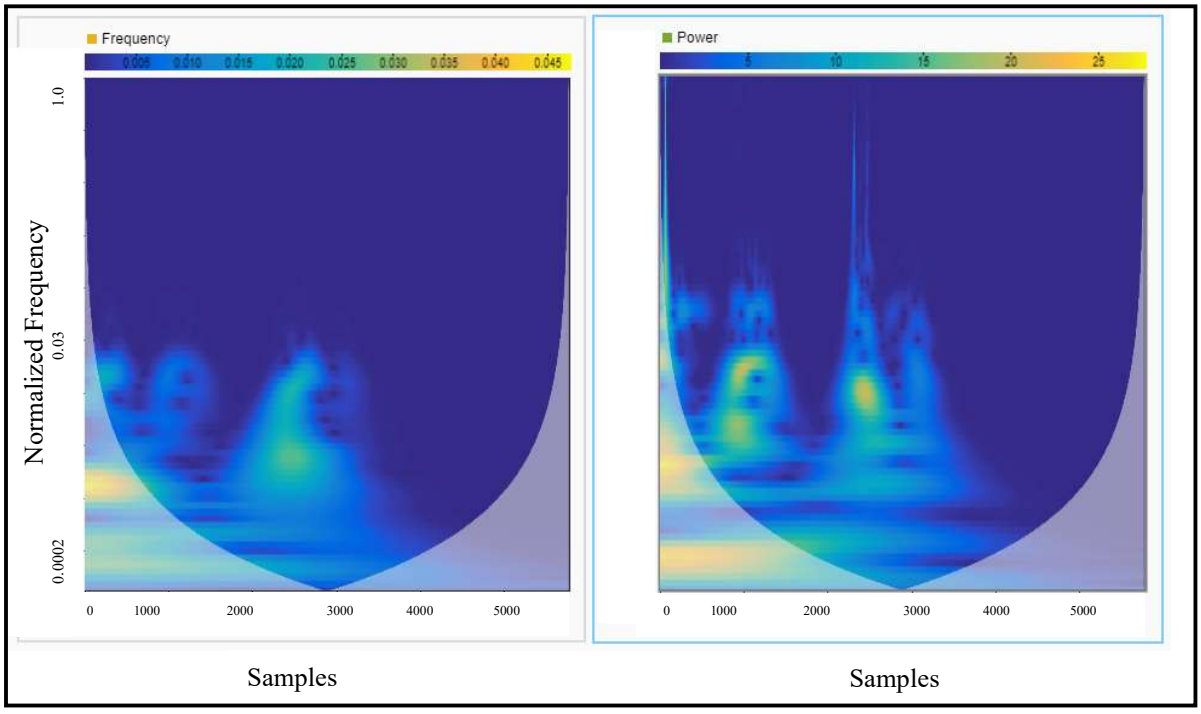

Figure 4.80: Time-Frequency/Scalogram for Frequency, Power

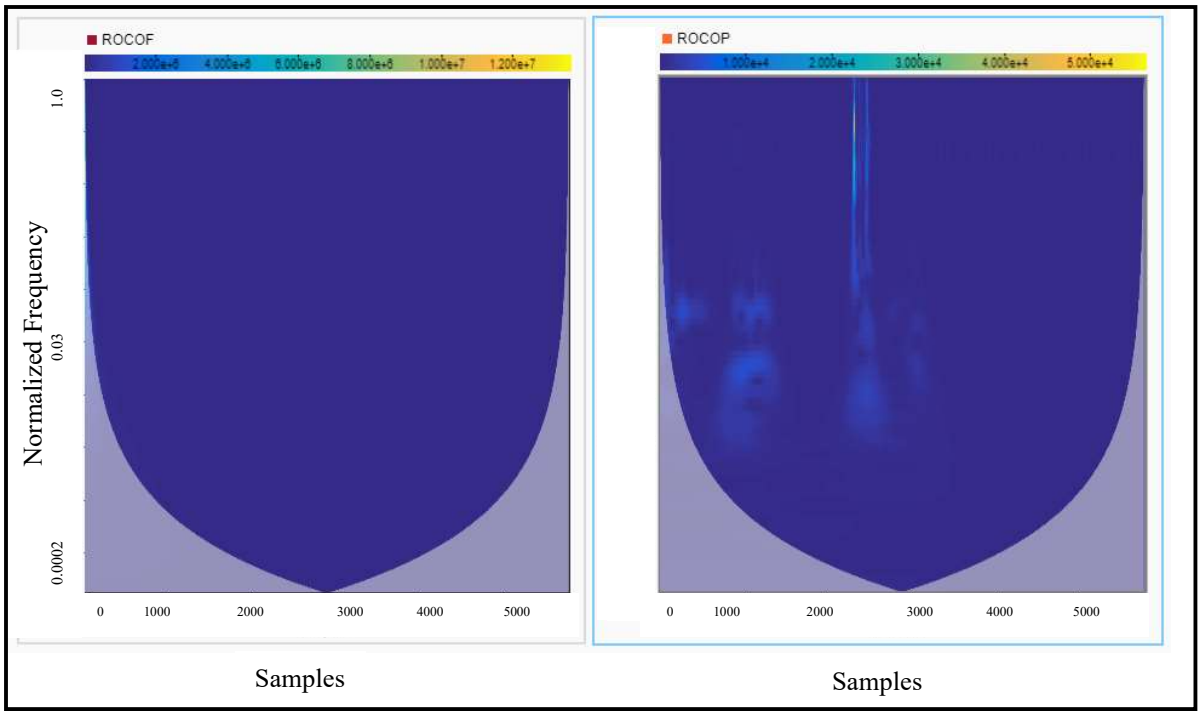

Figure 4.81: Time-Frequency/Scalogram for $ROCOF, ROCOP$

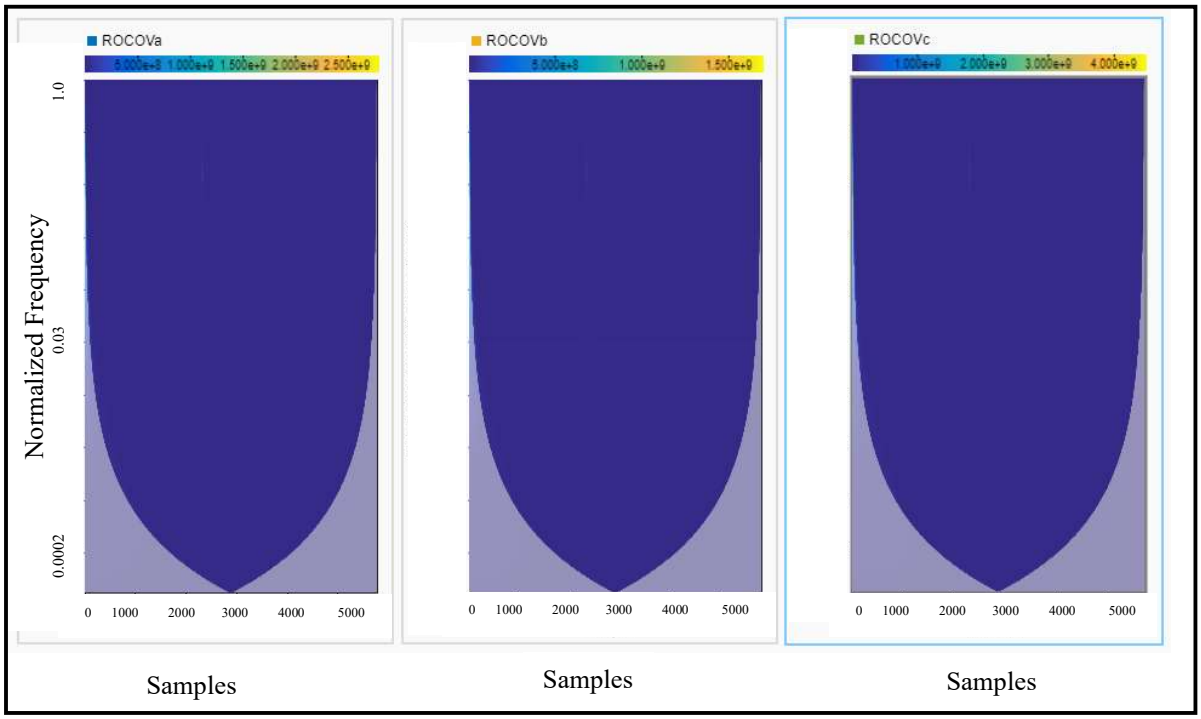

Figure 4.*82*: Time-Frequency/Scalogram for $ROCOVa, ROCOVb, ROCOVc$

4.3 Model Training

Each of the cases presented in previous section, utilized 31 measurements/indices having a length of 5,770 samples/measurement, which is based on Fs=3.84 kHz [70] and the 1.5 second duration. Hence, the data set generated from running all 46 cases is a matrix of 1,426 (31 measurements × 46 cases) × 5770 (signal length). The data set is divided into islanding and non-islanding subsets, as follows: a set of 527 (31 measurements ×17 cases) × 5770 (signal length) for islanding cases, and another set of 899 (31 measurements ×29 cases) × 5770 (signal length) for non-islanding cases. By applying the CWT and the filter bank to the measurements, the time-frequency coefficients/features will be generated and converted to images (scalograms) that will be fed to the deep learning hidden layers. The data set is split into 80% to be used to train the model while the remaining 20% is used for the model testing.

The next step is to use CNN network. In this work, the Alex pre-trained CNN network uses the training data set to train the model and to develop the classification [72]. Fig. 4.83 shows the training progress using 12 epochs (training processes), 1,236 iterations, and learning rate of 0.0001. These parameters were identified after several attempts to achieve the highest training accuracy, lowest training loss of 0.0006, and the best testing results with the highest testing accuracy and the shortest detection time.

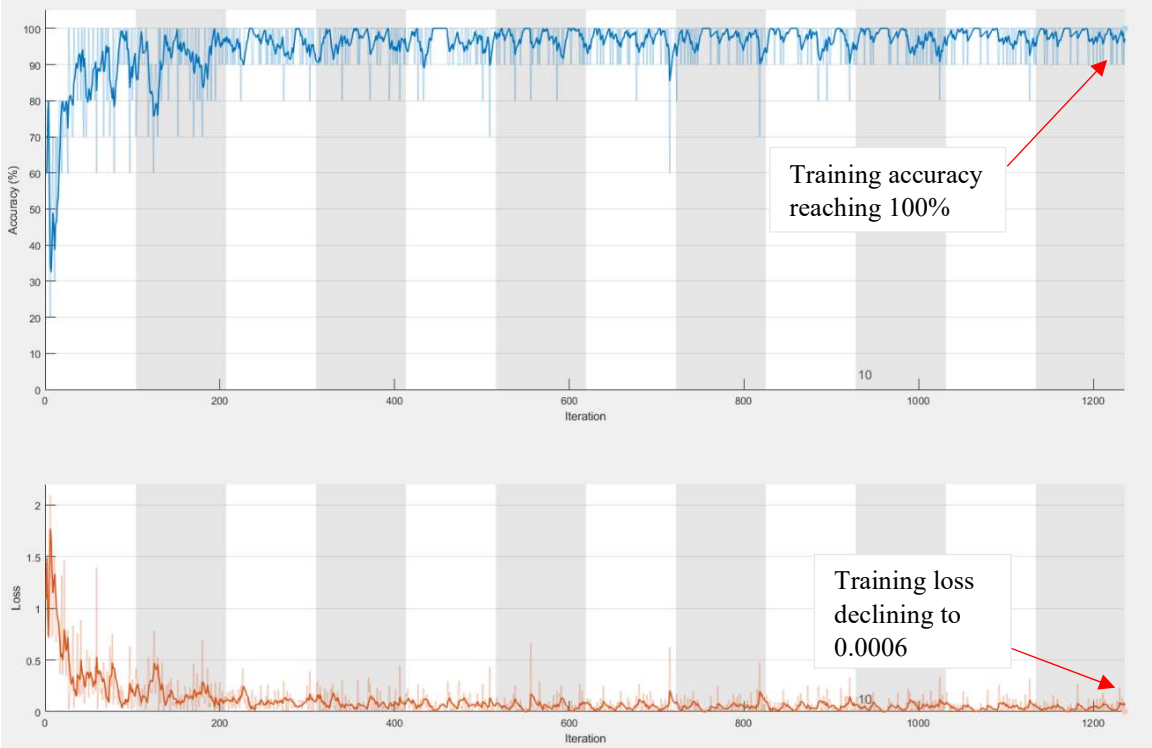

Figure 4.83: The Accuracy and Loss for the Model's Training

4.4 Model Testing

The testing set is used to test and assess the performance of the classifier to predict the islanding and the non-islanding cases for the data that the model never sees a priori. In order to test the model, 20% of the data set is used for testing the trained model.

Most input data is taken for model training to ensure the model is well trained on large amount of data, and therefore, the 20% of the input data is deemed sufficient for testing the model to make sure the trained model is working efficiently with an acceptable accuracy. The testing set is selected randomly from the input data to ensure the model has never seen this data before and the results are unbiased. Dividing the data set into training and testing sets to maximize training and testing is made through cross-validation that split the data differently to find the best algorithm for the model.

Table 4.5 shows the confusion matrix that identifies the number of testing cases that are correctly (T) or incorrectly (F) classified by the trained model. The testing accuracy calculated by the model is 98.1%.

By applying (3.14) & (3.15) to confusion matrix counts, the model accuracy, precision, recall, and F-measure are 1, 0.95, 1, and 0.974 respectively.

Table 4.5: Confusion Matrix

		Actual Class	
		Islanding	Non-Islanding
Predicted Class	Islanding	**90 (TP)**	**5 (FP)**
	Non-Islanding	0 (FN)	162 (TN)

4.5 Detection Time

The computational time was executed on a laptop with Intel processor, Core™ i7-7500U CPU @ 2.7 GHz. The installed memory (RAM) is of 8.00 GB, an operating system of 64-bit and windows 10. The time required to complete the training is 26 minutes and 53 seconds (1613 seconds) for all measurement. Hence, the time spent for each signal is 1.25 second using laptop's processor.

However, the simulation was done offline, but if the relay was employed to perform the training, it would require shorter time than the laptop's processor used for the work in this thesis. This is because the relay has a processor of a higher sampling frequency of 3.84 kHz [70] that reduces the detection time. The computed time for the relay using the new proposed method is 0.88 second including the time of 0.6 second prior to islanding and 0.9 second after islanding. If the time prior to islanding is excluded, then 0.28 second will be required to detect the islanding by the relay when adopting the new proposed method. The outcome is in compliance with the IEEE 1547 [5].

By applying the proposed method when islanding occurs at 0.6 second, the D-RER will trip at 0.6+0.28=0.88 second. Fig. 4.84 to Fig. 4.92 show a few selected signals when islanding occurs at 0.6 second, and D-RER trips at 0.88 second as a result of applying the proposed method.

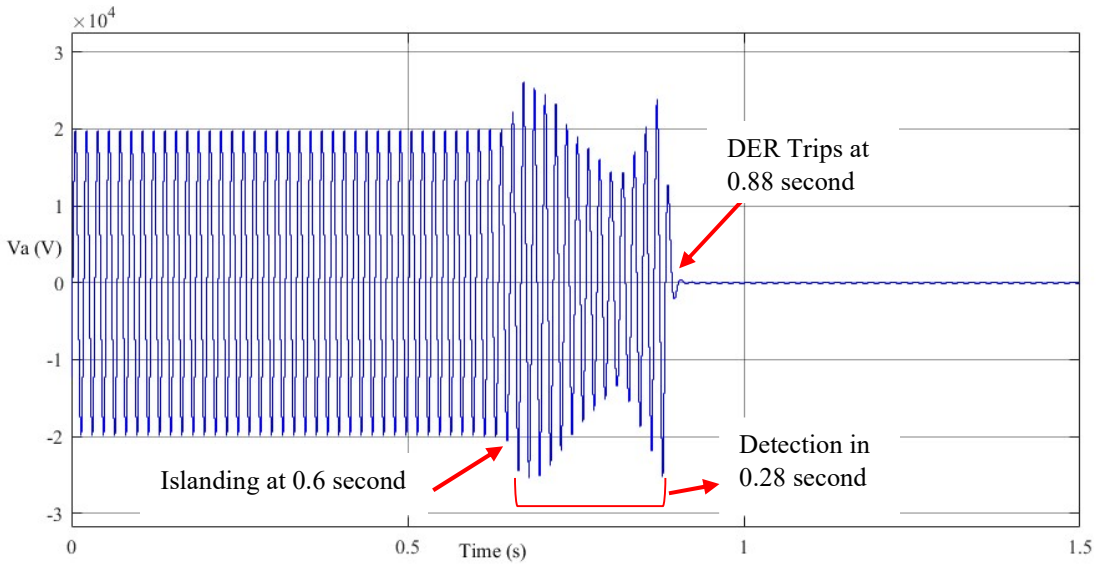

Figure 4.84: Islanding Occurrence and D-RER Tripping for Va Signal

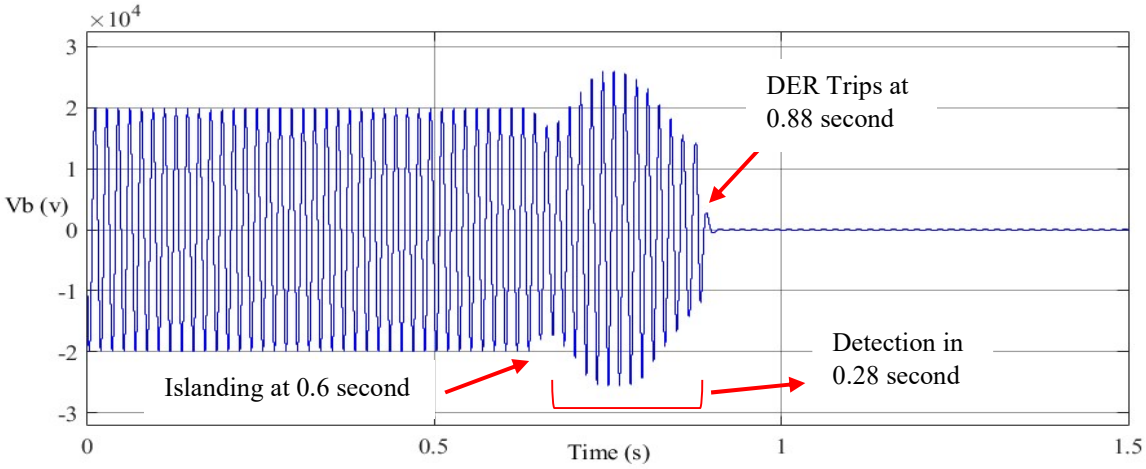

Figure 4.85: Islanding Occurrence and D-RER Tripping for Vb Signal

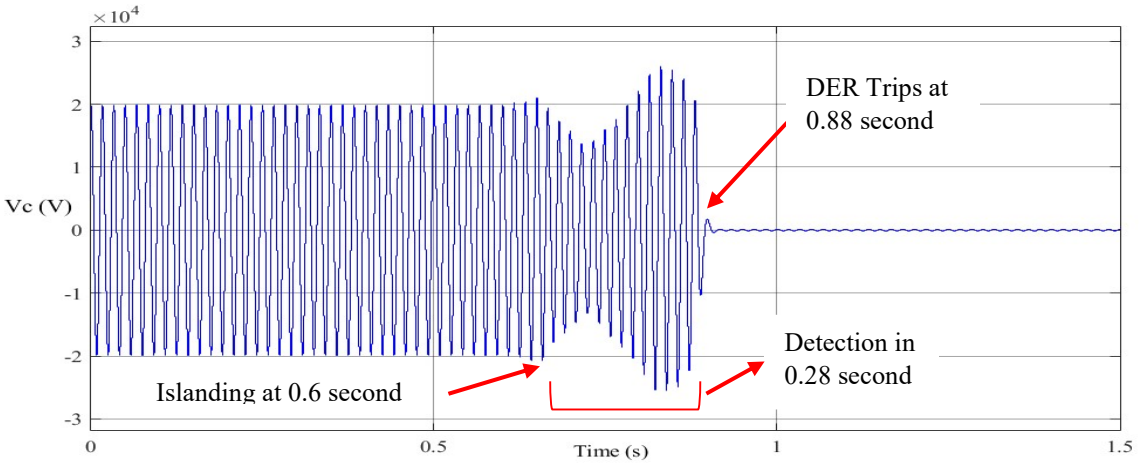

Figure 4.86: Islanding Occurrence and D-RER Tripping for Vc Signal

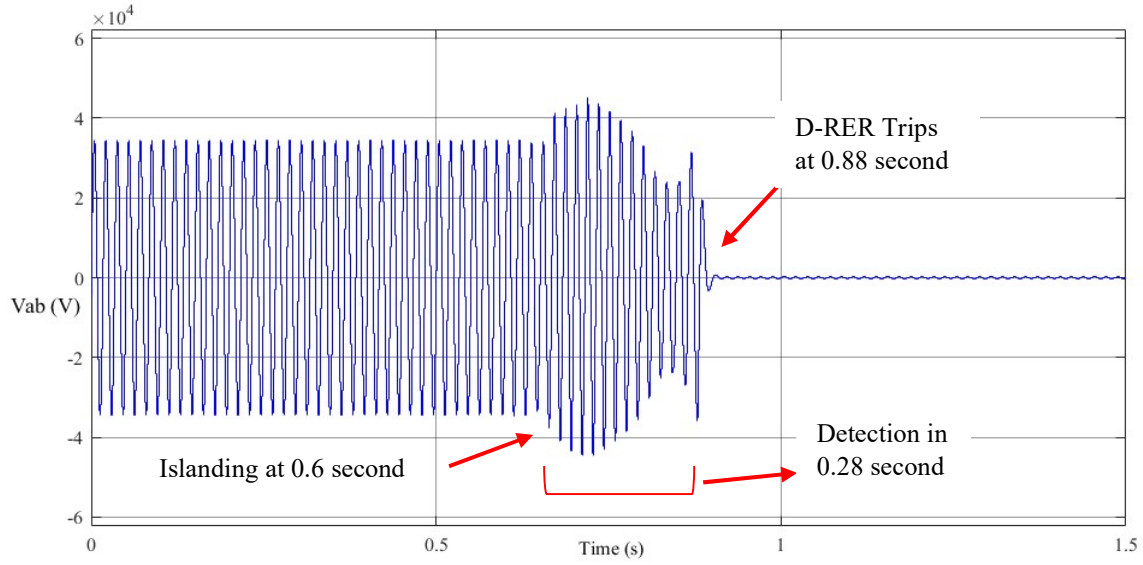

Figure 4. 87: Islanding Occurrence and D-RER Tripping for Vab Signal

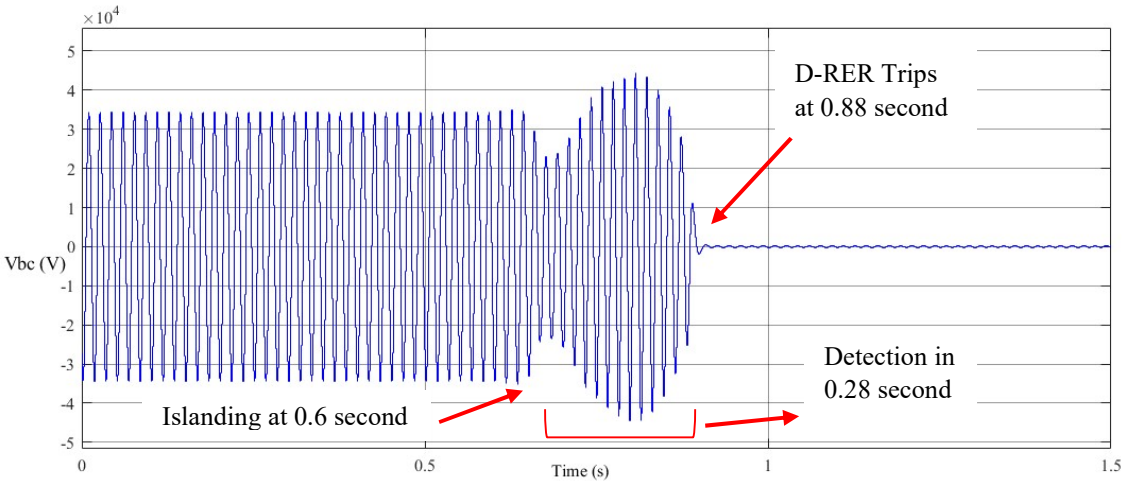

Figure 4. 88: Islanding Occurrence and D-RER Tripping for Vbc Signal

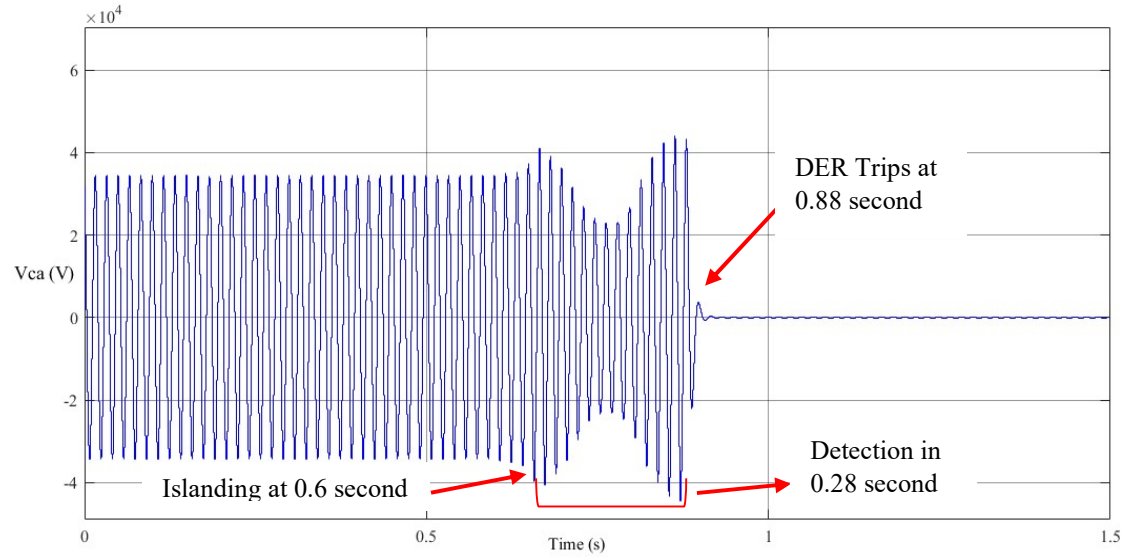

Figure 4. 89: Islanding Occurrence and D-RER Tripping for Vca Signal

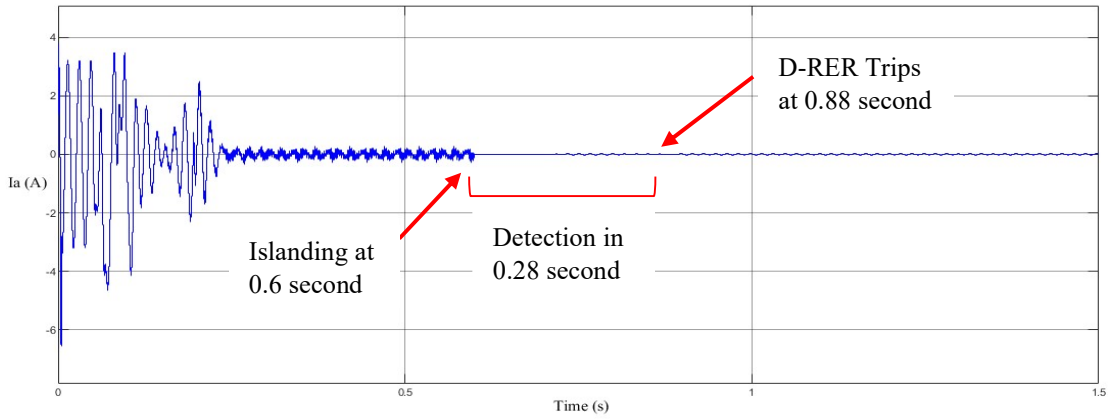

Figure 4. 90: Islanding Occurrence and D-RER Tripping for Ia Signal

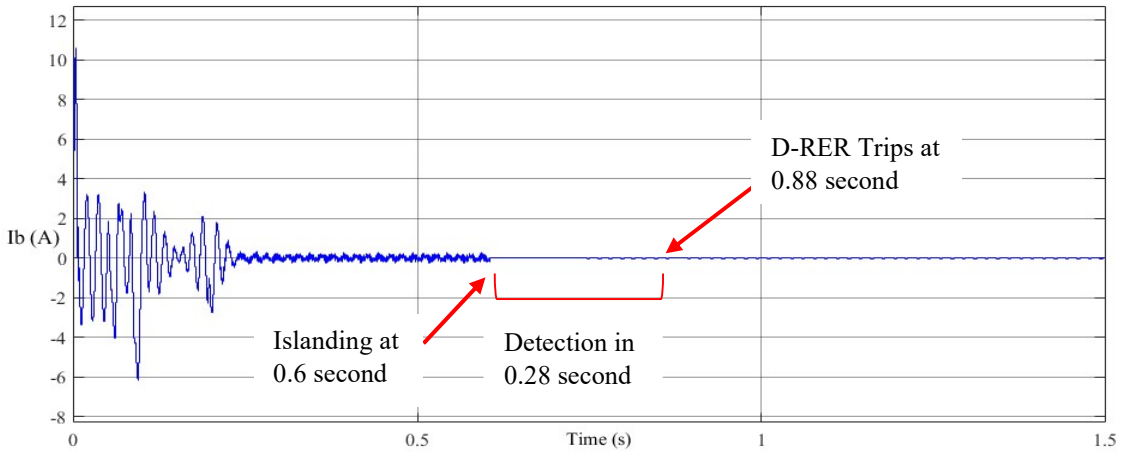

Figure 4.91: Islanding Occurrence and D-RER Tripping for Ib Signal

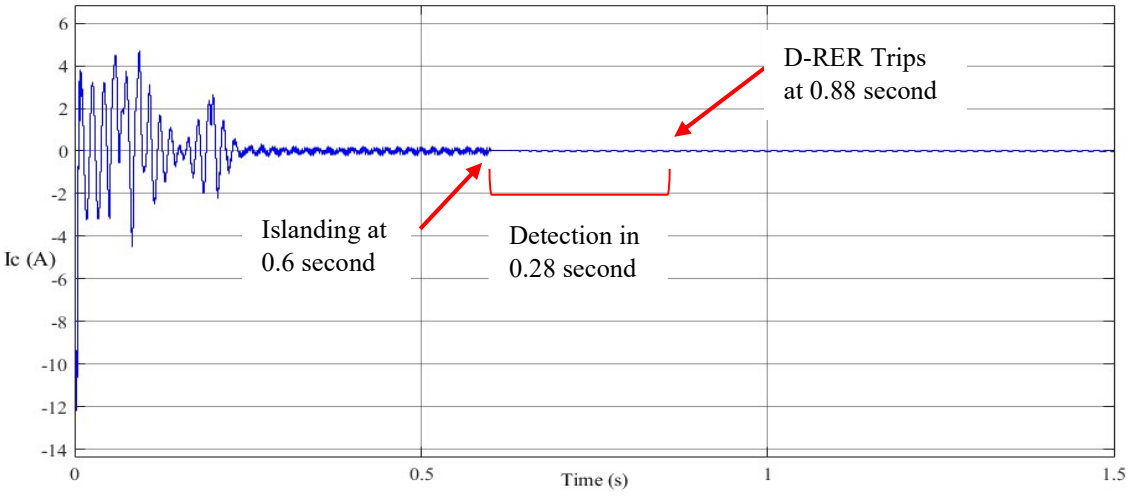

Figure 4. 92: Islanding Occurrence and D-RER Tripping for Ic Signal

4.6 Summary and Discussion

This section shows a summary of the work in comparison with other studies that used AI techniques for passive islanding detection. The proposed method shows outstanding performance in terms of the accuracy and the detection time of all studied cases.

4.6.1 Comparison with Non-Deep Learning Studies

In comparison with the Random Forest Classification used in [38] although this method shows higher accuracy of 100%, but this result was not manually calculated and verified. Besides, the method in [38] took longer detection time than the proposed method. In addition, the work in [38] used machine learning that deals with classified data, whereas the proposed method uses deep learning that can deal with unclassified (raw) data. The Slantlet Transform and the Ridgelet Probabilistic Neural Network in [27] shows accuracy of 100% and detection time of 0.17 second. However, the work in [27] used machine learning method, whereas the proposed method utilized deep learning networks that deal with raw data and hence the feature extraction process is already included in the modeling stage instead of being done manually before the modeling stage as explained earlier.

4.6.2 Comparison with Deep Learning Studies

The auto-encoder in [37] shows an accuracy of 98.3% and a detection time of 0.18 second. The work in [37] took only two cases to train and assess the model. Also, the auto-encoder used three hidden layers only, which may not be applicable in case of massive data that may require multi-layer (deeper) neural networks for better classification. The frequency used in [37] is 30 kHz, which is not a standard relay frequency. The deep leaning approach (Multi-Layer Perceptron) proposed in [22] shows accuracy of 99.88%, but it took two seconds to detect the islanding, which is marginal to the maximum time specified by IEEE 1547. Also, the study in [22] looked only to the synchronous generators (DER) but it did not consider the D-RERs and their complexities to the islanding detection and hence the performance of the approach in [22] in case of D-RER could not be evaluated.

As mentioned in 4.6.1, the proposed method in this thesis stands out from other works by its ability to automatically detect, learn, and extract the features by the deep layers in the modeling stage which enables this technique of dealing with raw data from the grid.

Chapter 5. Conclusion and Recommendations

5.1 Conclusion

The work presented in the thesis aims to enhance the passive islanding detection in smart distribution system considering the integration of renewable-based distributed energy resources. As the literature review revealed, the current passive islanding detection methods have several advantages but they also still have limitations. The proposed method uses one of the advanced artificial intelligence techniques called the deep learning neural networks for achieving an effective way to passively detect the islanding when considering the renewable-based distributed solar photovoltaic, which are usually problematic to detect due to the power electronic interface.

The proposed method like other passive islanding detection uses local system signals measured at the PCC as the input data for feature extraction in the deep learning algorithms. Furthermore, in order to simulate study-case scenarios, the work introduced 46 cases of islanding and non-islanding for the analysis and simulation. A smart grid consisting of microgrid interconnected with utility grid at the PCC was used in the simulation to consider all cases and measurements. The islanding cases were studied when the breaker at the PCC opens at 0.6 second with different scenarios of power flow through the PCC. All scenarios of power flow through the PCC were studied including the positive power flow when the generated power is greater than local load demand within the microgrid, negative power flow when the local generated power by the D-RER is less than the local load demand. Lastly, the cases of zero power mismatch were also studied and considered. Many traditional islanding detection methods failed to detect the islanding when there is no power flowing through PCC, which made the detection harder and led to larger NDZ.

Following the process of obtaining the local signals in all the simulated cases, the continuous wavelet transform was used in the thesis to transform the signals into the time-frequency representations. The data was then split into 80% for training and 20% for testing. The data set was used to train one of the CNN pre-trained neural network called the Alex network. The results show a 100% training's accuracy with training loss reduces to zero. Furthermore, the trained model was tested on new data that the model has never seen to verify the testing accuracy and the detection time. The trained model was able to

successfully detect 90 islanding cases (TP). Also, the trained model was able to classify properly 162 non-islanding cases. There are only 5 cases that were incorrectly classified (FP) by the model as islanding cases while they are non-islanding cases. There were zero islanding cases that were misclassified by the model as non-islanding. The accuracy and the detection time prove that this new approach has an outstanding performance in detecting the islanding within the time specified in IEEE 1547 [5]. The proposed method could detect the islanding in smart distribution containing D-RER with zero power mismatch cases.

5.2 Recommendations

According to the analysis and the work done in this thesis, the following recommendations are introduced:

- The thesis proves that the passive islanding detection can be enhanced to successfully detect the islanding and minimizing the NDZs.
- The work presented various types of local measurements that can be best used for the islanding detection.
- The thesis recommends the use of the continuous wavelet transform to obtain the time-frequency representations of the local measurements to be used as data set for islanding detection.
- In order to detect the islanding successfully in smart grids, the thesis recommends the use of deep learning as one of the advanced AI techniques to deal with the data received from the smart grids to automatically extract and learn the features for robust and reliable event classification.
- A detailed review to the scalograms of the islanding and the non-islanding cases shows that:
    a. The current and voltage measurements and indices respond effectively to islanding occurrence, which was observed through the scalograms of the islanding cases as they are different from the scalograms of the non-islanding cases. Therefore, these measurements were successful in classifying the events and detecting islanding events.

b. The scalograms for ROCOV (abc), ROCOF, and impedance indices were very similar in both islanding and non-islanding cases, which led to misclassification. Therefore, ROCOV, ROCOF, and impedance indices are not recommended for use in islanding detection using deep learning for any future work.

5.3 Future Work

Further research can be conducted in the future to continue improving the islanding detection based on the work presented in this thesis. The proposed work can be applied throughout the smart grid on multiple microgrids at the same time. Future research may include the investigation of deep learning into active methods as well as enhancing the classification accuracies when incorporating multiple islands.

Besides, the processes of measuring the signals, obtain the time-frequency components, and model training are all made external to the DER. The future work can combine and integrate all processes to be all part of the DER or the inverter, so that the DER can automatically detect the islanding and trips itself.

References

[1] "Chapter 6 - Energy Sustainability, Part 3b | Principles of Sustainability | University of Idaho." https://www.webpages.uidaho.edu/sustainability/chapters/ch06/ch06-p3a.asp (accessed Oct. 30, 2020).

[2] W. H. Kersting, *Distribution System Modeling and Analysis*. CRC Press, 2017.

[3] B. Guha, "Smart Distributed Generation Systems Using Improved Islanding Detection and Event Classification," *Electron. Theses Diss.*, Jan. 2015, [Online]. Available: https://digitalcommons.georgiasouthern.edu/etd/1262.

[4] N. Jenkins, C. Long, and J. Wu, "An Overview of the Smart Grid in Great Britain," *Engineering*, vol. 1, no. 4, pp. 413–421, Dec. 2015, doi: 10.15302/J-ENG-2015112.

[5] "IEEE Standard for Interconnection and Interoperability of Distributed Energy Resources with Associated Electric Power Systems Interfaces," *IEEE Std 1547-2018 Revis. IEEE Std 1547-2003*, pp. 1–138, Apr. 2018, doi: 10.1109/IEEESTD.2018.8332112.

[6] M. E. Ropp, M. Begovic, and A. Rohatgi, "Analysis and performance assessment of the active frequency drift method of islanding prevention," *IEEE Trans. Energy Convers.*, vol. 14, no. 3, pp. 810–816, Sep. 1999, doi: 10.1109/60.790956.

[7] Guo-Kiang Hung, Chih-Chang Chang, and Chern-Lin Chen, "Automatic phase-shift method for islanding detection of grid-connected photovoltaic inverters," *IEEE Trans. Energy Convers.*, vol. 18, no. 1, Art. no. 1, Mar. 2003, doi: 10.1109/TEC.2002.808412.

[8] C. Li, C. Cao, Y. Cao, Y. Kuang, L. Zeng, and B. Fang, "A review of islanding detection methods for microgrid," *Renew. Sustain. Energy Rev.*, vol. 35, pp. 211–220, Jul. 2014, doi: 10.1016/j.rser.2014.04.026.

[9] B. Yu, M. Matsui, and G. Yu, "A review of current anti-islanding methods for photovoltaic power system," *Sol. Energy*, vol. 84, no. 5, pp. 745–754, May 2010, doi: 10.1016/j.solener.2010.01.018.

[10] M. Hanif, M. Basu, and K. Gaughan, "A discussion of anti-islanding protection schemes incorporated in a inverter based DG," in *2011 10th International Conference on Environment and Electrical Engineering*, May 2011, pp. 1–5, doi: 10.1109/EEEIC.2011.5874710.

[11] L. A. C. Lopes and Huili Sun, "Performance assessment of active frequency drifting islanding detection methods," *IEEE Trans. Energy Convers.*, vol. 21, no. 1, pp. 171–180, Mar. 2006, doi: 10.1109/TEC.2005.859981.

[12] A. S. Aljankawey, W. G. Morsi, L. Chang, and C. P. Diduch, “Passive method-based islanding detection of Renewable-based Distributed Generation: The issues,” in *2010 IEEE Electrical Power Energy Conference*, Aug. 2010, pp. 1–8, doi: 10.1109/EPEC.2010.5697253.

[13] H. Laaksonen, “Advanced Islanding Detection Functionality for Future Electricity Distribution Networks,” *IEEE Trans. Power Deliv.*, vol. 28, no. 4, pp. 2056–2064, Oct. 2013, doi: 10.1109/TPWRD.2013.2271317.

[14] W. Xu, G. Zhang, C. Li, W. Wang, G. Wang, and J. Kliber, “A Power Line Signaling Based Technique for Anti-Islanding Protection of Distributed Generators—Part I: Scheme and Analysis,” *IEEE Trans. Power Deliv.*, vol. 22, no. 3, pp. 1758–1766, Jul. 2007, doi: 10.1109/TPWRD.2007.899618.

[15] A. Almalaq and G. Edwards, “A Review of Deep Learning Methods Applied on Load Forecasting,” in *2017 16th IEEE International Conference on Machine Learning and Applications (ICMLA)*, Dec. 2017, pp. 511–516, doi: 10.1109/ICMLA.2017.0-110.

[16] S. D. Kermany, M. Joorabian, S. Deilami, and M. A. S. Masoum, “Hybrid Islanding Detection in Microgrid With Multiple Connection Points to Smart Grids Using Fuzzy-Neural Network,” *IEEE Trans. Power Syst.*, vol. 32, no. 4, pp. 2640–2651, Jul. 2017, doi: 10.1109/TPWRS.2016.2617344.

[17] D. Motter and J. C. de M. Vieira, “The Setting Map Methodology for Adjusting the DG Anti-Islanding Protection Considering Multiple Events,” *IEEE Trans. Power Deliv.*, vol. 33, no. 6, pp. 2755–2764, Dec. 2018, doi: 10.1109/TPWRD.2018.2816400.

[18] A. Etxegarai, P. Eguía, and I. Zamora, “Analysis of remote islanding detection methods for distributed resources,” *Renew. Energy Power Qual. J.*, pp. 1142–1147, May 2011, doi: 10.24084/repqj09.580.

[19] P. Radoglou-Grammatikis, P. Sarigiannidis, I. Giannoulakis, E. Kafetzakis, and E. Panaousis, “Attacking IEC-60870-5-104 SCADA Systems,” in *2019 IEEE World Congress on Services (SERVICES)*, Jul. 2019, vol. 2642–939X, pp. 41–46, doi: 10.1109/SERVICES.2019.00022.

[20] A. Shukla, S. Dutta, and P. K. Sadhu, “An island detection approach by μ-PMU with reduced chances of cyber attack,” *Int. J. Electr. Power Energy Syst.*, vol. 126, p. 106599, Mar. 2021, doi: 10.1016/j.ijepes.2020.106599.

[21] A. Pouryekta, V. K. Ramachandaramurthy, N. Mithulananthan, and A. Arulampalam, “Islanding Detection and Enhancement of Microgrid Performance,” *IEEE Syst. J.*, vol. 12, no. 4, pp. 3131–3141, Dec. 2018, doi: 10.1109/JSYST.2017.2705738.

[22] V. L. Merlin, R. C. Santos, A. P. Grilo, J. C. M. Vieira, D. V. Coury, and M. Oleskovicz, "A new artificial neural network based method for islanding detection of distributed generators," *Int. J. Electr. Power Energy Syst.*, vol. 75, pp. 139–151, Feb. 2016, doi: 10.1016/j.ijepes.2015.08.016.

[23] N. Liu, C. Diduch, L. Chang, and J. Su, "A Reference Impedance-Based Passive Islanding Detection Method for Inverter-Based Distributed Generation System," *IEEE J. Emerg. Sel. Top. Power Electron.*, vol. 3, no. 4, pp. 1205–1217, Dec. 2015, doi: 10.1109/JESTPE.2015.2457671.

[24] N. Liu, A. Aljankawey, C. Diduch, L. Chang, and J. Su, "Passive Islanding Detection Approach Based on Tracking the Frequency-Dependent Impedance Change," *IEEE Trans. Power Deliv.*, vol. 30, no. 6, pp. 2570–2580, Dec. 2015, doi: 10.1109/TPWRD.2015.2418580.

[25] D. Bejmert and T. S. Sidhu, "Investigation Into Islanding Detection With Capacitor Insertion-Based Method," *IEEE Trans. Power Deliv.*, vol. 29, no. 6, pp. 2485–2492, Dec. 2014, doi: 10.1109/TPWRD.2014.2347032.

[26] A. G. Abd-Elkader, S. M. Saleh, and M. B. Magdi Eiteba, "A passive islanding detection strategy for multi-distributed generations," *Int. J. Electr. Power Energy Syst.*, vol. 99, pp. 146–155, Jul. 2018, doi: 10.1016/j.ijepes.2018.01.005.

[27] M. Ahmadipour, H. Hizam, M. L. Othman, M. A. M. Radzi, and A. S. Murthy, "Islanding detection technique using Slantlet Transform and Ridgelet Probabilistic Neural Network in grid-connected photovoltaic system," *Appl. Energy*, vol. 231, pp. 645–659, Dec. 2018, doi: 10.1016/j.apenergy.2018.09.145.

[28] I. Y.-H. Gu and E. Styvaktakis, "Bridge the gap: signal processing for power quality applications," *Electr. Power Syst. Res.*, vol. 66, no. 1, pp. 83–96, Jul. 2003, doi: 10.1016/S0378-7796(03)00074-9.

[29] Zwe-Lee Gaing, "Wavelet-based neural network for power disturbance recognition and classification," *IEEE Trans. Power Deliv.*, vol. 19, no. 4, pp. 1560–1568, Oct. 2004, doi: 10.1109/TPWRD.2004.835281.

[30] Chia-Hung Lin and Chia-Hao Wang, "Adaptive wavelet networks for power-quality detection and discrimination in a power system," *IEEE Trans. Power Deliv.*, vol. 21, no. 3, pp. 1106–1113, Jul. 2006, doi: 10.1109/TPWRD.2006.874105.

[31] C.-T. Hsieh, J.-M. Lin, and S.-J. Huang, "Enhancement of islanding-detection of distributed generation systems via wavelet transform-based approaches," *Int. J. Electr. Power Energy Syst.*, vol. 30, no. 10, pp. 575–580, Dec. 2008, doi: 10.1016/j.ijepes.2008.08.006.

[32] M. Oleskovicz, D. V. Coury, O. D. Felho, W. F. Usida, A. A. F. M. Carneiro, and L. R. S. Pires, "Power quality analysis applying a hybrid methodology with wavelet

transforms and neural networks," *Int. J. Electr. Power Energy Syst.*, vol. 31, no. 5, pp. 206–212, Jun. 2009, doi: 10.1016/j.ijepes.2009.01.012.

[33] N. W. A. Lidula and A. D. Rajapakse, "A Pattern Recognition Approach for Detecting Power Islands Using Transient Signals—Part I: Design and Implementation," *IEEE Trans. Power Deliv.*, vol. 25, no. 4, pp. 3070–3077, Oct. 2010, doi: 10.1109/TPWRD.2010.2053724.

[34] N. W. A. Lidula and A. D. Rajapakse, "A Pattern-Recognition Approach for Detecting Power Islands Using Transient Signals—Part II: Performance Evaluation," *IEEE Trans. Power Deliv.*, vol. 27, no. 3, pp. 1071–1080, Jul. 2012, doi: 10.1109/TPWRD.2012.2187344.

[35] S. C. Paiva, R. L. de A. Ribeiro, D. K. Alves, F. B. Costa, and T. de O. A. Rocha, "A wavelet-based hybrid islanding detection system applied for distributed generators interconnected to AC microgrids," *Int. J. Electr. Power Energy Syst.*, vol. 121, p. 106032, Oct. 2020, doi: 10.1016/j.ijepes.2020.106032.

[36] N. Mohan, K. P. Soman, and R. Vinayakumar, "Deep power: Deep learning architectures for power quality disturbances classification," in *2017 International Conference on Technological Advancements in Power and Energy (TAP Energy)*, Dec. 2017, pp. 1–6, doi: 10.1109/TAPENERGY.2017.8397249.

[37] X. Kong, X. Xu, Z. Yan, S. Chen, H. Yang, and D. Han, "Deep learning hybrid method for islanding detection in distributed generation," *Appl. Energy*, vol. 210, pp. 776–785, Jan. 2018, doi: 10.1016/j.apenergy.2017.08.014.

[38] O. N. Faqhruldin, E. F. El-Saadany, and H. H. Zeineldin, "A Universal Islanding Detection Technique for Distributed Generation Using Pattern Recognition," *IEEE Trans. Smart Grid*, vol. 5, no. 4, pp. 1985–1992, Jul. 2014, doi: 10.1109/TSG.2014.2302439.

[39] S. Alshareef, S. Talwar, and W. G. Morsi, "A New Approach Based on Wavelet Design and Machine Learning for Islanding Detection of Distributed Generation," *IEEE Trans. Smart Grid*, vol. 5, no. 4, pp. 1575–1583, Jul. 2014, doi: 10.1109/TSG.2013.2296598.

[40] S. R. Samantaray, K. El-Arroudi, G. Joós, and I. Kamwa, "A Fuzzy Rule-Based Approach for Islanding Detection in Distributed Generation," *IEEE Trans. Power Deliv.*, vol. 25, no. 3, pp. 1427–1433, Jul. 2010, doi: 10.1109/TPWRD.2010.2042625.

[41] S. Vyas, R. Kumar, and R. Kavasseri, "Data analytics and computational methods for anti-islanding of renewable energy based Distributed Generators in power grids," *Renew. Sustain. Energy Rev.*, vol. 69, pp. 493–502, Mar. 2017, doi: 10.1016/j.rser.2016.11.116.

[42] Y. Fayyad and A. Osman, "Neuro-wavelet based islanding detection technique," in *2010 IEEE Electrical Power Energy Conference*, Aug. 2010, pp. 1–6, doi: 10.1109/EPEC.2010.5697180.

[43] A. Darabi, A. Moeini, and M. Karimi, "Distributed generation intelligent islanding detection using governor signal clustering," in *2010 4th International Power Engineering and Optimization Conference (PEOCO)*, Jun. 2010, pp. 345–351, doi: 10.1109/PEOCO.2010.5559212.

[44] K. El-Arroudi, G. Joos, I. Kamwa, and D. T. McGillis, "Intelligent-Based Approach to Islanding Detection in Distributed Generation," *IEEE Trans. Power Deliv.*, vol. 22, no. 2, pp. 828–835, Apr. 2007, doi: 10.1109/TPWRD.2007.893592.

[45] M. Heidari, G. Seifossadat, and M. Razaz, "Application of decision tree and discrete wavelet transform for an optimized intelligent-based islanding detection method in distributed systems with distributed generations," *Renew. Sustain. Energy Rev.*, vol. 27, pp. 525–532, Nov. 2013, doi: 10.1016/j.rser.2013.06.047.

[46] O. N. Faqhruldin, E. F. El-Saadany, and H. H. Zeineldin, "Naive Bayesian islanding detection technique for distributed generation in modern distribution system," in *2012 IEEE Electrical Power and Energy Conference*, Oct. 2012, pp. 69–74, doi: 10.1109/EPEC.2012.6474982.

[47] N. W. A. Lidula, N. Perera, and A. D. Rajapakse, "Investigation of a fast islanding detection methodology using transient signals," in *2009 IEEE Power Energy Society General Meeting*, Jul. 2009, pp. 1–6, doi: 10.1109/PES.2009.5275780.

[48] B. Matic-Cuka and M. Kezunovic, "Islanding Detection for Inverter-Based Distributed Generation Using Support Vector Machine Method," *IEEE Trans. Smart Grid*, vol. 5, no. 6, pp. 2676–2686, Nov. 2014, doi: 10.1109/TSG.2014.2338736.

[49] "Deep Learning for Signal Processing with MATLAB." https://www.mathworks.com/campaigns/offers/deep-learning-for-signal-processing-white-paper.html (accessed Oct. 31, 2020).

[50] A. Almalaq and G. Edwards, "A Review of Deep Learning Methods Applied on Load Forecasting," in *2017 16th IEEE International Conference on Machine Learning and Applications (ICMLA)*, Dec. 2017, pp. 511–516, doi: 10.1109/ICMLA.2017.0-110.

[51] R. Shi, J. Liu, K.-H. So, S. Wang, and Y. Liang, "E-LSTM: Efficient Inference of Sparse LSTM on Embedded Heterogeneous System," in *2019 56th ACM/IEEE Design Automation Conference (DAC)*, Jun. 2019, pp. 1–6.

[52] D. Zhang, X. Han, and C. Deng, "Review on the research and practice of deep learning and reinforcement learning in smart grids," *CSEE J. Power Energy Syst.*, vol. 4, no. 3, pp. 362–370, Sep. 2018, doi: 10.17775/CSEEJPES.2018.00520.

[53] W. G. Morsi, C. P. Diduch, and L. Chang, "A new islanding detection approach using wavelet packet transform for wind-based distributed generation," in *The 2nd International Symposium on Power Electronics for Distributed Generation Systems*, Jun. 2010, pp. 495–500, doi: 10.1109/PEDG.2010.5545860.

[54] C. Burrus, R. Gopinath, and H. Guo, "Introduction to Wavelets and Wavelet Transform—A Primer," *Recherche*, vol. 67, Jan. 1998.

[55] S. M. A. Bhuiyan, J. Khan, and G. Murphy, "WPD for Detecting Disturbances in Presence of Noise in Smart Grid for PQ Monitoring," *IEEE Trans. Ind. Appl.*, vol. 54, no. 1, pp. 702–711, Jan. 2018, doi: 10.1109/TIA.2017.2753720.

[56] J. Khan, S. Bhuiyan, G. Murphy, and J. Williams, "Data Denoising and Compression for Smart Grid Communication," *IEEE Trans. Signal Inf. Process. Netw.*, vol. 2, no. 2, pp. 200–214, Jun. 2016, doi: 10.1109/TSIPN.2016.2539680.

[57] C. Gargour, M. Gabrea, V. Ramachandran, and J. Lina, "A short introduction to wavelets and their applications," *IEEE Circuits Syst. Mag.*, vol. 9, no. 2, pp. 57–68, Second 2009, doi: 10.1109/MCAS.2009.932556.

[58] S. C. Olhede and A. T. Walden, "Generalized Morse wavelets," *IEEE Trans. Signal Process.*, vol. 50, no. 11, pp. 2661–2670, Nov. 2002, doi: 10.1109/TSP.2002.804066.

[59] J. M. Lilly and S. C. Olhede, "Higher-Order Properties of Analytic Wavelets," *IEEE Trans. Signal Process.*, vol. 57, no. 1, pp. 146–160, Jan. 2009, doi: 10.1109/TSP.2008.2007607.

[60] J. M. Lilly and S. C. Olhede, "Generalized Morse Wavelets as a Superfamily of Analytic Wavelets," *IEEE Trans. Signal Process.*, vol. 60, no. 11, pp. 6036–6041, Nov. 2012, doi: 10.1109/TSP.2012.2210890.

[61] C. Mateo and J. A. Talavera, "Short-time Fourier transform with the window size fixed in the frequency domain.(Report)," *Digit. Signal Process.*, vol. 77, pp. 13–21, 2018, doi: 10.1016/j.dsp.2017.11.003.

[62] G. G. Amiri and A. Asadi, "Comparison of Different Methods of Wavelet and Wavelet Packet Transform in Processing Ground Motion Records," vol. 7, no. 4, p. 10, 2009.

[63] D. Zhang, X. Han, and C. Deng, "Review on the research and practice of deep learning and reinforcement learning in smart grids," *CSEE J. Power Energy Syst.*, vol. 4, no. 3, pp. 362–370, Sep. 2018, doi: 10.17775/CSEEJPES.2018.00520.

[64] "Deep Learning Toolbox Getting Started Guide." https://www.mathworks.com/help/pdf_doc/deeplearning/index.html?s_cid=doc_ftr (accessed Nov. 14, 2020).

[65] N. Mohan, K. P. Soman, and R. Vinayakumar, “Deep power: Deep learning architectures for power quality disturbances classification,” in *2017 International Conference on Technological Advancements in Power and Energy (TAP Energy)*, Dec. 2017, pp. 1–6, doi: 10.1109/TAPENERGY.2017.8397249.

[66] H. Shi, M. Xu, and R. Li, “Deep Learning for Household Load Forecasting—A Novel Pooling Deep RNN,” *IEEE Trans. Smart Grid*, vol. 9, no. 5, pp. 5271–5280, Sep. 2018, doi: 10.1109/TSG.2017.2686012.

[67] N. Singhal, N. Singhal, and Srishti, “Comparing CNN and RNN for Prediction of Judgement in Video Interview Based on Facial Gestures,” in *2018 5th International Conference on Signal Processing and Integrated Networks (SPIN)*, Feb. 2018, pp. 175–180, doi: 10.1109/SPIN.2018.8474256.

[68] “Detailed Model of a 100-kW Grid-Connected PV Array - MATLAB & Simulink.” https://www.mathworks.com/help/physmod/sps/ug/detailed-model-of-a-100-kw-grid-connected-pv-array.html (accessed Nov. 01, 2020).

[69] I. V. Banu, M. Istrate, D. Machidon, and R. Pantelimon, “A study on anti-islanding detection algorithms for grid-tied photovoltaic systems,” in *2014 International Conference on Optimization of Electrical and Electronic Equipment (OPTIM)*, May 2014, pp. 655–660, doi: 10.1109/OPTIM.2014.6850940.

[70] T. S. A. A. Sewilam, “Automated wavelet-based fault detection and diagnosis for smart distribution systems and microgrids,” Aug. 2017, Accessed: Nov. 01, 2020. [Online]. Available: http://ir.library.dc-uoit.ca/handle/10155/817.

[71] “IEEE Standard Conformance Test Procedures for Equipment Interconnecting Distributed Energy Resources with Electric Power Systems and Associated Interfaces,” *IEEE Std 15471-2020*, pp. 1–282, May 2020, doi: 10.1109/IEEESTD.2020.9097534.

[72] K. Devleker, “Signal Processing for Deep Learning and Machine Learning,” p. 42, Jul. 2020.